

Carbon and water exchange in Amazonian rainforests

A thesis presented

by

Lucy Hutyra

to

The Department of Earth and Planetary Sciences

in partial fulfillment of the requirements

for the degree of

Doctor of Philosophy

in the subject of

Earth and Planetary Sciences

Harvard University
Cambridge, Massachusetts
April, 2007

Carbon and water exchange in Amazonian rainforests

Abstract

The Amazon rainforest contains approximately 25% of the earth's terrestrial carbon stores and is responsible for cycling vast amounts of carbon and water between the atmosphere and biosphere. This thesis addresses several important issues surrounding the controls on carbon and water exchange and ecosystem stability in Amazonian rainforests through the use of eddy-covariance data, ground-based measurements, long-term climate records, and numerical models.

Based on four years of eddy-covariance data for CO₂ and H₂O fluxes in an evergreen, old-growth tropical rainforest we found that this forest was a small net source of carbon to the atmosphere with an average loss of $0.9 \pm 0.22 \text{ Mg C ha}^{-1} \text{ yr}^{-1}$. This estimate was independently confirmed through biometric methods which also showed the forest to be losing carbon at a rate of $1.5 \pm 0.57 \text{ Mg C ha}^{-1} \text{ yr}^{-1}$ due to excess respiratory losses. The annual carbon balance was very sensitive to weather anomalies, particularly the timing of the dry-to-wet season transition, reflecting modulation of light inputs and respiration processes.

We found that this forest maintained high rates of photosynthesis throughout the year due to adequate water supplies, high year-round temperatures, and high light levels. Canopy carbon uptake rates were largely controlled by phenology and light with no indication of seasonal water limitation during the 5-month dry season. Photosynthetic efficiency declined late in the wet season, before leaf senescence, and increased after new leaf elongation midway through the dry season. However, ecosystem respiration was inhibited by moisture limitations on heterotrophic respiration during the dry season.

Historical records and charcoal found in soils show that fires have occurred in many evergreen tropical forests. Future climate scenarios suggest that temperatures in the Amazon may increase while precipitation decreases, likely decreasing water availability and increasing drought and flammability. We found that over 600,000 km², more than 11% of the Brazilian Amazon, could shift to transitional forests or savanna, if aridity increases as predicted by climate change models. Our analysis showed that increased aridity may lead to bisection of Amazonian equatorial forests.

| | |
|--|--------|
| Abstract..... | iii |
| Acknowledgements..... | vii |
| Chapter 1: Introduction..... | - 1 - |
| 1.1 The global carbon cycle & tropical rainforests..... | - 1 - |
| 1.2 Methods for measuring forest CO ₂ and H ₂ O exchange..... | - 4 - |
| 1.2.1 Eddy-covariance measurements..... | - 5 - |
| 1.2.2 Ground-based measurements..... | - 6 - |
| 1.3 Thesis Overview..... | - 7 - |
| Chapter 2: Seasonal controls on the exchange of carbon and water in an Amazonian rainforest..... | - 11 - |
| 2.1 Abstract..... | - 12 - |
| 2.2 Introduction..... | - 13 - |
| 2.3 Methods..... | - 16 - |
| 2.3.1 Site Description..... | - 16 - |
| 2.3.2 Instrumentation..... | - 17 - |
| 2.3.3 Data Processing & Analysis..... | - 19 - |
| 2.4 Results..... | - 24 - |
| 2.4.1 Weather and climate..... | - 24 - |
| 2.4.2 Energy balance..... | - 29 - |
| 2.4.3 Ecosystem carbon fluxes..... | - 31 - |
| 2.4.4 Ecosystem water fluxes..... | - 34 - |
| 2.4.5 Independent Estimates of Carbon Flux..... | - 36 - |
| 2.5 Discussion..... | - 39 - |
| 2.5.1 Controls on NEE..... | - 39 - |
| 2.5.2 Controls on Gross Primary Production..... | - 40 - |
| 2.5.3 Controls on Ecosystem Respiration..... | - 43 - |
| 2.5.4 Is forest growth water limited?..... | - 47 - |
| 2.6 Summary & Conclusions..... | - 50 - |
| 2.7 Acknowledgments..... | - 53 - |
| Chapter 3: Resolving systematic errors in estimates of net ecosystem exchange of CO ₂ and ecosystem respiration in a tall-stature forest: application to a tropical forest biome..... | - 54 - |
| 3.1 Abstract..... | - 55 - |
| 3.2 Introduction..... | - 56 - |
| 3.3 Methods..... | - 59 - |
| 3.3.1 Site description..... | - 59 - |
| 3.3.2 Ground-based Measurements..... | - 60 - |
| 3.3.3 Eddy-covariance measurements..... | - 62 - |
| 3.3.4 Canopy CO ₂ storage models..... | - 64 - |
| 3.4 Results..... | - 65 - |
| 3.4.1 Ground-based measurements..... | - 65 - |
| 3.4.1.1 Respiration..... | - 65 - |
| 3.4.1.2 Net Carbon fluxes..... | - 68 - |

| | |
|--|---------|
| 3.4.2 Evidence of lost nighttime flux | - 70 - |
| 3.4.3 Canopy CO ₂ storage | - 72 - |
| 3.4.4 Tower-based respiration flux measurements..... | - 79 - |
| 3.4.4.1 Best estimates of ecosystem respiration | - 79 - |
| 3.4.4.2 Treatments of canopy CO ₂ storage | - 81 - |
| 3.4.5 Tower-based net ecosystem exchange measurements..... | - 83 - |
| 3.4.6 Diurnally varying storage models | - 84 - |
| 3.5 Discussion & Conclusions..... | - 85 - |
| 3.6 Implications and future research..... | - 87 - |
| 3.7 Acknowledgements | - 89 - |
| Chapter 4: Climatic variability and vegetation vulnerability in Amazônia | - 90 - |
| 4.1 Abstract..... | - 91 - |
| 4.2 Introduction | - 92 - |
| 4.3 Measurements & Empirical model | - 94 - |
| 4.4 Drought assessment | - 96 - |
| 4.5 Results | - 99 - |
| 4.5.1 Forest evapotranspiration | - 99 - |
| 4.5.2 Drought and vulnerable vegetation areas | - 99 - |
| 4.6 Discussion..... | - 102 - |
| 4.7 Acknowledgements | - 105 - |
| Chapter 5: Conclusion..... | - 106 - |
| 5.1 Controls on ecosystem carbon balance..... | - 107 - |
| 5.2 Validation of flux measurements..... | - 109 - |
| 5.3 Future Amazon stability | - 110 - |
| 5.4 Future research..... | - 112 - |
| Appendix A..... | - 114 - |
| A.1 Water vapor concentrations | - 114 - |
| A.2 Latent heat flux calculation..... | - 116 - |
| A.3 Sensible Heat Flux | - 117 - |
| A.4 Supplemental Figures and analyses for chapter 2..... | - 118 - |
| References..... | - 125 - |

Acknowledgements

I have many people to thank for making this work possible and so successful. First, I have to thank my advisors Steven Wofsy and J. William Munger who are constantly full of ideas and always have their doors open. I have been lucky to have Steve and Bill as mentors and can only hope that someday I will be as successful in guiding others.

The Wofsy group is a team of incredibly talented and dedicated scientists and engineers. Allison Dunn has been my great friend and provided incredible support throughout all my years at Harvard. This thesis would really not have been possible without her constant encouragement, humor, and proof reading. The eddy-covariance system deployed in the Amazon was the brainchild of Steve Wofsy and Bill Munger, but it was engineered into a reality by Scott Saleska, Bill Munger, Bruce Daube, Alfram Bright, and John Budney. I never would have imagined that it would be such a challenge to keep an instrument running in the middle of a rainforest, but I learned a great deal in the process of all the repairs. I am also grateful to Elaine Gottlieb for her good humor and continual assistance with data processing and coding. Scott Saleska was a wonderful scientific mentor throughout the years; his efforts are still clearly evident in the dataset today. An army of people contributed their sweat and blood to the ground-based biometric measurements including Elizabeth Hammond-Pyle, Scott Saleska, Simone Vieira, Plinio de Carmargo, Daniel Curran, Amy Rice, Greg Santoni, VY Chow, and John Budney.

The community within EPS has been a constant source of information and support. In particular, I would like to thank Chenoweth Moffat and Paul Kelly who are the backbone of this department and keep everything running so smoothly. I also appreciate the support of current and former Wofsy group post-docs and technicians including Carol Barford, Valeriy Ivanov, Christine Jones, Pathmathevan Mahadevan, Katheryn McCain, and Shawn Urbanski. I sincerely thank my thesis committee members, the LBA project office, and NASA for their generous funding of this research.

I would also like to thank my wonderful community of friends and family who were continually interested, encouraging, and supportive. Finally, and most importantly, I would like to thank my husband Bob Reeder and my wonderful parents Stanley and Halina Hutyra for their never ending kindness and patience which has been critical in sustaining me throughout my entire education.

Chapter 1: Introduction

Terrestrial ecosystems significantly contribute to the global carbon cycle, constituting a very large pool of readily exchangeable carbon. Approximately 2200 Pg of carbon are contained in terrestrial ecosystems and the annual flux between the terrestrial biosphere and the atmosphere is about 20 times larger than the CO₂ released through the burning of fossil fuels. Changes in the net carbon balance of terrestrial ecosystems due to climate change, fire, and/or anthropogenic activities have the potential to significantly perturb the global carbon cycle and feedback onto climate change. In this chapter I (1) review the role of the tropical rainforests in the global carbon cycle; (2) discuss methods for measuring forest CO₂ and H₂O exchange; and (3) briefly overview the issues explored in the remaining chapters of this thesis.

1.1 The global carbon cycle & tropical rainforests

Atmospheric CO₂ concentrations have increased from approximately 270 ppm in pre-industrial times [*Petit et al.*, 1999] to over 380 ppm in 2007 (Figure 1.1). CO₂ is a greenhouse gas which absorbs longwave radiation emitted by the earth and is known to have significant effects on global temperatures [*IPCC*, 2001]. The rate of atmospheric CO₂ accumulation has been roughly a constant fraction of CO₂ emissions through the burning of fossil fuels, deforestation, land-use change, and cement production [*Tans et al.*, 1990; *Prentice et al.*, 2001]. A significant fraction of the CO₂ emitted through

industrial activities has not accumulated in the atmosphere, but has instead been taken up by carbon sinks in the terrestrial biosphere and oceans [Prentice *et al.*, 2001; Houghton *et al.*, 2001]. In the terrestrial biosphere, carbon is primarily removed from the

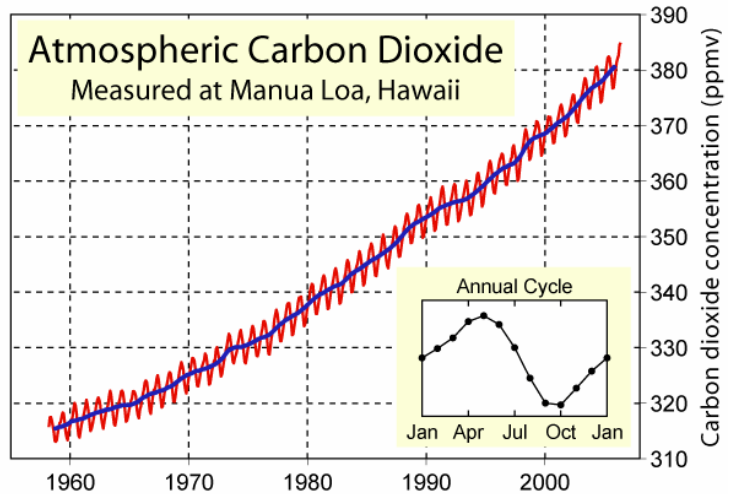


Figure 1.1: Measurements of CO₂ concentration from Manua Loa, Hawaii show a steady rate of accumulation in the atmosphere. The annual cycle of CO₂ accumulation and loss is driven by deciduous vegetation leaf litter dynamics. Figure courtesy of NOAA and Global Warming art:

http://www.globalwarmingart.com/wiki/Image:Mauna_Loa_Carbon_Dioxide.png

atmosphere through plant photosynthesis and returned through ecosystem respiration (Figure 1.2). The residence time of carbon in terrestrial ecosystems is short, ~12 years, but changes in the rates of carbon exchange have the potential to alter both the size of the terrestrial carbon pools and the residence time. Temperature, rainfall, atmospheric CO₂ concentration, and radiation (direct and diffuse) all affect photosynthesis and/or respiration and can modify the net carbon exchange, carbon allocation patterns, and/or overall productivity.

Forests are closely coupled to the climate, exerting a strong influence on temperature and precipitation patterns whilst these same weather and climate patterns dictate where particular forest types can establish and persist [Holdridge, 1947; Wang and Eltahir, 2000]. Significant departure from the current climatic conditions could result in shifts in

plant and animal ranges [Cox *et al.*, 2000; Cox *et al.*, 2004]. The global distribution, stability, and controls on the terrestrial carbon sink are highly uncertain, but the future global climate and ecology of the earth are likely to be very sensitive to changes in CO₂ concentrations.

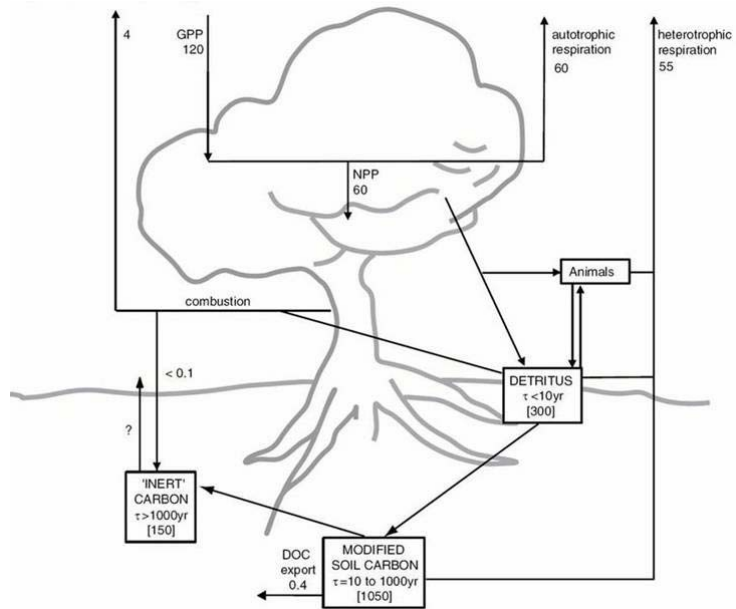


Figure 1.2: The terrestrial carbon cycle is currently out of equilibrium with forested ecosystems removing ~120 PgC yr⁻¹ from the atmosphere through gross primary production (GPP) and releasing ~115 PgC yr⁻¹ through respiration (autotrophic and heterotrophic), resulting in a net terrestrial carbon sink [IPCC, 2001].

Tropical rainforests exist across the earth's warm and moist climates, occurring roughly within the land areas bounded by the Tropic of Cancer (23.5° N) and the Tropic of Capricorn (23.5° S). This region is characterized by high annual precipitation inputs and minimal seasonal variations in temperature. These forests are typically very large in stature (>30 m), contain high species diversity (~200 species per hectare), and a wide range of plant functional forms (buttressing, climbers, epiphytes, etc). Tropical rainforests occupy about 18.1 x 10¹² m² of land, corresponding to approximately 12% of the terrestrial surface, and may contain as much as 55% of the carbon stored in terrestrial biomass [Houghton and Skole, 1990; Whittaker and Likens, 1975]. The Amazon Basin accounts for 50% of the world's undisturbed tropical rainforest [FAO, 1993], ~10% of

global terrestrial net primary productivity [Melillo *et al.*, 1993], and a major portion of global surface evaporation [Choudhury *et al.*, 1998].

Primary tropical rainforests have long been assumed to be in overall carbon balance with the atmosphere [Anderson and Spencer, 1991], with patches of the forest at all stages of recovery from both small and large-scale natural disturbances. However, early results from both eddy-covariance measurements (uptake of 2.2 MgC ha⁻¹ yr⁻¹; Grace *et al.*, 1995) and ground-based biometric studies (uptake of 0.7 MgC ha⁻¹ yr⁻¹; Phillips *et al.*, 1998) suggested that primary Amazonian rainforests were taking up carbon, providing a significant component of the terrestrial carbon sink. An ongoing, vigorous scientific debate has emerged about the carbon budget of Neotropical forests. Despite the importance of tropical rainforests as a carbon store, their role in the carbon cycle still remains poorly understood because they are very spatially extensive, highly heterogeneous, and are generally more difficult to study than other ecosystems. The controls on CO₂ exchange and the likely future response of tropical rainforests to changes in climate are among the largest uncertainties in climate change models [Schaphoff *et al.*, 2006].

1.2 Methods for measuring forest CO₂ and H₂O exchange

In this thesis both micrometeorological and ground-based measurements of carbon stocks and fluxes were utilized to estimate photosynthesis, respiration, and the net carbon exchange. Water exchange was measured through micrometeorological techniques.

1.2.1 Eddy-covariance measurements

Eddy-covariance is the standard micrometeorological method used to investigate the fluxes of CO₂ and H₂O above forest canopies [Wofsy *et al.*, 1993]. The technique is based on decomposing high frequency measurements of 3D wind and a scalar (CO₂, H₂O) into its mean and fluctuating components (Figure 1.3). The net ecosystem exchange (NEE) of CO₂ between the forest and the atmosphere was computed as

$$NEE = \overline{w'c'} + \frac{\partial}{\partial t} \int_0^h c(z) dz \quad (1.1)$$

where the first term on the right hand side is the covariance between vertical wind velocity fluctuations (w') and fluctuations in the concentration of the scalar (c' , CO₂). The second term is the change in the canopy CO₂ storage, where z is the height above the ground surface, h is the

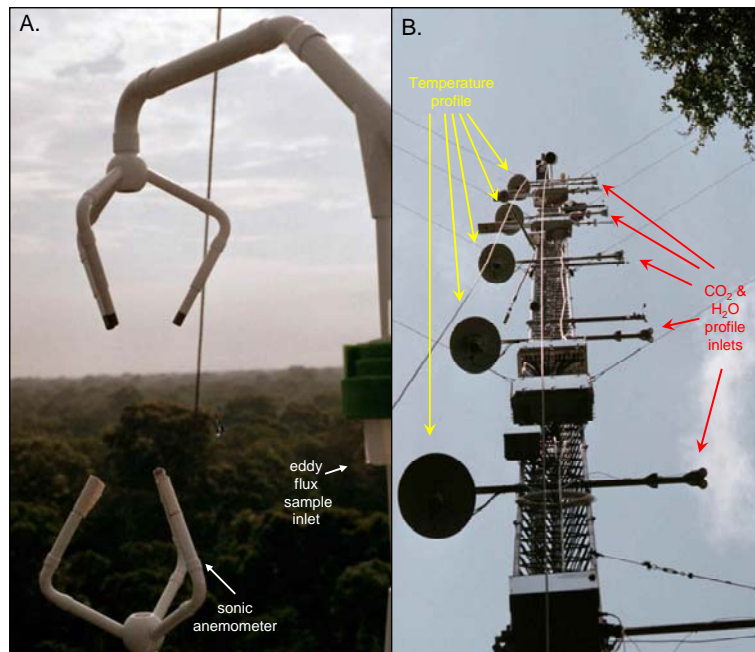


Figure 1.3: Eddy-covariance measurements of the net ecosystem exchange of CO₂, H₂O were made in a primary Amazonian rainforest from 2001 – 2006. High frequency measurements of the 3D winds and gas concentrations at the top of a tower (A) in conjunction with canopy profile measurements (B) allowed for the estimation of the net vertical exchange of CO₂ and H₂O.

flux measurement height, t is time, and the overbar denotes a time average [Baldocchi *et al.*, 1988]. Eddy-covariance is a direct method for measuring the net exchange over approximately 1 km² and can be readily correlated with climate data to gain insights into the processes controlling ecosystem production and exchange.

Observed NEE is the small residual difference between carbon uptake through photosynthesis and carbon loss through respiration. During the daytime hours, measured NEE is the combination of photosynthesis and autotrophic (roots, stem, leaves) and heterotrophic (microorganisms) respiration. In the nighttime, NEE represents ecosystem respiration because photosynthesis can be assumed to be zero. Evapotranspiration is based on measurements of water vapor vertical flux, representing the sum of surface evaporation/condensation and plant transpiration.

1.2.2 Ground-based measurements

The aboveground stock of biomass and the carbon fluxes in tropical rainforests are notoriously difficult to measure [Clark, 2007]. Accurate tropical rainforest mensuration requires large (> 1 ha), multiple, unbiased sample plots which are typically difficult to access [Philips, 1994]. The global average carbon stock in tropical rainforests is 150 Mg C ha⁻¹ in aboveground live biomass [Grace *et al.*, 2001] with as much as another ~ 50 Mg C ha⁻¹ stored in aboveground dead biomass [Rice *et al.*, 2004] (Figure 1.4). Repeated measurement of forest structure (biomass, growth, mortality, recruitment) can elucidate the ecological mechanisms controlling longer term (years to decades) dynamics of ecosystem carbon exchange, the overall carbon balance, and provide an important

constraint for eddy-covariance measurements on the time scale of several years. Finer scale measurements of ecosystem respiration (soil, coarse woody debris, etc.) can quantify the flux rates for different components of the forests and provide an independent estimate of ecosystem respiration to further constrain the eddy-covariance data and the partitioning of NEE into its component processes.

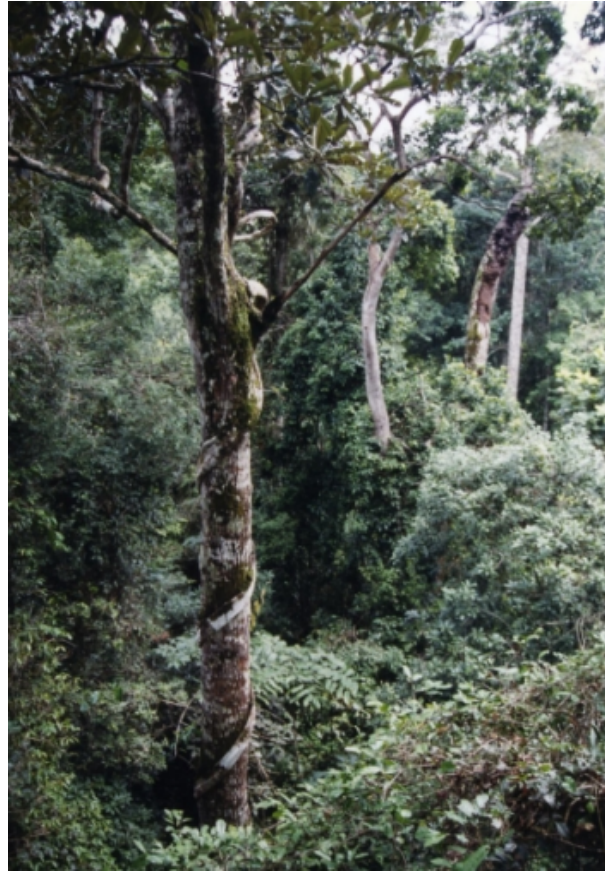


Figure 1.4: View from the forest canopy of a gap in the Tapajós National Forest, Pará, Brazil .

1.3 Thesis Overview

This thesis addresses several important issues surrounding the controls on carbon and water exchange in tropical rainforests through the use of eddy-covariance data, ground-based measurements, long-term climate records, and numerical models. Chapters 2, 3, and 4 are presented as self-contained scientific papers. Chapter 2 is currently undergoing peer-review [Hutyra *et al.*, 2007], chapter 3 is in preparation for submission, and chapter 4 was published in 2005 [Hutyra *et al.*, 2005].

In chapter two I use four years of eddy-covariance data for CO₂ and H₂O exchange in an evergreen, old-growth tropical rainforest to examine the forest responses to seasonal variations and to weather anomalies. Canopy carbon uptake rates were largely controlled by phenology and light with no indication of seasonal water limitation during the 5-month dry season. Photosynthetic efficiency declined late in the wet season, before leaf senescence, and increased after new leaf elongation midway through the dry season. Rates of evapotranspiration were inelastic and did not depend on dry season precipitation. However, ecosystem respiration was inhibited by moisture limitations on heterotrophic respiration during the dry season. The net carbon balance for this ecosystem was very close to neutral, with mean net loss of $890 \pm 220 \text{ kg C ha}^{-1} \text{ yr}^{-1}$, and a range of -221 ± 453 (uptake) to $+2677 \pm 488$ (loss) $\text{kg C ha}^{-1} \text{ yr}^{-1}$ over 4 years. The annual carbon balance was very sensitive to weather anomalies, particularly the timing of the dry-to-wet season transition, reflecting modulation of light inputs and respiration processes.

In chapter three I focus on constraining the measurements of NEE and ecosystem respiration at a Central Amazonian forest through a combination of four years of high quality eddy-covariance measurements and independent ground-based measurements. Integration of eddy-covariance data to daily, seasonal and annual timescales involves several assumptions about which data are representative and must account for unrepresentative periods using carefully evaluated and validated filling methods. Small errors and biases in these approaches can have a significant effect on compiled ecosystem carbon balances when integrated over long timescales, and must therefore be minimized to accurately determine net carbon balances. This chapter focuses on the biases

associated with lost nocturnal flux and missing storage measurements that need to be considered and applied at all sites employing the eddy-covariance technique. Multiple independent estimates for the net carbon balance and ecosystem respiration are presented, including a carefully constructed budget bottom-up for respiration, to validate the correction approaches. The inclusion of canopy storage is essential to accurate assessments of net carbon exchange, but we found that short-term measurements of storage may be adequate to accurately model storage over longer timescales. The chapter presents a framework for analysis and validation that could and should be utilized at other flux tower locations around the globe.

In chapter four I expand my focus from a single study location to examine the vulnerability and resilience of Amazonian vegetation to climate change. Models of climate change predict close coupling between increases in aridity and conversion of Amazonian forests to savanna. The hypothesis explored in this chapter is that higher order climate statistics are important in determining the boundary between tropical rainforests and fire-adapted savanna vegetation. I explored climate-vegetation relationships using climate data, observed vegetation distributions, and evapotranspiration rates inferred from eddy-covariance data. Drought frequency was found to be an excellent predictor of the Amazonian forest-savanna boundary, indicating the key role of extreme climatic events for inducing vegetation change, and highlighting particularly vulnerable regions in the Amazon.

Finally, in chapter five I summarize the main finding of this thesis work and offer suggestions for future research.

The research presented in this thesis was the product of a highly collaborative environment and the extensive efforts of many different people. This work was supported by grants NASA NCC5-341, NASA NCC5-684, and NASA NNG06GG69A to Harvard University.

Chapter 2: Seasonal controls on the exchange of carbon and water in an Amazonian rainforest

Submitted for publication to *Journal of Geophysical Research – Biogeosciences* on
November 7, 2006

Hutyra, L.R., Munger, J.W., Saleska, S.R., Gottlieb, E., Daube, B.C., Dunn, A.L.,
Amaral, D.F., de Camargo, P.B., Wofsy, S.C., Seasonal controls on the exchange of
carbon and water in an Amazonian rainforest, *Journal of Geophysical Research –
Biogeosciences*, in review.

2.1 Abstract

The long-term resilience of Amazonian forests to climate changes and the fate of their large stores of organic carbon depend on the ecosystem response to climate and weather. This study presents four years of eddy covariance data for CO₂ and water fluxes in an evergreen, old-growth tropical rainforest examining the forest's response to seasonal variations and to short-term weather anomalies. Photosynthetic efficiency declined late in the wet season, before appreciable leaf litter fall, and increased after new leaf production midway through the dry season. Rates of evapotranspiration were inelastic and did not depend on dry season precipitation. However, ecosystem respiration was inhibited by moisture limitations on heterotrophic respiration during the dry season. The annual carbon balance for this ecosystem was very close to neutral, with mean net loss of $890 \pm 220 \text{ kg C ha}^{-1} \text{ yr}^{-1}$, and a range of -221 ± 453 (C uptake) to $+2677 \pm 488$ (C loss) $\text{kg C ha}^{-1} \text{ yr}^{-1}$ over 4 years. The trend from large net carbon release in 2002 towards net carbon uptake in 2005 implies recovery from prior disturbance. The annual carbon balance was sensitive to weather anomalies, particularly the timing of the dry-to-wet season transition, reflecting modulation of light inputs and respiration processes. Canopy carbon uptake rates were largely controlled by phenology and light with virtually no indication of seasonal water limitation during the 5-month dry season indicating ample supplies of plant-available-water and ecosystem adaptation for maximum light utilization.

2.2 Introduction

Tropical forests are closely coupled to climate, exerting a strong influence on temperature and precipitation patterns whilst these same weather and climate patterns dictate where particular forest types can establish and persist [Holdridge, 1947]. The interactions between regional and global climate and the Amazonian rainforest are uncertain. Both model results and field studies show wide variability in the spatial patterns and seasonality of forest growth, respiration, and water exchange [e.g. Saleska *et al.*, 2003; Schaphoff *et al.*, 2006]. Mechanistic understanding of the forest responses to climatic factors (particularly temperature, light, and moisture) is required to improve ecosystem process models for tropical forests and to enable more accurate projections of possible responses to changes in climate.

The Amazon Basin accounts for 50% of the world's undisturbed tropical rainforest [FAO 1992], 10% of global terrestrial net primary productivity [Melillo *et al.*, 1993], and a major portion of the global surface evaporation [Choudhury and DiGirolamo, 1998]. Much of the Amazon maintains a green canopy throughout the dry season by acquiring water through deep roots [Nepstad *et al.*, 1994] and possibly by hydraulic redistribution of water by plants [Oliveira *et al.*, 2005]. Huete *et al.* [2006] found widescale 'green-up' of Amazonian rainforest during the dry season, with new leaf production during the period of maximum temperature, the most sunlight, and minimum precipitation.

Previous Amazonian studies have reported diverse seasonal patterns in the net ecosystem exchange of CO₂ from forests. Some sites found enhanced uptake of CO₂ during the dry season [Saleska *et al.*, 2003; Goulden *et al.*, 2004], others reported decreased uptake during the dry season [Malhi *et al.*, 1998; Araujo *et al.*, 2002; von Randow *et al.*, 2004], and others showed no seasonality in the exchange patterns [Carswell *et al.*, 2002]. A data-model comparison for the Tapajós National Forest found that the Terrestrial Ecosystem Model (TEM) [Tian *et al.*, 1998] and Integrated Biosphere Simulator (IBIS) [Botta *et al.*, 2002] model predicted seasonality opposite to observed patterns [Saleska *et al.*, 2003]. Net carbon uptake was observed in the dry season due to lower seasonal respiration rates [Saleska *et al.*, 2003], whereas models predicted carbon release in the dry season due to water limitations on photosynthetic uptake of CO₂.

Similarly, evapotranspiration (ET), the combination of surface evaporation and plant transpiration, has been found to peak at some forest sites during the dry season when radiation inputs were highest [Hutyra *et al.*, 2005; da Rocha *et al.*, 2004; Carswell *et al.*, 2002; van Randow *et al.*, 2002; Shuttleworth, 1988], but at other sites maximum ET occurred during the wet season when water availability was highest [Malhi *et al.*, 2002; Vourlitis *et al.*, 2002]. The observed divergence between sites is likely due to differences in the actual water available to the vegetation, plus differences in phenology and radiative drivers. The amount of moisture available to a forest affects the forest's physical structure, ecophysiology, and flammability. Moisture availability is a function of not only incoming precipitation, but also the depth and texture of the soil, the depth of the water table, transpiration demands of the forest, soil capillarity, site hydrology, and the vertical

distribution of roots. Drier forests can behave like moister forests if deep roots and/or favorable soils provide access to water throughout the dry season months.

Global Climate Models (GCM) generally predict decreases in Amazonian ET during the dry season, in phase with precipitation [*Dickinson and Henderson-Sellers, 1988; Werth and Avissar, 2004*]. *Lee et al.* [2005] updated the National Center for Atmospheric Research Community Atmospheric Model to include both hydraulic redistribution and deep roots in the Amazon. This model produced higher dry season ET relative to control runs, but ET still maximized during the wet season. Evidently we need better understanding of the controls on H₂O exchange in order to improve models to predict forest flammability and to forecast the effects of drought on forest species abundances, biomass distributions, and rates of photosynthesis and ecosystem respiration.

To gain insight into the mechanisms controlling the exchange of carbon and water at the Tapajós old-growth forest, we first summarize observed local meteorology and energy exchange, and then present detailed methods, data processing techniques and validation strategies necessary for making accurate, unbiased eddy covariance measurements in a remote rainforest. We address two major scientific questions: (1) What are the controls on seasonal and inter-annual variations of net ecosystem exchange of CO₂, respiration, and photosynthesis, and water exchange? (2) Is forest growth water-limited during the dry season, or on an annual basis?

2.3 Methods

2.3.1 Site Description

Our study was part of the Brazilian-led Large-Scale Biosphere-Atmosphere Experiment in Amazonia (LBA-ECO). The site is located in the Tapajós National Forest (TNF; 54°58'W, 2°51'S, Pará, Brazil) near Km 67 of the Santarém-Cuiabá highway (BR-163). The TNF is bounded by the Tapajós River to the west and the BR-163 highway on the east, extending from 50 km to 150 km south of the city of Santarém, Pará, Brazil. East of BR-163 the landscape is extensively developed for agriculture. The tower was located ~ 6 km west of the BR-163 highway and ~ 6 km east of the Tapajós River, in an area of largely contiguous forest extending for tens of kilometers to the north and south.

The soils at this site are predominately nutrient-poor oxisols with pockets of sandy ultisols, both having low organic content and cation exchange capacity [*Silver et al.*, 2000]. During well drilling at a nearby site with similar soils, the water table was found to be at ~ 100 m depth [*Nepstad et al.* 2002]. The forest is on flat terrain and has a closed canopy with a mean height of approximately 40-45 m and emergent trees reaching up to 55 m. There are few indications of recent anthropogenic disturbance other than small hunting trails. This forest can be classified as 'primary' with abundant large logs, numerous epiphytes, an uneven age distribution, and emergent trees [*Clark*, 1996]. Ground-based biometric plots were established at this site in July, 1999. See *Rice et al.* [2004] and *Vieira et al.* [2004] for more complete descriptions of the forest structure and growth dynamics.

2.3.2 Instrumentation

A 64 m tower (Rohn 55G, Peoria, IL) was instrumented for eddy covariance measurements which commenced in April, 2001 and continued until the tower was destroyed when a falling tree hit the guy wires in January 2006. Three modular enclosures (approximately 1 m x 0.6 m x 0.2 m) containing all the key instruments and dataloggers were mounted on the tower to keep inlet tubes short (~ 2 m) (Figure 2.1). Eddy-flux measurements were made at a height of 57.8 m with a sample rate of 8 Hz. A 3-axis sonic anemometer (CSAT-3, Campbell Scientific, Logan, UT) was mounted with the air sample inlet located 20 cm from the anemometer. The flux system drew sample air from the inlet through a 50 mm diameter Teflon filter and 9.5 mm (inner diameter) Teflon PFA tubing to a closed-path infrared gas analyzer (IRGA, LI-6262, Licor, Lincoln, NE). The eddy system sample cell (11.9 cm³) was pressure-controlled at 66.6 kPa with a mass flow rate of 6000 sccm, providing a cell-flushing time of 0.078 s. This system design maintains the advantages of the closed-path sensor (e.g. precise instrument calibration,

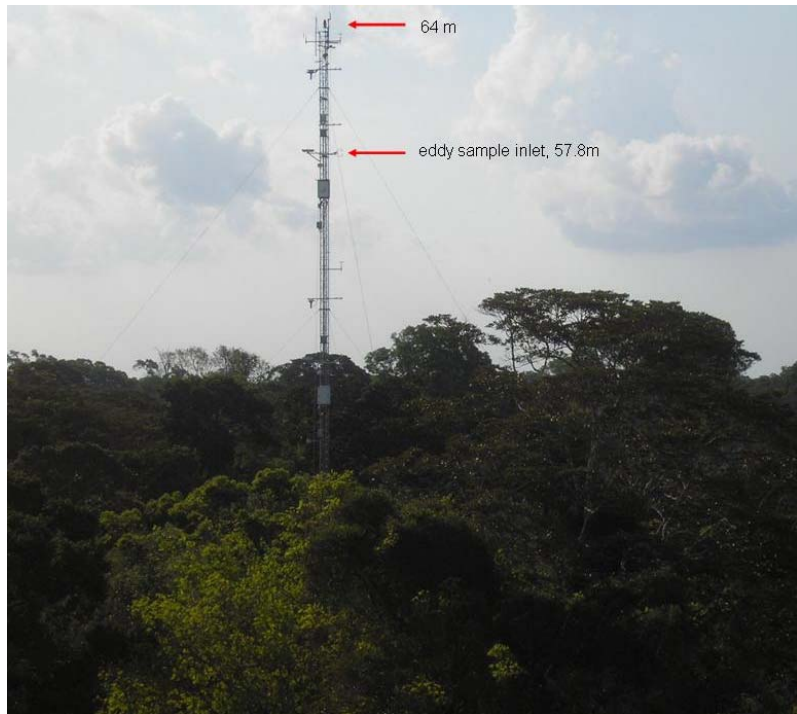


Figure 2.1: Eddy flux tower and forest canopy in the TNF.

constant pressure and temperature), while also adding some of the advantages (e.g. minimal attenuation of high-frequency fluctuations) attributed to open-path designs. This system is particularly suitable for deployment with very tall vegetation where problems accrue due to long sample-tubes from the top of the tower.

Calibrations of the eddy system for CO₂ were made every 6 hours (April 2001 – November 11, 2002 & March 29, 2003 – November 15, 2003) or 12 hours (November 12, 2002 – March 29, 2003 & November 15, 2003 – January 24, 2006) using 325, 400, and 475 ppm CO₂ standard gases traceable to world standards. The instrument was zeroed every 2 hours using a zero air generator (Parker Balston 74-5041, Haverhill, MA). The long-term accuracy of the instruments was ensured by measuring a surveillance standard (traceable to NOAA/CMDL standards at 380.45 ppm) once per week, this tank lasted through the duration of the measurements. Calibrations for water vapor were made using the daily fluctuations of $T_v - T_k$, where T_v is the sonic temperature (derived from the speed of sound provided by the sonic anemometer, closely approximating the virtual temperature) and T_k is the ambient temperature. This approach was necessary due to failures in the chilled mirror hydrometers originally installed for this purpose (see Appendix A for addition details about calibration methods).

Vertical profiles of CO₂ and H₂O concentrations were measured at 8 levels on the tower (62.2, 50, 39.4, 28.7, 19.6, 10.4, and 0.91 m). Sample air was drawn at 1000 sccm through the 8 profile inlets in sequence (2 minutes at each level). The profile concentration data were used to estimate the change in vertical average concentration

between the ground and flux measurement height in order to calculate the column average storage of CO₂. The profile IRGA was zeroed between each profile sequence and an absolute calibration at 325, 400, and 475 ppm was made every 6 or 12 hours, as it was for the eddy CO₂ measurements.

A suite of environmental measurements was also made on the tower (Table 2.1). Dataloggers (CR-10X, Campbell Scientific, Logan, UT), controlled the overall operation of the system. The data were downloaded via coaxial cable to a computer, housed in a climate controlled hut near the tower.

| <i>Measurement</i> | <i>Instrument</i> | <i>Height on tower</i> |
|---|---|--|
| Net Radiation | Rebs Q7.1 with RV2 ventilation | 64.1 m |
| Photosynthetically Active Radiation (PAR) | Licor 190-SA | 63.6 m and 15.1 m |
| Aspirated air temperature | Met One 076B-4 aspirations with YSI 44032 thermistors | 61.9, 49.8, 39.1, 28.4, 18.3, 10.1, 2.8, and 0.6 m |
| Atmospheric pressure | MKS 627A Baratron pressure transducer | Ground-level |
| Dew point hygrometers | EdgeTech 200M | 57.9 m |
| Wind speed | Spinning cup anemometer, Met One 010C | 64.1, 52, 38.2, and 30.7 m |
| Wind direction | Met One 020C | 64.1 m |
| Precipitation | Texas Electronics 076B-4 | 42.6 m |

Table 2.1: List of environmental measurements, instruments, and measurement heights on the tower.

2.3.3 Data Processing & Analysis

The net ecosystem exchange (NEE) of CO₂ between the forest and the atmosphere was computed as

$$NEE = \overline{w'c'} + \frac{\partial}{\partial t} \int_0^h \overline{c(z)} dz \quad (2.1)$$

where the first term on the right hand side is the covariance between vertical wind velocity fluctuations (w') and fluctuations in the concentration of the scalar (c' , CO_2). The second term is the rate of change in the canopy storage, where z is the height above the ground surface, h is the flux measurement height, t is time, and the overbar denotes a time average [Baldocchi *et al.*, 1988]. The vertical coordinate for wind velocities is positive upward, thus positive values for fluxes denote emission and negative values denote uptake. Concentrations of CO_2 and H_2O were calculated using output from the IRGA's raw signal using a third order polynomial fit to the calibration data. CO_2 concentrations were corrected for water vapor. The temperature and pressure inside the sample cell were constant and thus no density fluctuation corrections were required (the data were represented as mole fraction in dry air; see [Webb *et al.*, 1980]).

Cospectral analyses of CO_2 , H_2O , and heat flux measurements were done to assess the reliability of the flux data and to verify if appropriate averaging intervals have been used to capture all of the flux-carrying eddies [Kaimal *et al.*, 1972]. An ogive analysis [Lee *et al.*, 2004] provided an independent check on the adequacy of sampling intervals by looking for an asymptotic plateau in the cumulative sums of the cospectra (between 1 Hz and 34.2 minutes). The daytime ogives for CO_2 , H_2O , and heat fluxes (Appendix A, Figure A.1) indicate that for this site a 30 minute averaging period was appropriate. We did not examine averaging intervals beyond 34.2 minutes due to the instrument calibration schedule, but the ogives indicate that the low frequency fluxes were adequately captured. There was some attenuation of high frequency (above 0.1 Hz) components of the water vapor flux due to adsorption and desorption along the sample

tube walls and inlet filters, but attenuation losses were low (< 2%) because of the short sample tube lengths. We corrected for attenuation as described by *Goulden et al.* [1996]. There may also be a small loss of water flux (<5%) at frequencies longer than 30 minutes, but we don't have a reliable method for accounting for that portion of the cospectrum.

Eddy fluxes (CO₂, H₂O, momentum, and sensible heat) were calculated as 30-minute block averages, after rotating the wind field to a plane of zero mean vertical wind for each 30-minute period [*McMillen*, 1988], then averaged to hourly means. Time lags, due to sample travel time and adsorption in the sample line, were determined by maximizing the correlation between w' and c' and were found to be approximately 1 s and 2 s for CO₂ and H₂O, respectively. See Appendix A for more details about energy flux calculations and calibration methods.

Rainy periods were not explicitly excluded in the processing. However, half-hourly data were filtered to exclude high rates of error in the sonic and IRGA error flags, typically attributable to heavy rainfall and extreme temperatures. We required a minimum of 70 % and 20 % IRGA and sonic data coverage, respectively, for each half-hour period to be included in the time series. This filtering had the effect of excluding periods of heavy rainfall. The sonic transducers were coated with hydrophobic grease and wicking material to minimize the down time after rain ended.

ET and latent heat flux (LE) are both based on measurements of water vapor flux (F_{H_2O}) and represent the sum of surface evaporation, condensation, and plant transpiration. LE is

computed as the product of the latent heat of vaporization and the measured $F_{\text{H}_2\text{O}}$, reported in energy units (W m^{-2}). ET is the sum of half-hourly net water vapor fluxes ($F_{\text{H}_2\text{O}}$) reported in mm day^{-1} for analyses of water budget. Negative ET and LE fluxes denote condensation and positive ET and LE fluxes indicate evaporation plus transpiration.

Measurements of NEE were separated into the component fluxes of ecosystem respiration (R) and gross primary production (GPP) in order to examine the mechanisms controlling the observed patterns of exchange. R was estimated using nighttime NEE measurements during well-mixed periods where the friction velocity,

$$u^* = \sqrt{-1^* w' u'}, \quad (2.2)$$

was greater than or equal to 0.22 m s^{-1} (see section 3.5 for additional information on constraining R estimates). Appendix A, Figure A2 shows the relationship between nighttime NEE and u^* . We have critically assessed potential errors and biases associated with lost nocturnal flux and missing canopy storage measurements at this site [Hutyra *et al.*, 2007]. This analysis strongly supports the appropriateness of the u^* filter and the threshold value, using a suite of independent validation methods for both the NEE and R.

Filling of data gaps was required to obtain a continuous time series for R. Filling for this data set was based on the mean nocturnal NEE within short, sub-seasonal intervals. The 4-year dataset was divided into sample bins each containing 50 hours of well-mixed nighttime observations with a median sample bin size of 12 days. Values of R during the daytime and calm nighttime hours were estimated based on the mean of the valid

nighttime observations within a given sample bin. We did not find a statistically significant correlation between R and nighttime temperature at this site within the gap-filling time scales (see section 4.3 for discussion about the temperature relationships). Therefore, the gap filling was based on mean nighttime NEE values, capturing seasonal patterns but not imposing any diel patterns on the R flux estimates.

GPP refers to canopy carbon uptake such that

$$\text{NEE} = \text{R} - \text{GPP}. \quad (2.3)$$

Since we use only nighttime observations to estimate R, the magnitude of daytime R should be considered a first order estimate. To obtain a continuous time series of GPP, the dataset was divided into sample bins each containing 75 good hours of observations (well-mixed, daytime hours) and missing GPP values were replaced using a fit between GPP and photosynthetically active radiation (PAR). If the curvature in the relationship between GPP and PAR was significant ($p\text{-value} \leq 0.05$), a hyperbolic fit was used, otherwise a linear fit was utilized. The hyperbolic fit was employed in 95% of the periods, with a linear fit being used when there was insufficient low light data to accurately capture the curvature in the GPP-light relationship. The median sample bin size was 8 days.

From January 2002 to January 2006 CO₂ flux data were recorded for 81.2% of possible hours. After accounting for both weak atmospheric turbulence and instrument failures, 48.3% of all possible hours were utilized in this analysis. Missing NEE values were filled using the derived R and GPP estimates. The mean difference between the measured and

derived NEE for periods with valid observations was 0. Unless noted otherwise, all parenthetically reported errors are 95% confidence intervals calculated by bootstrapping the error distributions during similar (*e.g.* season, hour, PAR level) time periods [Richardson *et al.*, 2005]. Seasonal mean results are based on the mean dry season interval extending from July 15 – December 15 with the remainder of the year being considered the wet season.

2.4 Results

2.4.1 Weather and climate

Tables 2.2 and 2.3 provide the observed monthly and seasonal mean climatic conditions, energy fluxes, GPP, R, and NEE for the study period from January 2002 through January 2006. The TNF averages 1920 mm per year of precipitation with a mean dry season of 5 months duration (months with <100 mm precipitation), typically extending from July 15 to December 15 [Parotta *et al.*, 1995]. This site is in the 27th percentile (\pm 2-3%) for both annual precipitation and length of the wet season in the Amazon basin [Saleska *et al.*, 2003, supplement]. There is a regional minimum in annual precipitation in the North-Central Amazon, the location of the TNF, because the propagating sea-breeze front that provides an important trigger for convective precipitation arrives at night [Garstang *et al.*, 1994; Mitchell *et al.*, 2003]. There was also a tendency for precipitation to occur in the late afternoon (1300-1500, local time (LT)) during all seasons, due to convective activity stimulated by surface heating. Climatic conditions during our four years of observation were sufficiently variable to allow us to examine both seasonal and inter-

| year | month | P (mm day ⁻¹) | H (W m ⁻²) | ET (mm day ⁻¹) | R _n (mm day ⁻¹) | T (°C) | NEE (μmol m ⁻² s ⁻¹) | GPP (μmol m ⁻² s ⁻¹) | R (μmol m ⁻² s ⁻¹) |
|------|-------|------------------------------|---------------------------|-------------------------------|---|-----------|--|--|--|
| 2002 | Jan | 10.4 | 20.4 | 2.43 | 4.09 | 25.0 | 2.7 | 7.0 | 9.9 |
| 2002 | Feb | 9.1 | 17.0 | 3.2 | 3.98 | 25.1 | 2.2 | 7.8 | 10.2 |
| 2002 | Mar | 11.8 | 16.1 | 2.71 | 4.12 | 24.7 | 2.2 | 8.0 | 10.3 |
| 2002 | Apr | 17.1 | 21.0 | 2.98 | 4.39 | 24.7 | 1.7 | 7.5 | 9.5 |
| 2002 | May | 6.3 | 18.0 | 2.84 | 4.42 | 25.7 | 1.5 | 7.2 | 8.8 |
| 2002 | Jun | 3.3 | 18.8 | 3.04 | 4.6 | 25.3 | 1.4 | 6.5 | 8.0 |
| 2002 | Jul | 2.0 | 26.8 | 3.06 | 5.07 | 26.1 | 1.8 | 6.5 | 8.4 |
| 2002 | Aug | 0.3 | 31.9 | 3.2 | 5.63 | 26.6 | 1.0 | 7.1 | 8.2 |
| 2002 | Sep | 0.5 | 33.6 | 3.6 | 6.08 | 27.1 | 0.2 | 7.4 | 7.7 |
| 2002 | Oct | 0.7 | 24.7 | 3.59 | 5.89 | 27.0 | -1.1 | 8.4 | 7.5 |
| 2002 | Nov | 5.4 | 18.4 | 3.2 | 4.27 | 26.7 | 0.1 | 8.1 | 8.4 |
| 2002 | Dec | 3.0 | 12.1 | 3.03 | 4.26 | 26.1 | 0.7 | 8.1 | 9.1 |
| 2003 | Jan | 0.9 | 21.1 | 2.96 | 4.79 | 26.4 | -0.5 | 7.9 | 7.6 |
| 2003 | Feb | 8.4 | 14.2 | 2.4 | 3.91 | 24.7 | 1.0 | 7.9 | 9.1 |
| 2003 | Mar | 9.6 | 15.8 | 2.61 | 4.25 | 24.8 | 1.5 | 7.8 | 9.6 |
| 2003 | Apr | 8.1 | 19.8 | 2.75 | 4.74 | 25.0 | 1.4 | 7.5 | 9.1 |
| 2003 | May | 8.1 | 19.2 | 2.72 | 4.68 | 25.3 | 1.8 | 7.1 | 9.1 |
| 2003 | Jun | 5.1 | 20.0 | 2.73 | 4.53 | 25.3 | 2.3 | 6.6 | 9.0 |
| 2003 | Jul | 2.1 | 24.7 | 3.13 | 4.54 | 26.0 | 1.7 | 6.4 | 8.2 |
| 2003 | Aug | 2.3 | 22.8 | 3.1 | 5.03 | 26.4 | 1.3 | 6.4 | 7.7 |
| 2003 | Sep | 3.3 | 23.9 | 3.6 | 5.55 | 26.6 | 0.3 | 8.6 | 9.0 |
| 2003 | Oct | 1.7 | 20.7 | 3.43 | 5.11 | 26.7 | -0.2 | 9.0 | 8.9 |
| 2003 | Nov | 4.9 | 15.9 | 3.63 | 4.7 | 26.6 | -0.3 | 8.5 | 8.4 |
| 2003 | Dec | 3.0 | 12.4 | 3.62 | 4.75 | 26.6 | -0.7 | 8.1 | 7.7 |
| 2004 | Jan | 13.7 | 17.0 | 3.19 | 4.42 | 26.0 | 0.9 | 7.4 | 8.5 |
| 2004 | Feb | 15.7 | 16.1 | 2.81 | 4.06 | 24.6 | 1.3 | 8.0 | 9.5 |
| 2004 | Mar | 8.5 | 14.1 | 2.94 | 4.4 | 24.9 | 1.0 | 8.2 | 9.4 |
| 2004 | Apr | 9.9 | 16.4 | 2.73 | 4.2 | 25.2 | 1.3 | 8.4 | 9.9 |
| 2004 | May | 10.3 | 16.6 | 2.65 | 4.16 | 25.6 | 1.7 | 7.7 | 9.5 |
| 2004 | Jun | 3.1 | 22.8 | 3.16 | 4.62 | 25.6 | 1.5 | 7.4 | 9.0 |
| 2004 | Jul | 4.9 | 21.0 | 3.12 | 4.92 | 25.7 | 1.2 | 7.2 | 8.5 |
| 2004 | Jul | 4.9 | 21.0 | 3.12 | 4.92 | 25.7 | 1.2 | 7.2 | 8.5 |
| 2004 | Aug | 2.3 | 24.3 | 3.31 | 5.34 | 26.3 | 1.0 | 6.9 | 8.0 |
| 2004 | Sep | 3.3 | 21.7 | 3.37 | 5.38 | 26.7 | -0.2 | 7.9 | 7.8 |
| 2004 | Oct | 2.2 | 23.4 | 3.52 | 5.13 | 27.0 | -0.9 | 8.1 | 7.3 |
| 2004 | Nov | 0.8 | 19.1 | 3.42 | 4.44 | 27.7 | -1.6 | 7.5 | 6.0 |
| 2004 | Dec | 2.0 | 19.3 | 3.04 | 3.47 | 27.4 | -1.3 | 8.0 | 6.7 |
| 2005 | Jan | 7.8 | 21.1 | 2.77 | 4.41 | 27.0 | 0.3 | 7.7 | 8.2 |
| 2005 | Feb | 8.8 | 18.1 | 2.54 | 3.42 | 25.3 | 1.6 | 7.9 | 9.6 |
| 2005 | Mar | 9.8 | 21.1 | 2.8 | 4.31 | 25.5 | 0.3 | 8.9 | 9.4 |
| 2005 | Apr | 13.0 | 21.4 | 2.67 | 4.44 | 25.5 | 1.5 | 8.4 | 10.0 |
| 2005 | May | 9.0 | 16.8 | 2.62 | 4.4 | 25.3 | 1.7 | 7.2 | 8.9 |

Table 2.2 Continued: Monthly, 24 hour averages of precipitation (P), sensible heat flux (H), Evapotranspiration (ET), net radiation (R_n), temperature (T), net ecosystem exchange (NEE), gross primary production (GPP), and ecosystem respiration (R). Data gaps have been filled, see text for details.

| year month | P (mm day ⁻¹) | H (W m ⁻²) | ET (mm day ⁻¹) | R _n (mm day ⁻¹) | T (°C) | NEE (μmol m ⁻² s ⁻¹) | GPP (μmol m ⁻² s ⁻¹) | R (μmol m ⁻² s ⁻¹) |
|------------|------------------------------|---------------------------|-------------------------------|---|-----------|--|--|--|
| 2005 Jul | 1.6 | 25.0 | 3.19 | 4.81 | 26.3 | 1.4 | 6.7 | 8.2 |
| 2005 Aug | 1.3 | 28.1 | 3.76 | 5.22 | 27.1 | 1.2 | 6.4 | 7.7 |
| 2005 Sep | 1.3 | 27.2 | 3.73 | 5.69 | 27.1 | -0.8 | 8.2 | 7.5 |
| 2005 Oct | 1.8 | 24.9 | 3.95 | 5.77 | 27.5 | -2.2 | 8.5 | 6.5 |
| 2005 Nov | 4.2 | 21.8 | 3.29 | 4.9 | 27.4 | -0.4 | 8.9 | 8.6 |
| 2005 Dec | 10.9 | 15.8 | 2.43 | 3.43 | 25.2 | 2.0 | 7.6 | 9.7 |
| 2006 Jan | 9.2 | 19.8 | 2.57 | 3.12 | 25.3 | 1.2 | 8.2 | 9.6 |

Table 2.2 Continued: Monthly, 24 hour averages of precipitation (P), sensible heat flux (H), Evapotranspiration (ET), net radiation (R_n), temperature (T), net ecosystem exchange (NEE), gross primary production (GPP), and ecosystem respiration (R). Data gaps have been filled, see text for details.

| | NEE (kg C ha ⁻¹ season ⁻¹) | GPP (kg C ha ⁻¹ season ⁻¹) | R (kg C ha ⁻¹ season ⁻¹) | T (°C) | P (mm season ⁻¹) |
|----------|--|--|--|-----------|---------------------------------|
| Wet 2002 | 2893 ± 376 | 17550 | 20474 | 25.2 | 1833 |
| Dry 2002 | -217 ± 287 | 12998 | 12756 | 26.7 | 279 |
| Wet 2003 | 1376 ± 400 | 18079 | 19439 | 25.3 | 1316 |
| Dry 2003 | -470 ± 275 | 13632 | 13162 | 26.5 | 424 |
| Wet 2004 | 1194 ± 390 | 18924 | 20040 | 25.4 | 1904 |
| Dry 2004 | -1416 ± 274 | 13023 | 11589 | 26.8 | 407 |
| Wet 2005 | 1489 ± 356 | 18640 | 20121 | 25.6 | 1818 |
| Dry 2005 | -1097 ± 262 | 13415 | 12327 | 27.0 | 383 |

Table 2.3: Seasonal mean net ecosystem exchange (NEE), gross primary production (GPP), ecosystem respiration (R), temperature (T) at 57.8 m, and cumulative precipitation (P). The dry season extends from July 15 – December 15 and the fluxes reported are the seasonal sums for NEE, GPP, R, and precipitation.

annual variability, but did not include major climatic extremes or significant El Niño events.

Meteorology in the TNF is characterized by persistent trade winds [Lu *et al.*, 2005].

Winds at the top of the tower (64 m) were predominantly from the east and northeast.

During the afternoons, a westerly river breeze sometimes developed due to differential heating between the forest and the Tapajós River. The river breeze circulation was strongest during hot dry season afternoons, but was also present during dry afternoons in the rainy season. River breezes on average lasted 1.7 hours and developed during approximately 28% of the days.

The mean daily (24-hour average) wind speed recorded at the top of tower by the sonic anemometer was $2.1 \pm 0.01 \text{ m s}^{-1}$ during the wet season and $2.2 \pm 0.01 \text{ m s}^{-1}$ during the dry season. The mean daytime (0700 – 1500, LT) u^* was 0.42 ± 0.004 and $0.44 \pm 0.006 \text{ m s}^{-1}$ during the wet and dry seasons, respectively. The mean nighttime (2300 – 0500, LT) u^* was $0.21 \pm 0.004 \text{ m s}^{-1}$ for both the wet and dry seasons.

Observed net radiation flux (Rn) and temperature were higher during the dry season (Tables 2.2 and 2.3, Figures 2.2 and 2.3). Latent heat flux (LE) and vapor pressure deficit (VPD) closely followed the diel patterns in Rn and temperature. During the study period, the daily mean temperature was $25.9 \pm 0.74 \text{ }^\circ\text{C}$, with mean daily minimum and maximum temperatures of $23.5 \pm 0.05^\circ\text{C}$ and $29.0 \pm 0.08 \text{ }^\circ\text{C}$, respectively. Air temperature did not follow a symmetric diurnal cycle. Heating was rapid after sunrise (0600 local time), with

slow cooling in the afternoon after 1300 (LT). The observed mean RH and mixing ratio of water vapor were $78.2 \pm 0.1 \%$ and $16.2 \pm 0.07 \text{ g H}_2\text{O kg dry air}^{-1}$ over the study period, respectively.

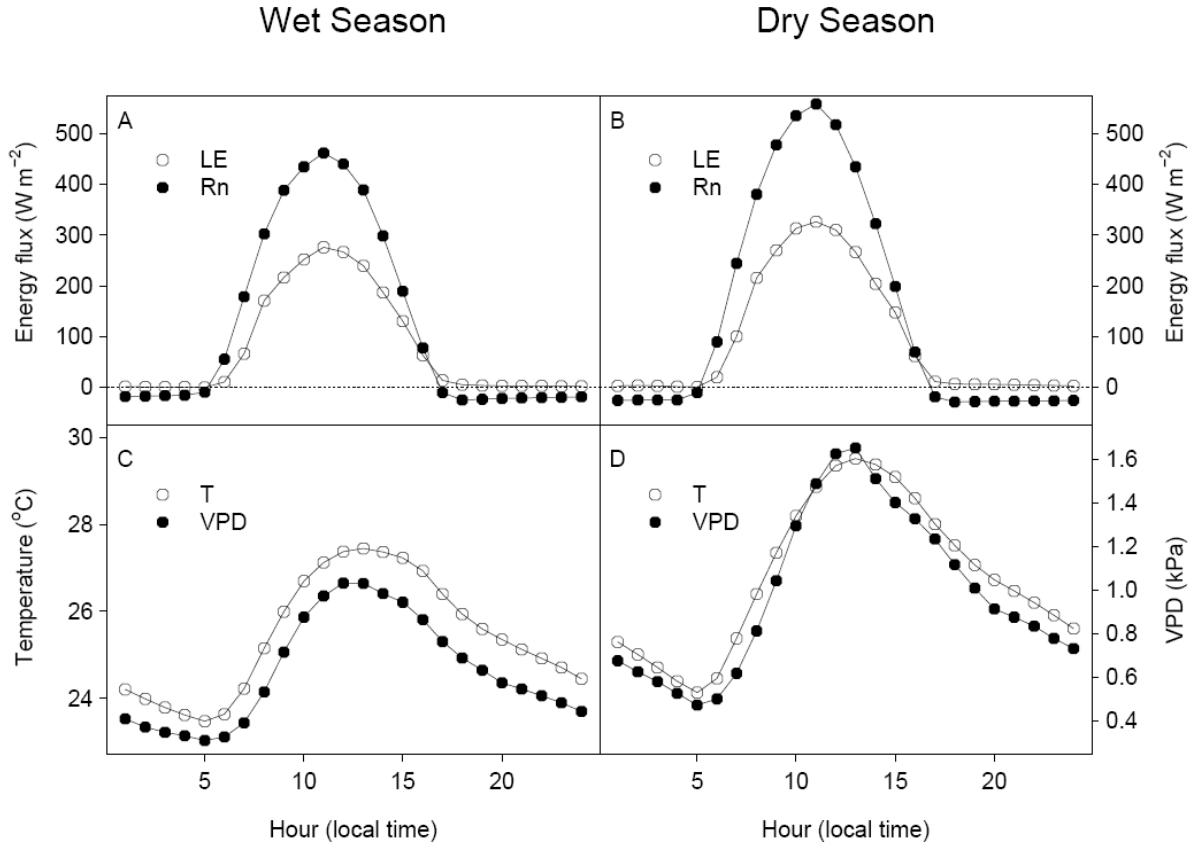


Figure 2.2: Monthly, 24 hour averages of precipitation (P), sensible heat flux (H), Evapotranspiration (ET), net radiation (R_n), temperature (T), net ecosystem exchange (NEE), gross primary production (GPP), and ecosystem respiration (R). Data gaps have been filled, see text for details.

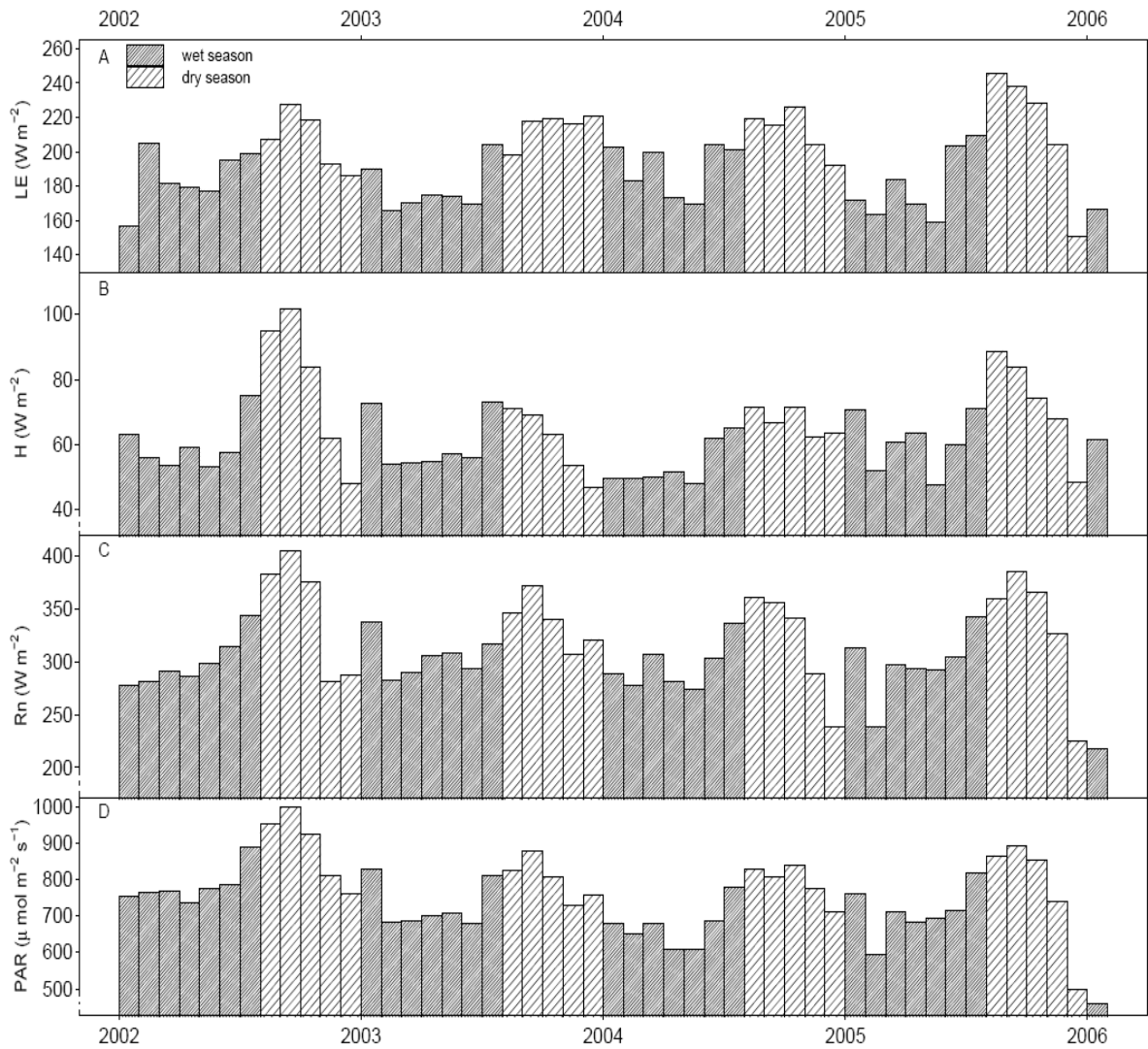


Figure 2.3: Seasonal mean net ecosystem exchange (NEE), gross primary production (GPP), ecosystem respiration (R), temperature (T) at 57.8 m, and cumulative precipitation (P). The dry season extends from July 15 – December 15 and the fluxes reported are the seasonal sums for NEE, GPP, R, and precipitation.

2.4.2 Energy balance

Net radiation flux (R_n) at the surface can be partitioned into ground heat flux (G), changes in biomass and canopy air heat content (S), atmospheric sensible (H) and latent heat (LE) fluxes, and net energy exchange due to precipitation inputs (ΔE_p , see below). Energy balance closure dictates that the sum of LE and H be equivalent to other energy sources and sinks such that

$$R_n - G - S = LE + H + \Delta E_p. \quad (2.4)$$

Energy balance closure is an important criterion used to assess the reliability and accuracy of surface flux measurements. G was not measured at this site, but has been estimated to be of order 3 W m^{-2} during the daytime [Hasler and Avissar, 2007] with its 24-hour integral approaching 0. In Amazonian ecosystems, where the quantity of biomass is very large, S has been estimated to be approximately 5 – 10% of incoming net radiation [Moore and Fisch, 1986], but also averages to 0 over daily intervals. S was estimated for this site using the empirical relationship reported in Moore and Fisch [1986] for a tropical forest near Manaus, Brazil.

To assess energy balance closure we examined the slope of an orthogonal distance regression of daytime hourly turbulent heat fluxes ($LE + H$) versus the total available energy ($R_n - S$) for all daytime hourly measurements (neglecting ground and ΔE_p fluxes); average closure was 85% (± 0.08) using this method. Energy closure was higher during the dry season ($88 \pm 0.1\%$) than the wet season ($83 \pm 0.08\%$). The seasonal closure difference may be a measure of unquantified heat exchanged by precipitation. For example, a 10 mm hr^{-1} rain event, with the water ten degrees cooler than ambient air,

could result in an apparent loss of 116 W m^{-2} from the ecosystem that is not captured in this analysis. On an annual basis the energy flux due to rain ($\sim 2000 \text{ mm yr}^{-1}$) is of order 3% of the total net radiation, and will have a larger impact in the wet season.

Measurement artifacts such as sensor separation and finite volume averaging also result in small, consistent losses in LE and H fluxes [Finnigan, 2004]. Given the overall consistency between wet and dry energy closure results, there is no reason to suspect our fluxes are significantly biased on seasonal timescales. Our observed 15% lack of closure in hourly data is similar to observations at most flux tower sites; global average closure was found to be 79% [Wilson *et al.*, 2002] and 82% within the Amazon tower sites [Hasler and Avissar, 2007]. The slope of the 24-hour energy closure (LE + H vs. Rn) was 93% (± 2.8), using only days with complete data coverage (more common in the wet season).

2.4.3 Ecosystem carbon fluxes

The annual (January – December) carbon balances at this site were 2677 ± 488 , 906 ± 491 , -221 ± 453 , and $392 \pm 449 \text{ kg C ha}^{-1} \text{ yr}^{-1}$, for 2002-2005, respectively, indicating a small net source of carbon to the atmosphere over the period, declining to approximate carbon balance over four years. The complete record analyzed here confirms the seasonal patterns initially reported for the TNF by Goulden *et al.* [2004] and Saleska *et al.* [2003]. During the wet season R was generally greater than GPP, resulting in a net carbon loss to the atmosphere (Tables 2.2 and 2.3, Figures 2.4 and 2.5). During the dry season the reverse was more common, with GPP exceeding R resulting in net carbon uptake from the atmosphere.

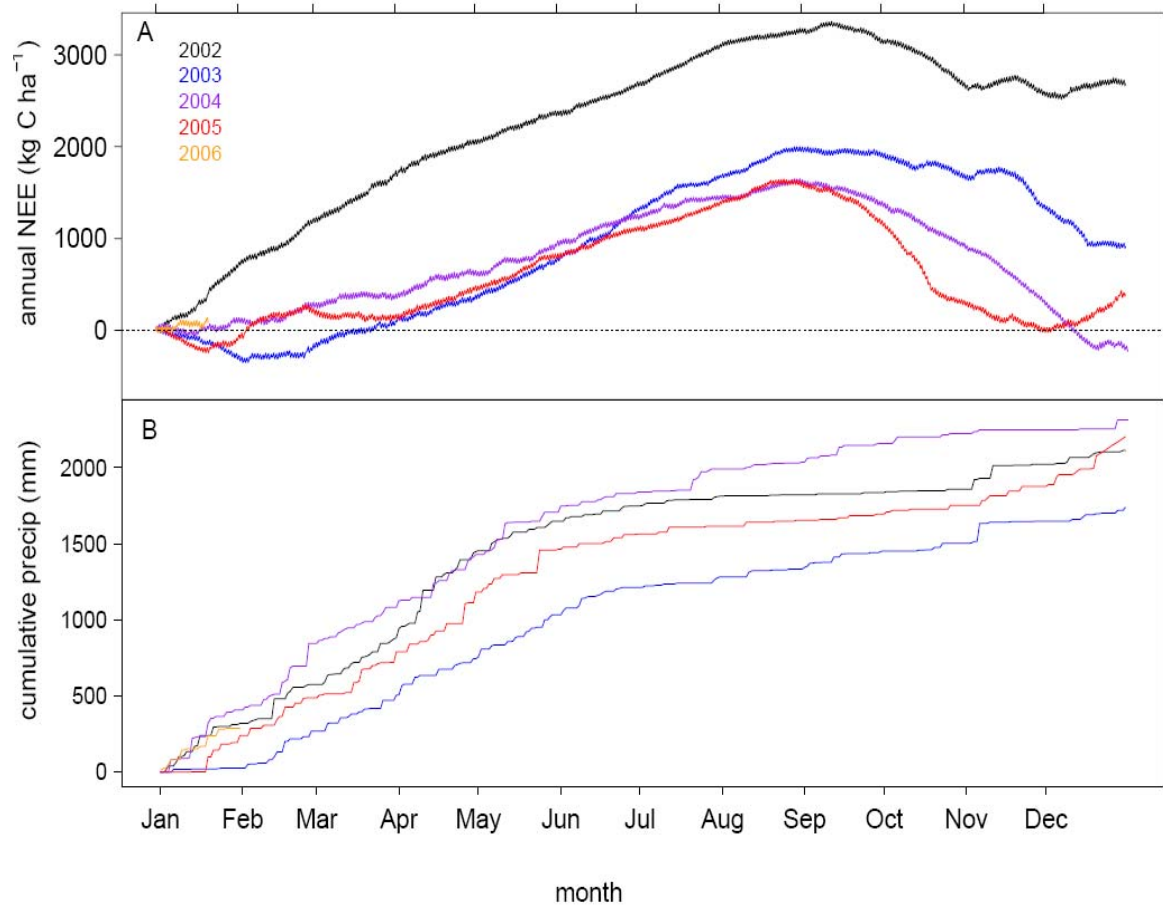


Figure 2.4: Time series of (a) cumulative net ecosystem exchange of CO₂ (annual NEE, kg C ha⁻¹) for January 1, 2002 – January 19, 2006 and (b) cumulative precipitation (mm).

The mean annual ecosystem respiration was $8.6 \pm 0.11 \mu\text{mol m}^{-2} \text{s}^{-1}$, with a mean of 9.2 ± 0.15 and $7.7 \pm 0.15 \mu\text{mol m}^{-2} \text{s}^{-1}$ for the wet and dry seasons, respectively. Maximum respiration was observed during the mid-wet season in March and minimum respiration was observed during the late dry season in October (Table 2.2, Figure 2.5). The mean annual GPP was $8.3 \pm 0.11 \mu\text{mol m}^{-2} \text{s}^{-1}$ with no statistically significant seasonal difference in carbon uptake, $2614 \pm 93 \text{ kg C ha}^{-1} \text{ month}^{-1}$ and $2653 \pm 79 \text{ kg C ha}^{-1} \text{ month}^{-1}$ for the wet and dry seasons, respectively.

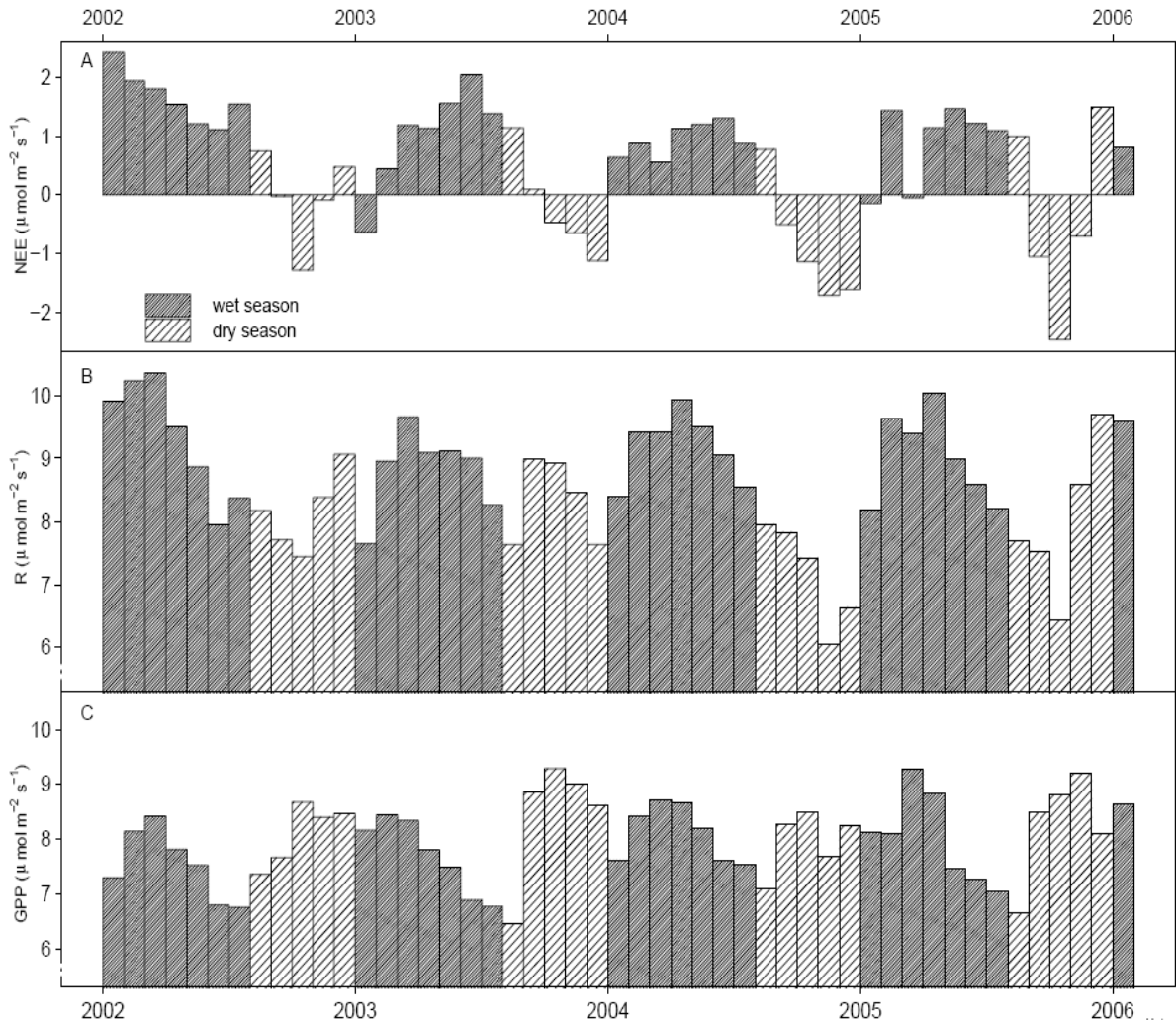


Figure 2.5: Monthly time series (49 months) of (a) net ecosystem exchange of CO_2 (NEE , $\mu\text{mol m}^{-2} \text{s}^{-1}$), (b) ecosystem respiration (R , $\mu\text{mol m}^{-2} \text{s}^{-1}$), and (c) gross primary production (GPP , $\mu\text{mol m}^{-2} \text{s}^{-1}$). The shading patterns within the bars indicate the season.

The total ecosystem R was lower during the dry season, but the decline in R typically began during the latter part of the wet season, in synchrony with the decline in the canopy carbon uptake. R tended to remain low throughout the dry season even as canopy uptake increased. This observation appears to highlight differential responses of the autotrophic and heterotrophic components of R . Autotrophic R can be assumed to increase with increasing GPP . Hence, reduction of R in the dry season is very likely to represent

moisture limitations on heterotrophic R. Over four years, the TNF was a source of carbon to the atmosphere with an observed mean loss of $890 \pm 220 \text{ kg C ha}^{-1} \text{ yr}^{-1}$.

2.4.4 Ecosystem water fluxes

Observed ET ranged widely, from 0.67 to 6.24 mm day⁻¹, with average rates of 2.89 ± 0.15 and 3.41 ± 0.18 mm day⁻¹ for the wet and dry seasons, respectively. The annual mean total was 1135 mm. Across the four measurement years, ET consistently increased at the start of the dry season and remained elevated throughout the entire dry season (Figure 2.3). ET rates were within the range observed at other Amazonian flux sites [see Amazon-wide comparisons in *Hutyra et al.*, 2005], but the data were significantly lower than modeled ET reported by *Nepstad et al.* [2004] and *Lee et al.* [2005]. The annual fraction of precipitation lost through ET was fairly constant during the study period at 0.53 (1116mm/2111mm), 0.64 (1114mm/1740mm), 0.49 (1137mm/2311mm), 0.51 (1123/2201) for 2002-2005, respectively. The ratios of evaporation to precipitation during the dry seasons of 2002, 2003, 2004, and 2005 were 1.81 (503.3mm/278.5mm), 1.16 (521.8mm/448mm), 1.28 (514.4mm/402.4mm), and 1.40 (535.7mm/382.9mm), respectively. Dry season ET was insensitive to dry season precipitation, being nearly constant across years even though dry season precipitation varied by 40%.

There was no statistically significant difference observed between the wet and dry seasons in the slope of LE and H versus Rn (Figure 2.6). The mean annual evaporative fraction (LE/Rn) was 0.62. This invariance contrasts markedly with data reported by *Malhi et al.* [1998; 2002], who observed significant seasonal differences in the

evaporative fraction in an Amazonian forest near Manaus, Brazil, that actually receives more rainfall and has a shorter dry period. The observed patterns are consistent with the findings of *da Rocha et al.* [2004] for the nearby tower at km 83.

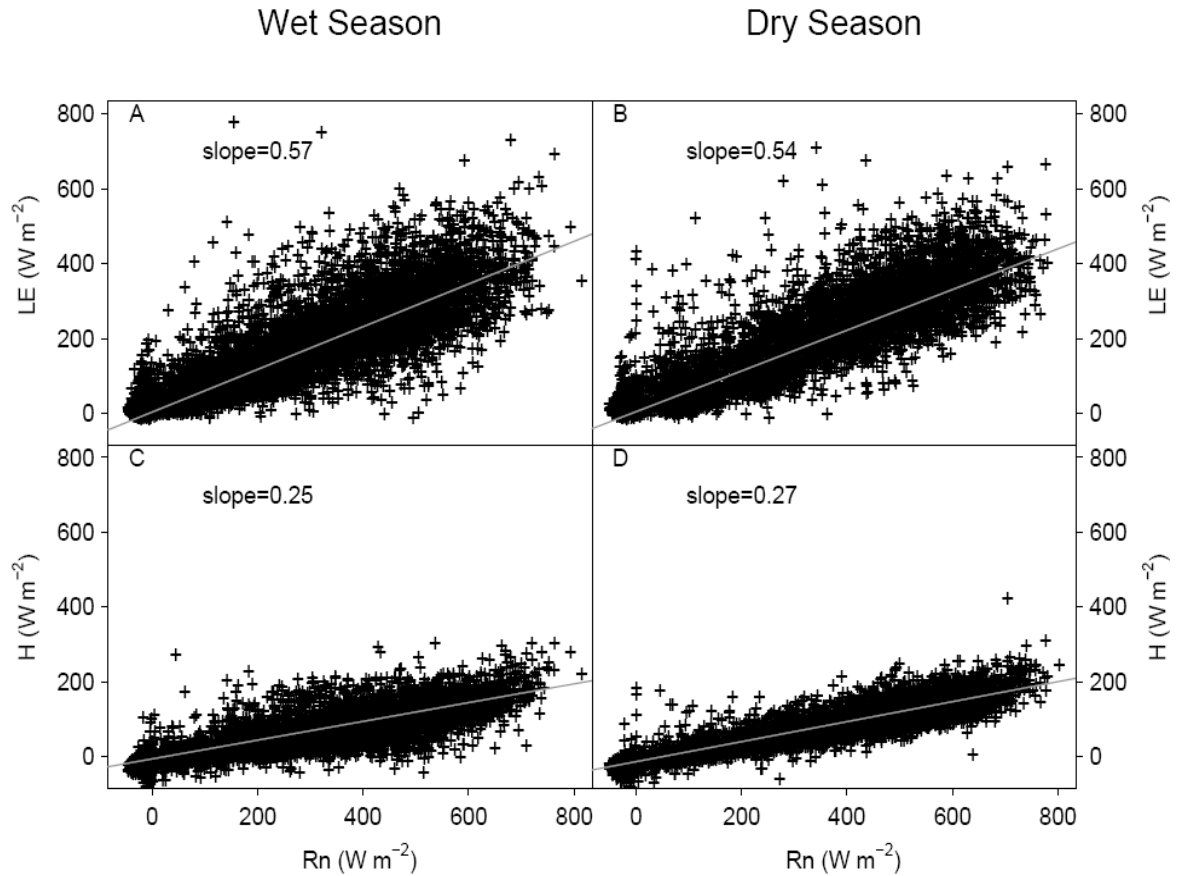


Figure 2.6: (a) Hourly latent heat flux (LE , $W m^{-2}$) as a function of net radiation ($W m^{-2}$) during the wet season. (b) Hourly LE as a function of net radiation during the dry season. (c) Hourly sensible heat flux (H , $W m^{-2}$) as a function of net radiation during the wet season. (d) Hourly H as a function of net radiation during the dry season. The slope reported is from an orthogonal distance regression.

2.4.5 Independent Estimates of Carbon Flux

It is critical to independently validate carbon flux measurements in order to ensure accurate cumulative sums and to examine the mechanisms controlling exchange. Biases in day/night measurements of CO₂ flux could significantly affect estimates of the overall carbon balance. A potential source of bias is the prevalence of weak vertical mixing during the nighttime hours, leading to a violation of the assumption of horizontal homogeneity required for eddy flux measurements and to ‘lost flux’ associated with horizontal advection [Finnigan, 2004]. We used three independent approaches to ensure unbiased data for nighttime fluxes and to validate flux measurements: (a) filtering the data according to u^* values to correct for underestimation of nighttime fluxes; (b) analysis of annual and seasonal light response relationships between PAR and NEE to derive independent estimates of nighttime NEE, avoiding any use of nighttime data or u^* filtering; (c) estimation of nighttime NEE by similarity of CO₂ with ²²²Rn.

(a) Respiration is a biological process that should be largely independent of the turbulence intensity. Since measured NEE decreased in calm conditions (Appendix A, Figure A.2), there appears to be some lost flux. Approximately 57% of the nighttime hours at this site were calm, with $u^* < 0.22 \text{ m s}^{-1}$. We corrected for lost flux by filtering calm night periods and replacing the data with the mean value for proximate well-mixed time periods (defined as $u^* \geq 0.22 \text{ m s}^{-1}$, see Saleska *et al.*, [2003] and Hutrya *et al.* [2007] for further discussion of u^* corrections and the relationship between canopy CO₂ storage and turbulence). Note that the prevalence of strong turbulence (high u^*) in both daytime and nighttime is higher at the TNF than observed at many Amazonian flux towers, giving

better mixing and fewer gaps in the nighttime flux [c.f. *Kruijt et al.*, 2004]. The observed mean nighttime NEE with u^* filtering was 9.2 ± 0.15 and $7.7 \pm 0.15 \mu\text{mol m}^{-2} \text{s}^{-1}$ for the wet and dry seasons, respectively; were no u^* filter applied the respective mean nighttime NEE would be 7.1 ± 0.09 and $5.8 \pm 0.10 \mu\text{mol m}^{-2} \text{s}^{-1}$.

(b) We examined NEE-light relationships (Figure 2.7) using a nonlinear least squares approximation (hyperbolic function)

$$NEE = a_1 + \frac{a_2 \times PAR}{a_3 + PAR} \quad (2.5)$$

fitted to NEE and PAR. We excluded data for $PAR \leq 40 \mu\text{mol m}^{-2} \text{s}^{-1}$, since these data points often correspond to periods of low turbulence and rapidly changing light levels, resulting in large uncertainties. The intercept, a_1 , of this fit provides an independent estimate of mean ecosystem R (limit of eq. (5) as $PAR \rightarrow 0$). The annual mean value of a_1 was $8.9 \pm 0.6 \mu\text{mol m}^{-2} \text{s}^{-1}$, based on all available data (no u^* filter applied), and statistically indistinguishable from the mean nighttime u^* filtered NEE ($8.6 \pm 0.13 \mu\text{mol m}^{-2} \text{s}^{-1}$). Note that the respective datasets are completely disjoint. Seasonal comparisons between a_1 and u^* -filtered mean nighttime NEE also agreed within 5% (Appendix A, Figure A.3).

(c) Data for ^{222}Rn can potentially define rates of forest-atmosphere exchange, since ^{222}Rn is conserved after emission from the soil (apart from slow radioactive decay). *Martens et al.* [2004] independently assessed raw and u^* corrected eddy flux NEE measurements at night by comparing CO_2 eddy flux data with CO_2 fluxes inferred from ^{222}Rn profiles and

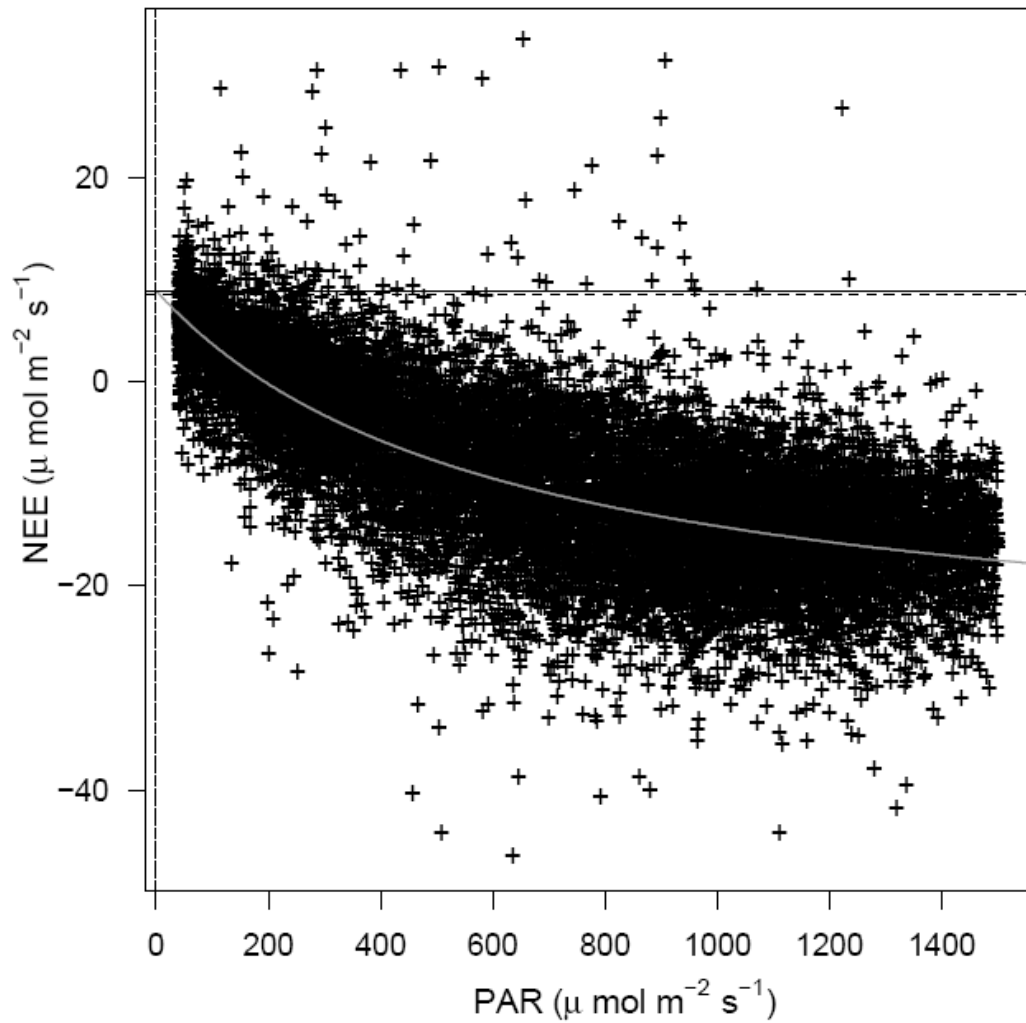


Figure 2.7: Net ecosystem exchange of CO_2 (NEE , $\mu\text{mol m}^{-2} \text{s}^{-1}$) as a function of photosynthetically active radiation (PAR , $\mu\text{mol m}^{-2} \text{s}^{-1}$). A nonlinear least squares approximation (hyperbolic function) is plotted through the data. The vertical line denotes $0 \mu\text{mol m}^{-2} \text{s}^{-1}$ PAR . The dashed horizontal line is the mean nighttime NEE ($8.6 \pm 0.1 \mu\text{mol m}^{-2} \text{s}^{-1}$, $u^* \geq 0.22$). The solid horizontal line is the a_1 intercept term from the hyperbolic fit (eq. 5) estimating of mean nighttime respiration ($8.9 \pm 0.6 \mu\text{mol m}^{-2} \text{s}^{-1}$).

^{222}Rn soil flux measurements. Nighttime NEE derived from ^{222}Rn was found to be $9.0 \pm 0.99 \mu\text{mol m}^{-2} \text{ s}^{-1}$ for the wet season (June-July 2001) and $6.4 \pm 0.59 \mu\text{mol m}^{-2} \text{ s}^{-1}$ in the dry season (November-December 2001), agreeing very well with u^* filtered NEE measurements during the same period (8.65 ± 1.07 and 6.56 ± 0.73 , respectively) [Martens *et al.*, 2004].

The independent light-curve and ^{222}Rn based estimates of nighttime NEE both agree extremely well with the u^* -filtered nighttime flux measurements. Failing to apply a u^* filter to the data would have changed the annual sum of carbon exchange from a small carbon source to a significant carbon sink, almost $10 \text{ Mg C ha}^{-1} \text{ yr}^{-1}$. This value would also markedly disagree with bottom-up estimates for this site [Rice *et al.*, 2004; Saleska *et al.*, 2003; Hutrya *et al.*, 2007].

2.5 Discussion

2.5.1 Controls on NEE

The carbon balance of an ecosystem is the result of disturbance and recovery dynamics over time scales of years and decades [Saleska *et al.*, 2003; Rice *et al.*, 2004; Vieira *et al.*, 2004], upon which is superimposed the influence of weather anomalies on seasonal and annual time scales. Figure 2.4 shows the cumulative annual cycles of NEE, highlighting the dominance of ecosystem respiration throughout the early portion of the calendar year (wet season) as the forest lost carbon to the atmosphere. By September, increases in canopy uptake generally began to dominate and the forest turned into a carbon sink for

the rest of the dry season. The transition back to a net carbon source followed the arrival of wetter weather.

Climate anomalies exerted strong control on the inter-annual variations in net carbon balance. In 2005, carbon losses in the wet season were relatively small and the transition to carbon uptake was very abrupt, and by November the year was on track to be a significant carbon sink. But, the early arrival of the wet season, with significant November and December rainfall, reversed the carbon uptake and the site was instead an overall carbon source in 2005 (Figures 2.4 and 2.5). In January 2003, low precipitation, totaling only 27 mm, resulted in reduced respiration rates. However, GPP rates remained high, leading to a carbon sink for the month despite the seasonal norm (Figure 2.4, Figure 2.5). The greatest variability in monthly total NEE was observed during the late dry season and early wet season (November – January). Respiration rates were the most variable and sensitive to precipitation and temperature anomalies (Figure 2.5).

2.5.2 Controls on Gross Primary Production

Many process-based biogeochemical models [*e.g. Botta et al., 2002; Tian et al., 1998*] predict that moisture limitation during the dry season should provide a strong constraint on canopy carbon uptake in tropical forests like the TNF. Four years of observations at the TNF do not support this paradigm. Uptake was indeed reduced early in the dry season, but the decline began before the onset of the dry weather. Moreover, uptake started to increase in the driest period, well before the onset of the rainy season (Table 2.2; Figures 2.4, 2.5). The forest maintained high rates of photosynthesis throughout the

year because of adequate water supplies, high year-round temperatures, and high light levels. *Goulden et al.* [2004] observed a similar seasonal pattern in photosynthesis at a nearby forest site between July 2000 and July 2001.

Peak litterfall rates were observed at the TNF in August [*Rice et al.*, 2004], early in the dry season, and the flush of new leaves across the Basin also occurred in the dry season, August-October [Figure 2.8, *Huete et al.*, 2006; *Rivera et al.*, 2002]. Younger leaves have higher photosynthetic efficiency [*Freeland*, 1952] and hence it is not surprising that higher rates of GPP were observed in the months following leaf-out in the dry season. Previous work by *Wright and van Schaik* [1994] also showed that tropical plants produce new leaves when irradiance is maximized.

To quantify the phenology effects on GPP at this site, we calculated “canopy photosynthetic capacity” (P_c) as the mean monthly GPP in a fixed light interval (PAR 725 – 875 $\mu\text{mol m}^{-2} \text{s}^{-1}$), and compared the time series of this quantity with leaf litterfall rates and with remotely sensed vegetation greenness (enhanced vegetation index, EVI) at the TNF [*Huete et al.*, 2006]. We examined P_c to remove the influence of seasonal differences in incoming radiation. Figure 2.8 shows that leaf litterfall rates were strongly correlated with P_c ($r^2 = 0.76$ or 0.83 , for lags of 0 or 1 months, respectively). In contrast, EVI correlated weakly with P_c , explaining at best only 56% of the observed variance with a long lag (3 months). EVI, lagged by 2 months, was somewhat better correlated with monthly litterfall ($r^2 = 0.63$). The temporally lagged correlations in EVI and/or litterfall are not surprising since it takes time for the leaves to fully elongate and develop their

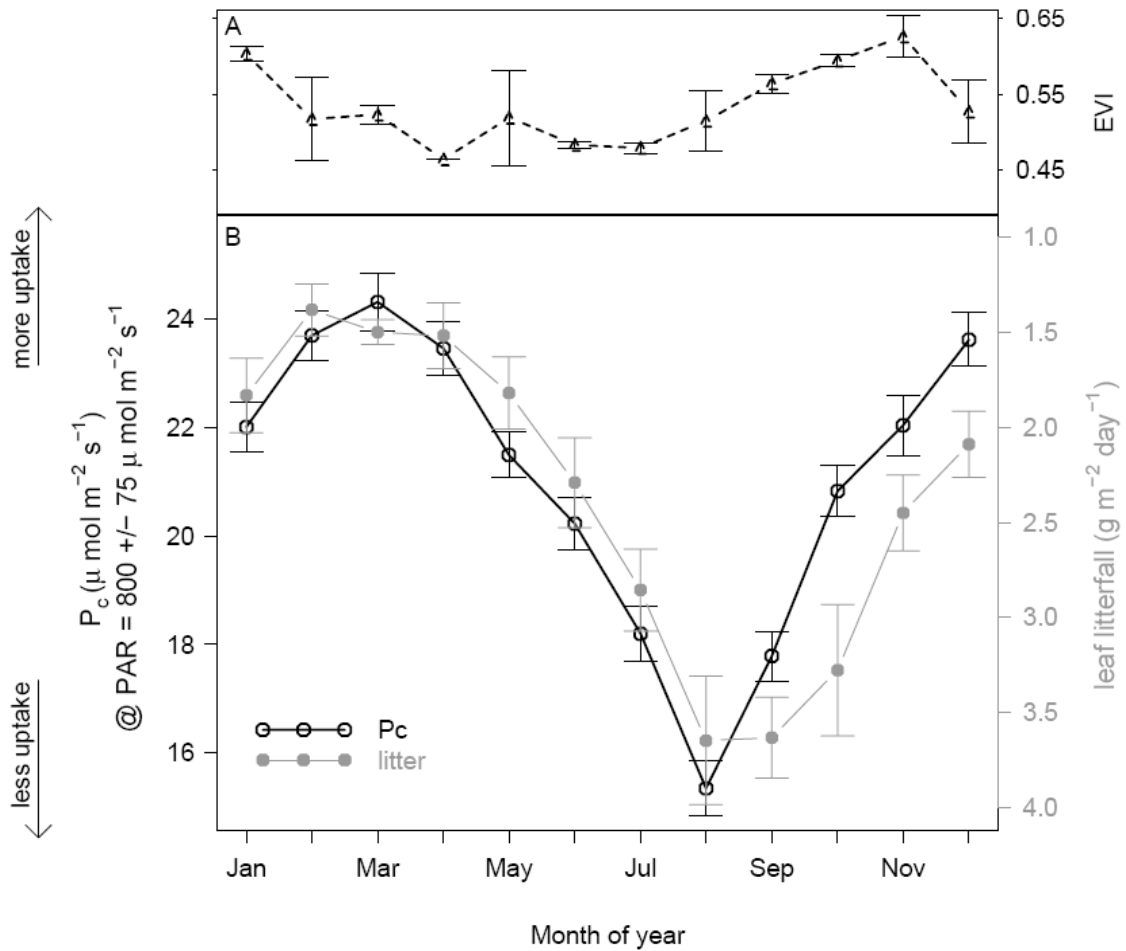


Figure 2.7: (a) Monthly mean Enhanced Vegetation Index (EVI), 2000-2005, triangles [Huete et al. 2006]. (b) The forest canopy efficiency is expressed as the monthly mean gross primary production (GPP) where photosynthetically active radiation is 725 – 875 $\mu\text{mol m}^{-2} \text{s}^{-1}$, open circles. Monthly mean leaf litterfall rate, July 2000 – May 2005, closed circles [see Rice et al. 2004 for methodological details]. The error bars denote standard error. Note that the axis for litterfall is inverted to highlight the correlation with P_c .

pigmentation. Note that total GPP, across all light levels, also correlated with litterfall ($r^2 = 0.63$, lagged by 2 months) and EVI ($r^2 = 0.40$, leading by 1 month).

During the late dry season there are also increased aerosol loadings due to land clearing and agricultural activities, resulting in higher diffuse light levels. *Oliveira et al.* [2007] observed maximum aerosol loading at the TNF between September and November.

Higher photosynthetic rates have been observed under diffuse light conditions [*Oliveira et al.*, 2007; *Gu et al.*, 2003]. Either or both leaf replacement and aerosol light scattering may account for increased P_c in the late dry season (October – December, Figure 2.8).

There was significant inter-annual variation in both EVI and P_c , see Appendix A Figure 4A for the full available time series.

2.5.3 Controls on Ecosystem Respiration

Ecosystem respiration is the sum of CO_2 released by plant leaves, stems, and roots (autotrophic respiration), and CO_2 released through decomposition of organic material (heterotrophic respiration). Temperature and moisture are key environmental factors regulating respiration rates, but the interaction among these parameters is still poorly understood [*Raich and Schlesinger*, 1992; *Trumbore*, 2006]. Temperature and soil moisture are typically inversely correlated, but both factors simultaneously influence R by affecting enzyme activity, diffusion of solutes and O_2 , growth of root tissue, and microbial populations [*Davidson et al.*, 2006]. Eddy covariance data cannot distinguish the components of respiration. However, our long dataset from the TNF does allow us to

examine the aggregate effects of climatic variability on total ecosystem respiration, over timescales from hourly to inter-annual.

Relationships between R and temperature have been reported in many ecosystems, and ecosystem models often use exponential relationships to describe these data, with Q_{10} values typically between 1 and 2 [e.g., Davidson *et al.*, 2006]. But decomposition of organic material in tropical forest soils is known to have a relatively low temperature sensitivity [Davidson and Janssens, 2006]. At the TNF, there was no statistically significant relationship between nighttime CO_2 flux and ground or canopy temperature, or precipitation, over any time interval from hourly to weekly (Table 2.4). Davidson *et al.* [2004], working at nearby site (~ 5 km), also found no significant relationship between soil volumetric water content and observed soil CO_2 respiration rates using chamber methods. The absence of a significant relationship between temperature and ecosystem R could be an artifact of high mean temperature, with canopy and ground mean temperatures averaging 24.8°C and 24.6°C, respectively, or of the small temperature range seasonally, diurnally, and during the nighttime. It is also possible that the entire temperature range is within a broad optimum for this ecosystem or that the temperature responses of multiple processes may cancel when aggregated to the ecosystem scale. The observations imply that models of tropical forests which include an exponential relationship between respiration and temperature may over-predict the temperature sensitivity of respiration rates at the ecosystem level.

When averaged on longer time scales, temperature and precipitation were significant correlates of total ecosystem respiration and a temperature regression could indeed explain the most significant portion of the total observed variance (Table 2.4). But, respiration was *negatively* correlated with temperature and *positively* correlated with precipitation, and the apparent relationship between R and temperature arises because temperature and precipitation are negatively correlated. We examined the intercept values (a_1) of morning versus afternoon light-curve extrapolations (eq. (5)) and found no significant difference in the respiration estimates in the dry season, although temperature differences were near their maximum (Appendix A, figure A5). In contrast, during the wet season we found that morning respiration estimates were higher than the afternoon estimates in three of four observed wet seasons (Appendix A, figure A5). Higher morning respiration highlights the dominance of moisture in controlling heterotrophic respiration rates since nighttime precipitation is very common while morning temperatures were lower. We conclude that the negative respiration-temperature correlation is likely a simple artifact that arises because wet seasons, which have higher respiration rates, are cooler than dry seasons.

Maximum litterfall rates (leaves, twigs, and fruits) were observed shortly after the onset of the dry season in August and September [Figure 2.8, *Rice et al.*, 2004]. Tropical forest litter typically has a short turnover time (less than 1 year [*Brown and Lugo*, 1982]), but during the dry season, following the peak input of litter, moisture levels are low in soil and litter. Hence, ecosystem respiration rates remain low, even though substrate abundance, temperatures, and canopy metabolic rates were highest in the dry season.

| | $\bar{T}_{daily\max}$ (°C) | $\sum P$ (mm) | $\bar{T}_{daily\max}$ & $\sum P$ | Best Model |
|---------------------|----------------------------|---------------|----------------------------------|---|
| Hourly time scale | - | - | - | - |
| Daily time scale | 0.05 | - | - | - |
| Weekly time scale | 0.12 | 0.06 | - | - |
| 14-day time scale | 0.29 | 0.24 | 0.32 | $R = 22.9 - 0.51 * T_{\max} + 0.05 * P$ |
| 21-day time scale | 0.45 | 0.32 | 0.47 | $R = 25.1 - 0.58 * T_{\max} + 0.03 * P$ |
| Monthly time scale | 0.67 | 0.54 | 0.72 | $R = 26.1 - 0.62 * T_{\max} + 0.03 * P$ |
| Seasonal time scale | 0.92 | 0.45 | 0.92 | $R = 39.9 - 1.1 * T_{\max}$ |

Table 2.4: Summary of explained variance (R^2) and best regression equations used to estimate ecosystem respiration (R) as a function of mean daily maximum temperature (T , °C) and cumulative precipitation (P , mm).

Chambers et al. [2004] estimated the mean ecosystem respiration rate to be $7.8 \mu\text{mol m}^{-2} \text{s}^{-1}$ at a site near Manaus, Brazil by measuring individual components of ecosystem respiration, compared to $8.4 \mu\text{mol m}^{-2} \text{s}^{-1}$ (7.5 – 9.4 95% CI) using eddy covariance method at that site. Using chamber-based methods, *Chambers et al.* [2004] estimated a mean soil respiration rate of $3.2 \mu\text{mol m}^{-2} \text{s}^{-1}$ at the Manaus site and reported that both soil respiration and total ecosystem respiration declined with increasing soil moisture, opposite to our observations. *Chambers et al.* [2004] speculated inadequate oxygen supplies in saturated soils led to lower respiration rates. Soil respiration measured at the TNF [*Varner et al.*, 2007] averaged $2.63 \mu\text{mol m}^{-2} \text{s}^{-1}$ annually and 2.91 and $2.29 \mu\text{mol m}^{-2} \text{s}^{-1}$ for the wet and dry seasons, respectively, and showed an increase with precipitation and a negative correlation with temperature, in harmony with our data for total ecosystem R . Thus, R at these two sites showed opposite seasonality, peaking during the wet season at the TNF but in the dry season at Manaus.

It is not known why these sites exhibit different seasonality in respiration. The TNF has much more coarse woody debris (CWD; $48 \pm 5.2 \text{ Mg C ha}^{-1}$; *Rice et al.*, 2004, *Santoni et*

al., 2007) than in Manaus (10.5 Mg C ha⁻¹, *Chambers et al.*, 2000; 15.7 ± 4.1 Mg C ha⁻¹, *Nascimento and Laurance* 2004, assuming that 1 kg dry biomass = 0.5 kg C biomass). In the TNF, CWD respiration was estimated to be a very significant component of the overall respiration budget contributing 1.2 ± 0.3 μmol m⁻² s⁻¹ (see *Hutyra et al.*, 2007 for a full breakdown of the TNF respiration budget). In contrast, CWD respiration estimates from Manuas are significantly smaller, contributing only ~0.50 μmol m⁻² s⁻¹ [*Chambers et al.*, 2004]. Seasonal patterns of CWD respiration are very poorly quantified for the tropics, but it is possible that the moisture and temperature responses of CWD respiration could differ significantly from soil R. The combination of a longer dry season and a larger stock of CWD at the TNF may contribute to changes in CWD respiration and help explain the seasonal differences versus Manaus. It is also possible that a different moisture optimum exists in Manaus due to the shorter dry season and greater annual rainfall. Further, topographic and soil differences between the Manaus and TNF sites are likely to also contribute to the opposite seasonal respiration patterns. The Manuas study site is located within an area of undulating topography with often inundated soils in the low-lying areas [*Araujo et al.*, 2002] while the TNF has very little topographic variation, no soil inundation, and an extremely deep water table. The physical reason for the seasonal differences in respiration remains an open question in need further research.

2.5.4 Is forest growth water limited?

Seasonal water limitations have the potential to reduce forest growth and place the forest at risk for fire. Future climate scenarios suggest that temperatures in the Amazon may increase while precipitation decreases [*Fung et al.*, 2005], likely decreasing water

availability and increasing drought and flammability. To assess the current sensitivity of this forest to water limitations we looked at the patterns in water flux, seasonal evaporative balances, water-use efficiencies, and light-use efficiency.

ET rates consistently increased at the start of the dry season and remained elevated throughout the period of maximum radiation inputs (Figures 2.2 and 2.3). Water losses consistently exceeded inputs during the dry season, large stores of water are evidently accessible to the trees. In the case of 2002, approximately 225 mm of water was withdrawn from storage during the dry season. If we adapt as representative the plant available water profile measured in a similar soil by *Nepstad et al.* [1994], the forest had to extract water from depths in excess of 4 m to support the observed dry season ET rates. The higher ET rates and the nearly inelastic total ET in the dry season are both strong indicators of adequate water availability at the TNF with the current climate.

Ecosystem water-use efficiency (WUE) can be defined as the ratio of GPP to F_{H_2O} (carbon uptake/water loss). Elevated values of WUE could indicate water stress as the scarce resource (water) is conserved. But, the mean observed WUE was 4.5 and 3.7 $\mu\text{mol CO}_2 / \text{mmol H}_2\text{O}$ for the wet and dry season, respectively, showing the opposite trend. Although this result is consistent with this ecosystem not experiencing seasonal water stress, it must be interpreted cautiously. Changes in the WUE can result from a change in either the canopy carbon uptake or F_{H_2O} . As the dry season approached, F_{H_2O} and the vapor pressure deficit started to increase while the GPP started to decrease, resulting in a

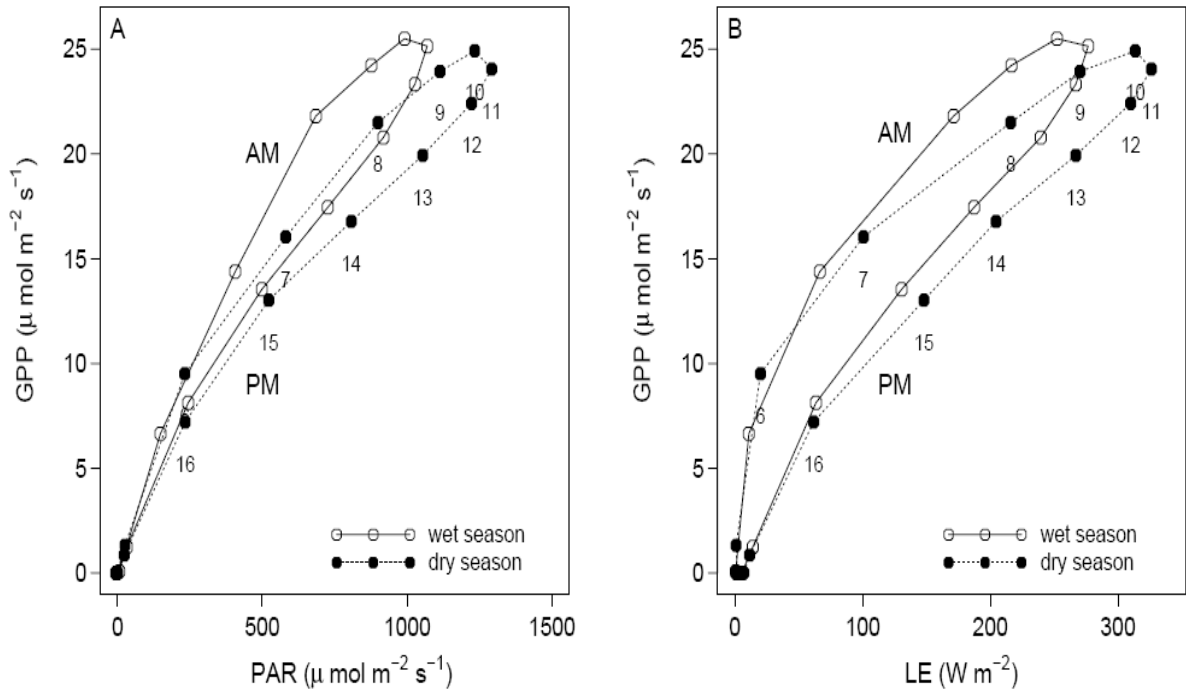


Figure 2.9: (a) Diel cycles of gross primary production (GPP) as a function of photosynthetically active radiation (PAR) for the wet (open circles) and dry (closed circles) seasons. (b) Diel cycle of GPP as a function of latent heat flux (LE) for the wet (open circles) and dry (closed circles) seasons. The numbers along the curve indicate the local time.

lower overall dry season WUE. The WUE started to increase again in October when canopy carbon uptake increased, while the $F_{\text{H}_2\text{O}}$ remained high (Table 2.2 and Table 2.3).

Both light-use efficiency (LUE) and WUE were significantly higher in the morning than afternoon (Figure 2.9). The diel patterns in the LUE and WUE are consistent with afternoon GPP being inhibited. The standard paradigm is that as VPD increases, plant water stress will increase and stomatal conductance will decrease, resulting in higher WUE and lower LE and LUE. However, at this site the LE remains high in the afternoon (Figure 2.2) and the overall evaporative fraction increased along with VPD, likely indicating abundant water supplies. The fraction of water lost through transpiration may

change diurnally, but the LE measurements can not be readily separated into the component processes. It is possible that the apparent afternoon reductions in GPP were due to differences in autotrophic respiration rates, but the analysis of light-curve intercepts (Appendix A, figure A.5) does not support that interpretation. The morning and afternoon differences in WUE and LUE are more likely due to limitation on stem conductance, plant circadian rhythms [*Doughty et al.*, 2006], metabolic cycles (e.g. respiration associated with sugar transport), or enzymatic limitations.

2.6 Summary & Conclusions

In this study we critically assessed flux measurements of CO₂ and H₂O and examined energy closure to ensure the validity of the observations, then we examined the controls on carbon and water exchange in an evergreen tropical rainforest. We found no significant signs of water limitation on photosynthesis: trees had adequate water supplies throughout the 5 month dry season. ET responded strongly to radiative drivers year-round and was insensitive to dry season precipitation totals. Observed dry season evaporative losses significantly exceeded precipitation inputs, drawing up to 225 mm of water from water reserves that had to extend many meters in depth. Evidently the annual input of precipitation and the capacity of the plants to use stored water over considerable depth provides the key to maintaining this closed canopy equatorial forest despite long periods of low rainfall.

We found that the seasonal course of canopy photosynthesis was largely controlled by phenology and light. Canopy photosynthetic efficiency declined before leaf senescence (late wet season) and increased after new leaf elongation (mid-dry season).

Unfortunately, the EVI parameter did not capture this pattern. Phenological control of the timing of peak carbon uptake capacity (P_c) again highlights adequate water availability and suggests that the assemblage of trees in this forest may have been selected to optimize for light, not water. The dominant influence of phenology versus water stress is a significant surprise for this forest.

Climate anomalies exerted a strong influence on net carbon exchange, principally through effects on R . Ecosystem R was lower during the dry season due to moisture limitations on heterotrophic respiration as evidenced by enhanced dry season GPP and P_c rates. We did not find a significant relationship between temperature and R on short timescales. The lack of temperature dependence raises uncertainty about the appropriateness of using Q-10 type relationships in ecosystem models of tropical rainforests. The largest variations in R , photosynthesis, and net carbon exchange were observed during the dry-to-wet season transition.

This forest currently does not exhibit signs of water limitations, with enough water to satisfy growth requirements. It was a small overall carbon source to the atmosphere, with the efflux rate declining over the period of study, consistent with the long-term ecosystem disturbance and recovery dynamics as proposed by *Rice et al.* [2004] and with the large contribution of CWD respiration to the observed high rates of respiratory carbon losses.

Live biomass stocks have increased significantly over the study period while CWD stocks have decreased [*Santoni et al*, 2007].

If precipitation rates were to decrease by a small amount, but water supplies remained adequate for the trees, it is possible that the net carbon uptake could increase due to higher insolation and slower heterotrophic respiration. However, a reduction in decomposition from drier conditions could result in increased flammability due to a build up of fuel. Alternatively, if the amount of available water for the trees were to decrease through logging (causing soil compaction), higher temperatures (increasing the evaporative demands), or large decreases in precipitation (slowing recharge of deep water reservoirs) the flammability of this forest might increase and the forest may convert to a fire adapted vegetation type. Accurate predictions of future climate and land-use changes require capturing these critical dependencies on precipitation and on ecosystem structure and function.

2.7 Acknowledgments

Thanks to David Fitzjarrald and the SUNY Albany team for providing weather station data which was critical for gap filling. The authors would like to thank Paul Moorcroft and Michael Keller's entire team for insightful comments and suggestions throughout this project. We thank Elizabeth Hammond-Pyle, Amy Rice, Alfram Bright, John Budney, and Daniel Curran for their engineering and field assistance; Bethany Reed, Lisa Merry, Dan Hodgkinson, Fernando Alves Leao and the staff of the LBA Santarem office for their extensive logistical and field assistance. Finally, we also thank the two anonymous reviewers whose useful comments improved the clarity of this paper. This work was supported by grants NASA NCC5-341 and NASA NCC5-684 to Harvard University.

Chapter 3: Resolving systematic errors in estimates of net ecosystem exchange of CO₂ and ecosystem respiration in a tall-stature forest: application to a tropical forest biome

Lucy R. Hutyra, J. William Munger, Elizabeth Hammond-Pyle, Scott R. Saleska, Natalia Restrepo-Coupe, Plinio B. de Camargo, Steven C. Wofsy, Resolving systematic errors in estimates of net ecosystem exchange of CO₂ and ecosystem respiration in a tall-stature forest: application to a tropical forest biome, *Agricultural and Forest Meteorology*, in review.

3.1 Abstract

The controls on tropical rainforest CO₂ exchange and the likely future responses to a changing climate are among the largest uncertainties in global climate change models. Eddy-covariance measurements potentially provide detailed data on CO₂ exchange in these forests, but accurate estimates of the net ecosystem exchange of CO₂ (NEE) and ecosystem respiration (R) require careful analysis of data representativity and treatment of data gaps. This study discusses the biases in NEE and R potentially associated with two sources of systematic error in eddy-covariance data, lost nighttime flux and missing canopy storage measurements, and we propose robust approaches to correct for these biases. Multiple independent estimates for the net carbon balance and ecosystem respiration are presented to validate the analyses, including a carefully constructed bottom-up budget for respiration and extrapolation of daytime data to zero light. We found that lost nocturnal flux can produce a significant bias and, where appropriate, a site-specific u^* threshold should be evaluated to avoid systematic bias in estimates of carbon exchange. The inclusion of canopy storage is essential to accurate assessments of net carbon exchange, due to day-night asymmetry in storage and turbulence. We found that short-term measurements of storage may be adequate to accurately model storage for use in obtaining ecosystem carbon balance. The analytical framework utilized in this study could be applied to any eddy-covariance site for validation of methodological techniques.

3.2 Introduction

Tropical rainforests contain large stores of biomass and rapidly cycle carbon through photosynthesis and respiration, giving them significant leverage on the global carbon cycle and rate of atmospheric CO₂ increase. Determining the net carbon balance in tropical rainforests is critical for quantifying the global carbon cycle, to understand the component processes of ecosystem respiration (R) and photosynthesis, and to define responses to environmental conditions.

Current research has not adequately constrained the magnitude, or even the sign, of the net carbon balance of tropical rainforests. Plot-level biometric measurements in undisturbed tropical rainforests have observed both significant carbon uptake [*Phillips et al.*, 1998; *Baker et al.*, 2004] and carbon emission [*Rice et al.*, 2004; *Miller et al.*, 2004]. Analysis of eddy-covariance measurements in the Amazon, which integrate carbon exchange over several square kilometers, have similarly observed a range of NEE in primary forest sites from net uptake [*Grace et al.*, 1995; *Malhi et al.*, 1998], neutral [*Miller et al.*, 2004], to small net release of carbon to the atmosphere [*Hutyra et al.*, 2007; *Saleska et al.*, 2003].

Many modeling studies have predicted net uptake of CO₂ in the wet season and emission in the dry season, driven by temperature and water effects on respiration and photosynthesis (respectively), but the opposite seasonality in NEE has been observed at some tropical forests [*Saleska et al.*, 2003; *Goulden et al.*, 2004]. The same models

predict divergent future scenarios in a changed climate, including collapse of the Amazon forest [Cox *et al.*, 2000] and possible feedbacks between warming, reduced forest cover, and increased aridity [Oyama and Nobre, 2003; Hutyra *et al.*, 2005].

Photosynthesis and its response to primary drivers (temperature and light) are relatively well understood at the leaf level and in environmental chambers [Farquhar, 1982].

However, given the significant variability in vertical and horizontal light interception within tropical ecosystem, it is a significant challenge to scale up leaf level results to the entire forest canopy. Ecosystem respiration (R) is a less understood process integrating both aboveground and belowground plant and microbial processes, each responding differently to environmental drivers [Davidson *et al.*, 2006].

Measurements from flux towers are a powerful tool for understanding the exchange of CO₂ between the atmosphere and biosphere. The eddy-covariance technique has been particularly useful for making direct, long-term measurements of CO₂ exchange in forests [e.g. Wofsy *et al.*, 1993; Urbanski *et al.*, 2007]. Observed NEE (the sum of eddy-covariance flux and changes in canopy CO₂ storage) represents the small residual difference between carbon uptake by photosynthesis and carbon loss through respiration.

During the daytime hours, NEE measures the combination of photosynthesis and autotrophic (roots, stem, leaves) and heterotrophic (microorganisms) respiration. In the nighttime, NEE represents ecosystem respiration since photosynthesis is zero. However, calm atmospheric conditions complicate the interpretation of nighttime fluxes, with

potentially significant affects on the computed ecosystem carbon budget. Estimates of integrated annual carbon balance may vary by several $\text{Mg C ha}^{-1} \text{ year}^{-1}$ depending on the treatment of flux measurements made under calm conditions [Miller *et al.*, 2004]. Stable atmospheric conditions at night are particularly problematic. The consequent carbon-balance problem is particularly large in the tropics, because the fluxes are large throughout the year and constitute a larger fraction of the overall observations, relative to temperate zones.

Eddy-covariance methods fail to measure NEE when turbulence is absent. Canopy storage, the change in average concentration below the eddy sensor, in principle should account for respiratory CO_2 that is not transported from the canopy by turbulent exchange, but in practice, some CO_2 flux is 'lost' from the system by transport processes that can not be measured at a single point. To complicate the problem further, canopy storage measurements are unavailable for long time periods at many flux towers in the Amazon [*c.f.* Iwata *et al.*, 2005], making the assessment of NEE in Amazonian rainforests particularly challenging and error prone. Very few studies of NEE have integrated across multiple years of data, or combined independent datasets, to link NEE to climate or to constrain the models of Amazonian carbon balance at regional scales.

Biometric observations provide another view of ecosystem carbon dynamics. Repeated measurement of forest structure (biomass, growth, mortality, recruitment) document changes in carbon stocks. They have the potential to elucidate the ecological mechanisms controlling longer term (years to decades) ecosystem carbon balance.

Biometric data can also provide an important independent check on flux tower measurements on the time scale of several years [Barford *et al.*, 2001; Saleska *et al.*, 2003]. Finer scale measurements of respiration (soil, coarse woody debris, etc.) can quantify the efflux rates for different forest components and provide an independent estimate of ecosystem respiration, to check estimates of R based on eddy-covariance data.

In this paper we scrutinize four years of high quality eddy-covariance and ground-based measurements in order to constrain measurements of NEE and ecosystem respiration at a Central Amazonian forest site. We demonstrate that not all methods of calculating NEE and R from flux data are equally plausible by using independent validation methods and conducting meticulous error analyses. Detailed bottom-up budgets for both ecosystem respiration and for net forest carbon balance are presented using repeated measurements and multiple datasets. We discuss the biases associated with lost nighttime flux and missing storage measurements that need to be considered at all flux tower sites. Finally, we propose a robust correction method for determining carbon balance in the absence of storage data and outline a validation framework for eddy-covariance results.

3.3 Methods

3.3.1 Site description

This study was part of the Brazilian-led Large-Scale Biosphere-Atmosphere Experiment in Amazonia (LBA-ECO). Measurements were made at a site in the Tapajós National Forest (TNF; 54°58'W, 2°51'S, Pará, Brazil) near km 67 of the Santarém-Cuiabá

highway (BR-163), in an area of largely contiguous forest extending for tens of kilometers to the north and south, ~ 6 km west of the BR-163 highway and ~ 6 km east of the Tapajós River. The forest is on flat terrain and has a closed canopy with a mean height of approximately 40 m. This forest can be classified as ‘old-growth’ with abundant large logs, numerous epiphytes, an uneven age distribution, and emergent trees [Clark, 1996]. The area averages a 5 month dry season, extending from approximately July 15 – December 15. See *Hutyra et al.* [2007] and *Rice et al.* [2004] for additional local site information and *Santoni et al.* [2007] for a regional analysis including the TNF.

3.3.2 Ground-based Measurements

Ground-based biomass inventories directly measure aboveground carbon stocks. Net aboveground carbon balance can therefore be determined through repeated surveys. Four permanent 50 x 1000 m biometry transects were established in 1999 adjacent to the eddy covariance tower along the prevailing wind directions (within the fetch of the tower). All live trees ≥ 35 cm dbh (diameter at breast height) were surveyed across 19.75 ha and trees ≥ 10 cm dbh were surveyed across 4.99 ha (a 10 m swath within four 1 km linear transects) in 1999, 2001, and 2005. Estimates of aboveground, whole tree biomass were calculated based on diameter measurements using the allometric relationships reported in *Chambers et al.* [2001]. Annual tree mortality and recruitment rates were estimated through multiple surveys [Rice et al., 2004].

Stocks of coarse woody debris (CWD) were surveyed using plot-based methods in 2001 [Rice *et al.*, 2004] and partially resurveyed in 2006. CWD respiration was estimated based on first-order kinetics,

$$CWD R = k x (\text{total CWD stock}). \quad (3.1)$$

An unbiased estimate of the mean k , assuming a normal distribution, was approximated by

$$\bar{k} = \exp\left(-4.117\rho + 0.5*[0.62\rho]^2\right) \quad (3.2)$$

where ρ (g cm^{-3}) is the wood density [Rice *et al.*, 2004; Chambers *et al.*, 2001; Gut, 1995]. Based on local measurements by Keller *et al.* [2005], a mean CWD density of 0.52 g cm^{-3} and a mean k of 0.124 yr^{-1} were used for respiration estimates. We modeled changes in CWD stocks and respiration from 2001 – 2006 by accounting for additional inputs and losses such that

$$CWD_i = CWD_{i-1} + \text{mortality input} - CWD R. \quad (3.3)$$

The distribution of CWD density and the mean mortality rates between 2001 and 2006 were assumed unchanged from the complete CWD survey in 2001 and the vegetation surveys in 2001 and 2005, respectively. Error estimates for the modeled CWD stock and respiration rates were obtained using bootstrap analysis [Efron and Tibshirani, 1997]. Complete descriptions of our biometric measurement methods, plot design, and early results are provided in Rice *et al.* [2004] and in a forthcoming paper by Santoni *et al.* [2007].

Soil CO₂ fluxes were measured at the km 67 tower site using dynamic, open chambers from March 18, 2001 to September 18, 2004 [Keller *et al.*, 2005]. Fluxes were calculated from the linear increase of concentration versus time adjusted for the ratio of chamber volume to area and the air density within the chamber. A full description of soil respiration measurement protocols is given in Keller *et al.* [2005].

Stem respiration data were obtained from Nepstad *et al.* [2002] based on measurements at the control plot of the ‘Seca Floresta’ experiment located approximately 5 km from the km 67 tower site at 2°54’ S, 54°57’ W. Stem respiration measurements were made on twenty individual trees in February, April, July, and October of 2004. Based on the relationship between tree diameter and total tree stem surface area reported in Chambers *et al.* [2004] and plot-based measurements of basal area, the respiration measurements were converted from m² stem area to m² ground area as follows:

$$\mu\text{mol} / \text{m}_g^2 / \text{s} = \mu\text{mol} / \text{m}_s^2 / \text{s} \times \frac{\text{tree.stem.index}(\text{m}^2)}{\text{tree.basal.area}(\text{m}^2)} \times \frac{\text{mean.basal.area}(\text{m}^2)}{\text{sample.area}(\text{m}^2)} \quad (3.4)$$

where m_g^2 is ground area, m_s^2 is stem area, the mean tree stem per tree basal area was 1.55 m² m⁻² [based on relationships reported in Chambers *et al.*, 2004], and the overall mean basal area per sample area was 0.0022 m² m⁻².

3.3.3 Eddy-covariance measurements

We used the eddy-covariance method to measure the CO₂ exchange between the forest and the atmosphere from January 2002 – January 2006. NEE was calculated every hour

as the sum of turbulent flux of CO₂ at 57.8 m and the change in canopy CO₂ storage in the column below [Wofsy *et al.*, 1993]. A 3-axis sonic anemometer (CSAT-3, Campbell Scientific, Logan UT) and a closed-path infrared gas analyzer (IRGA, LI-6262, Licor, Lincoln, NE) were used to measure the turbulent flux of CO₂ with a sample rate of 8 Hz. The vertical coordinate for wind velocities is positive upward, thus positive values for fluxes denote emission and negative values denote uptake. A profile system measured canopy concentration of CO₂ at eight levels throughout the canopy in sequence (2 minutes at each level). The profile measurements were used to estimate the change in the column average CO₂ mass between the ground and flux measurement height, to calculate the column average rate of change of CO₂ storage. In the case of canopy CO₂ storage, positive values indicate accumulation while negative values denote venting, thus NEE = flux + canopy storage. Full descriptions of the instrumentation, experimental design and data processing are given by *Hutyra et al.* [2007].

The storage and CO₂ flux measurements at this site provide evidence of ‘lost flux’ under calm conditions at night [see *Hutyra et al.*, 2007], with approximately 57% of the nighttime hours at this site being classified as calm ($u_* < 0.22 \text{ m s}^{-1}$). We corrected for lost flux by filtering out calm night periods and replacing the data with the mean value for proximate well-mixed time periods. The ‘best estimates’ of mean NEE and R were obtained during well-mixed periods. Data filling was then employed to obtain a continuous time series as needed for annual budgets, see *Hutyra et al.* [2007] for details of the filling algorithms. The 95% confidence intervals for the flux measurements were calculated by bootstrapping the error distributions during similar (*e.g.* season, hour, PAR

level) time periods [Richardson *et al.*, 2005]. Unless noted otherwise, all parenthetically reported errors are 95% confidence intervals.

3.3.4 Canopy CO₂ storage models

We tested two separate models for canopy CO₂ storage, to be used when direct measurements were unavailable. The first model was a simple diel storage model, S_d , based on the observed, mean hourly storage values from four years of profile storage measurements,

$$S_{d,i} = \bar{S}_i \text{ for } i = 1, 2, 3, \dots, 24 \quad (3.5)$$

where \bar{S}_i is the hourly mean storage at the i^{th} hour. The second storage model was proposed by *Iwata et al.* [2005] who estimated the total nighttime storage accumulation, S_c , from

$$S_c = a_1 + a_2 u_{*w} \quad (3.6)$$

where u_{*w} is a time-weighted friction velocity, such that

$$u_* = \sqrt{-1^* \langle w'u' \rangle}, \quad (3.7)$$

$$u_{*w} = \frac{\sum_{n=1}^{12} u_{*n} n}{\sum_{n=1}^{12} n}, \quad (3.8)$$

and a_1 and a_2 are empirical coefficients derived from periods when storage values were recorded. Daytime hourly storage, S_{ci} , was then estimated using a linear model,

$$S_{ci} = a_i S_c \text{ for } i = 1, 2, 3, \dots, 12 \quad (3.9)$$

where S_{ci} is the hourly daytime storage at the i^{th} hour, a_i is an hourly fitted parameter, and S_c is the modeled total CO_2 accumulation from the preceding night (equation 3.6). We denote the combination of *Iwata et al.* [2005] S_c and S_{ci} models as S_I . We forced both the S_I and the S_d models to have a zero mean storage over five day intervals to maintain physical realism, although this feature was apparently not included in the original formulation introduced by *Iwata et al.* [2005].

3.4 Results

3.4.1 Ground-based measurements

3.4.1.1 Respiration

The major components of ecosystem R include soil (litter, root, and microbial), stem, CWD, and leaf respiration. A bottom-up budget of total ecosystem R, based on measurements between 2000 and 2006, is shown in Figure 3.1, panel A.

Soil respiration, measured by *Keller et al.* [2005] at the TNF site, averaged $2.76 \pm 0.06 \mu\text{mol m}^{-2} \text{s}^{-1}$. The mean stem respiration measured by *Nepstad et al.* [2002] in the TNF averaged $0.62 \pm 0.08 \mu\text{mol m}_s^{-2} \text{s}^{-1}$ in stem area and $1.0 \pm 0.12 \mu\text{mol m}_g^{-2} \text{s}^{-1}$ relative to ground area. Local measurements of leaf respiration were not available. For budgeting purposes, we used the mean observed leaf respiration value of $2.59 \mu\text{mol m}_g^{-2} \text{s}^{-1}$ reported by *Chambers et al.* [2004] from a primary Amazonian forest site near Manaus, Brazil. No adjustments for possible differences in leaf area index (LAI) were considered since the LAI reported by *Chambers et al.* [2004] and the local observed LAI are very similar,

Estimates of ecosystem respiration

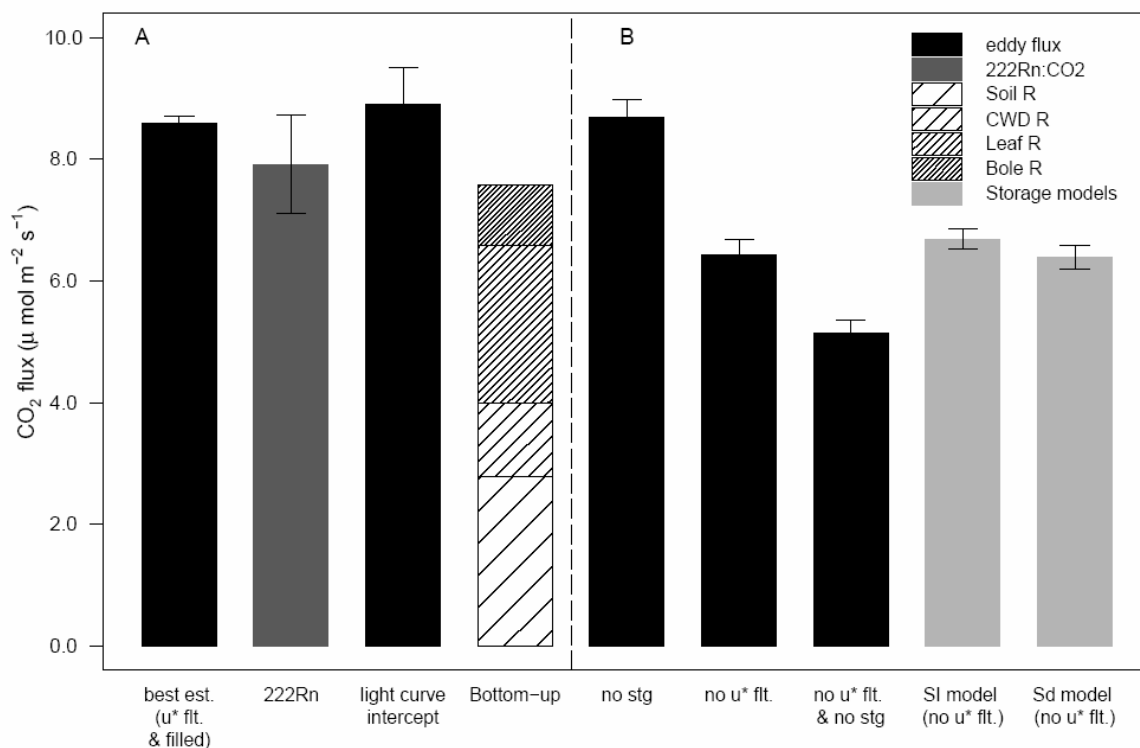


Figure 3.1: A.) Independent estimates of annual ecosystem Respiration. The ‘best estimate’ is based on four years of u_* filtered, gap filled nighttime flux measurements. The ^{222}Rn estimate is derived based on similarity to CO_2 flux [Martens et al., 2004]. The light curve intercept value is based on the fit between daytime PAR and NEE (no u_* filter). The bottom-up estimate includes the major components of the forest respiration budget (the sum is a lower bounds estimate on total respiration). B.) Alternative estimate of ecosystem R based on (1) exclusion of storage (flux only, u_* filter applied); (2) no u_* filtering (flux + measured storage); (3) flux only (no storage and no u_* filter); (4) measured CO_2 flux and storage as represented by the S_I and S_d storage models. The ‘best estimate’, ^{222}Rn , light curve intercept, bottom-up, and flux only (u_* filtered) respiration estimates agree within the error bounds.

4.7 and 4.5 $\text{m}^2 \text{m}^{-2}$ [Domingues et al., 2005], respectively. Temperature at the Manaus site was also similar in both the diurnal and seasonal patterns to the local observations [Malhi et al., 2002; Hutrya et al., 2007].

The mean CWD pool in July of 2001 at the TNF was $48 \pm 5.2 \text{ Mg C ha}^{-1}$ with a mean respiration rate of approximately $1.6 \pm 0.3 \mu\text{mol m}_g^{-2} \text{ s}^{-1}$ [Rice et al., 2004]. Additional

inputs to the CWD pool were estimated through repeated mortality surveys in 2001 and 2005. In the survey intervals of 1999 – 2001 and 2001 – 2005 the mean observed mortality was 2.4 ± 0.50 and 3.0 ± 0.44 Mg C ha⁻¹ yr⁻¹, respectively. Based on these CWD inputs and the site-specific decay rate constant (equation 3) we estimated a CWD pool of 37 ± 3.1 Mg C ha⁻¹ in July 2006, representing a ~23 % reduction in stock from the 2001 CWD pool. Based on the projected changes in CWD stock, the mean respiration rate was 1.2 ± 0.3 $\mu\text{mol } m_g^{-2} \text{ s}^{-1}$ (2001-2006). A partial resurvey of the CWD plots (diameter > 30 cm) in July 2006 found that the stock of large CWD was reduced by 22%, from 25.8 ± 4.2 to 20.2 ± 4.6 Mg C ha⁻¹. This partial resurvey CWD is in very good agreement with the estimated loss of total CWD and supports the modeled total CWD respiration rates for 2006.

Combining the respiration estimates for the individual components, our best bottom-up estimate for mean ecosystem R was $7.6 \mu\text{mol } m_g^{-2} \text{ s}^{-1}$. In one of the few other attempts to estimate ecosystem R using bottom-up methods in the Amazon, *Chambers et al.* [2004] reported a mean R of $7.8 \mu\text{mol } m_g^{-2} \text{ s}^{-1}$ for a primary forest near Manaus, Brazil.

However, our local, bottom-up estimate should be considered a lower bound on respiration since it does not include any contribution from the large amount of respiring organic material stored aboveground (e.g. rotting tree cores, termite nests, decomposition of suspended leaf litter, etc.). The components of the respiration budget included in this analysis are the largest in magnitude [*Chambers et al.*, 2004] and most amenable to direct measurement and scaling. Some of the terms in the respiration budget are known to have significant seasonal variations and deviations from steady state that can not be accounted

for in this budgeting exercise. A meaningful confidence interval could not be calculated for the bottom-up respiration estimate due to the compilation of wide array of data sets including published data without reported error estimates.

3.4.1.2 Net Carbon fluxes

To assess the net carbon balance in the TNF from the bottom-up, we repeatedly surveyed almost 3000 trees in 1999, 2001, and 2005. Between 2001 and 2005, the time interval which most closely overlaps with the eddy-covariance time series, the mean total aboveground biomass was $192 \pm 4.9 \text{ Mg C ha}^{-1}$ (trees with diameters $\geq 10 \text{ cm}$ and CWD $\geq 2 \text{ cm}$), with ~79% alive and 21% dead. The mean aboveground growth, recruitment (in-growth of new individual trees), and mortality rates were 3.2 ± 0.21 , 0.45 ± 0.045 and $3.01 \pm 0.44 \text{ Mg C ha}^{-1} \text{ yr}^{-1}$, respectively. Dividing the live aboveground biomass pool by inputs (growth + recruitment) or the outflow (mortality) gave notably short turnover times, 39 and 48 years, respectively, indicating a very dynamic forest [see *Santoni et al.* [2007] for further discussion].

The net flux in live biomass (growth + recruitment – mortality) was $-0.6 \pm 0.28 \text{ Mg C ha}^{-1} \text{ yr}^{-1}$, representing a small net uptake from the atmosphere. The net flux in dead biomass (mortality inputs – respiration) was $2.2 \pm 0.75 \text{ Mg C ha}^{-1} \text{ yr}^{-1}$, a sizable carbon loss to the atmosphere. The overall mean net carbon flux (net live flux + net dead flux) from this bottom-up budget was therefore $1.5 \pm 0.57 \text{ Mg C ha}^{-1} \text{ yr}^{-1}$ ($0.41 \pm 0.15 \mu\text{mol m}^{-2} \text{ s}^{-1}$, representing carbon loss to the atmosphere), Figure 3.2, panel A. This result confirms the earlier findings of $1.9 \pm 1.0 \text{ Mg C ha}^{-1} \text{ yr}^{-1}$ carbon loss from this site based on the 1999

Estimates of Net Ecosystem Exchange

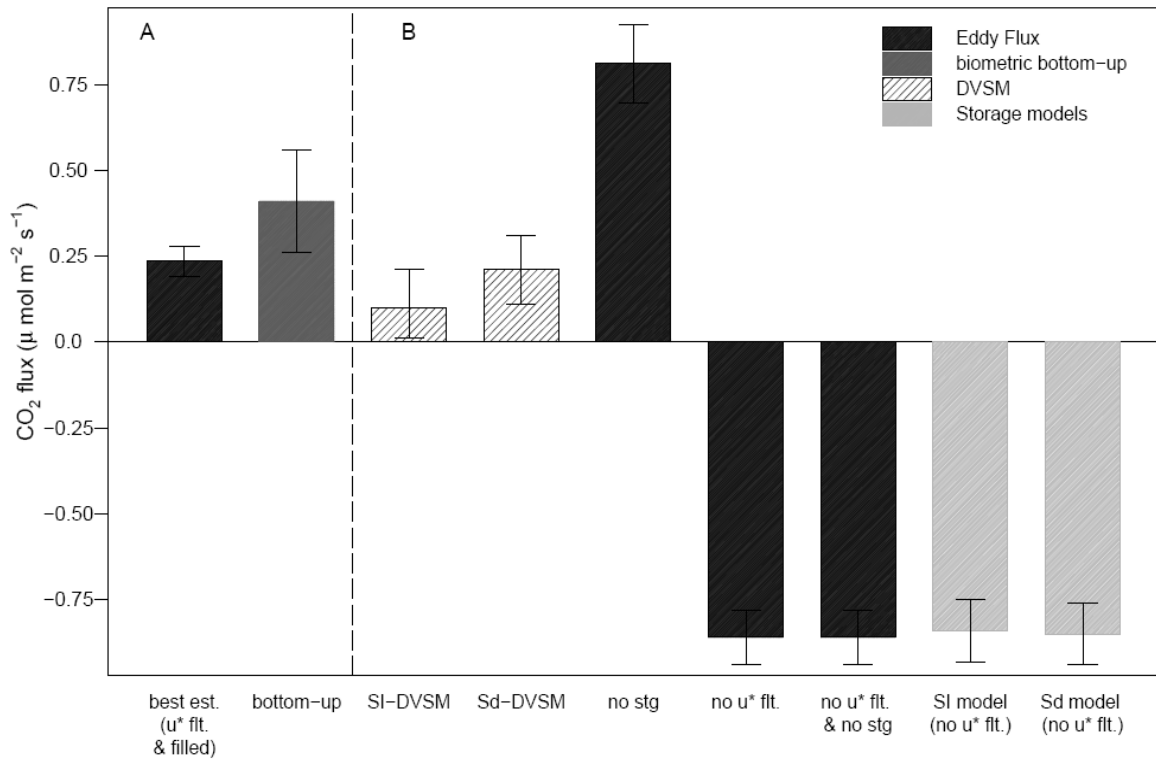


Figure 3.2: A.) Independent estimates of annual net ecosystem exchange (carbon balance) averaged from 2001 – 2005. The ‘best estimate’ is based on u^* filtered, gap filled flux measurements. The bottom-up biometry estimate is the result of repeated biometric surveys of forest structure (growth, recruitment, mortality). B.) Alternative estimates of the net carbon balance based on (1) measured flux and the diurnally varying storage models (S_I); (2) measured flux and the diurnally varying storage models (S_d) (3) exclusion of storage (flux only, u^* filter applied); (4) no u^* filtering (flux + measured storage); (5) flux only (no storage and no u^* filter); (6) measured CO_2 flux and storage as represented by the S_I and S_d storage models. The ‘best estimate’, bottom-up, S_I -DVSM, S_d -DVSM carbon balance estimates all agree within the error bounds.

and 2001 surveys. Further, this result is consistent with the hypothesis, proposed in Rice *et al.* [2004], that this forest is recovering from a prior disturbance. We have observed a decreasing stock of CWD, high growth rates, increasing biomass, and reversal of the sign of the annual NEE measured by eddy-covariance over the four year interval [Hutyra *et al.*, 2007; Santoni *et al.*, 2007; Saleska *et al.*, 2007].

3.4.2 Evidence of lost nighttime flux

As a biological process, nighttime ecosystem respiration should not depend on atmospheric turbulence. Under ideal conditions, the measurements of nighttime NEE (CO₂ flux + storage) would show no relationship with turbulence, but at many forest sites ideal conditions are not met and some flux is lost (Figure 3.3). Hence, measurements of canopy CO₂ storage and flux at the top of the tower are in fact strongly related to the occurrence of turbulence. This is not a surprising result. During periods of weak turbulence, the assumptions of horizontal homogeneity required for eddy-covariance may not be met and horizontal advection can result in ‘lost flux’ [Finnigan, 2004]. Our data confirms a decrease in CO₂ flux and an increase in storage flux under low turbulence nighttime conditions, but there was a pronounced reduction in nighttime NEE when turbulence was less than 0.22 m s⁻¹ (Figure 3.3).

On average, storage fluxes are negative (venting) and CO₂ fluxes are enhanced under windy nighttime conditions ($u_* > 0.3 \text{ m s}^{-1}$). The sum of the two terms appears to have little trend with u_* (Figure 3.3). To correct for the flux lost under low turbulence conditions, a u_* filter ($u_* \leq 0.22 \text{ m s}^{-1}$) was applied to remove periods with an apparent low bias, and data gaps were filled to maintain a complete time series (see *Hutyra et al.* [2007] for further gap filling details and see *Saleska et al.* [2003] and *Hutyra et al.* [2007] for details on the determination of an objective u_* threshold). From January 2002 – January 2006, the mean lost nocturnal flux was 16 kg C ha⁻¹ night⁻¹, approximately 40% of the nocturnal respiration flux (Figure 3.4). Figures 3.1 and 3.2, panels B, also show the bias if no flux correction is made.

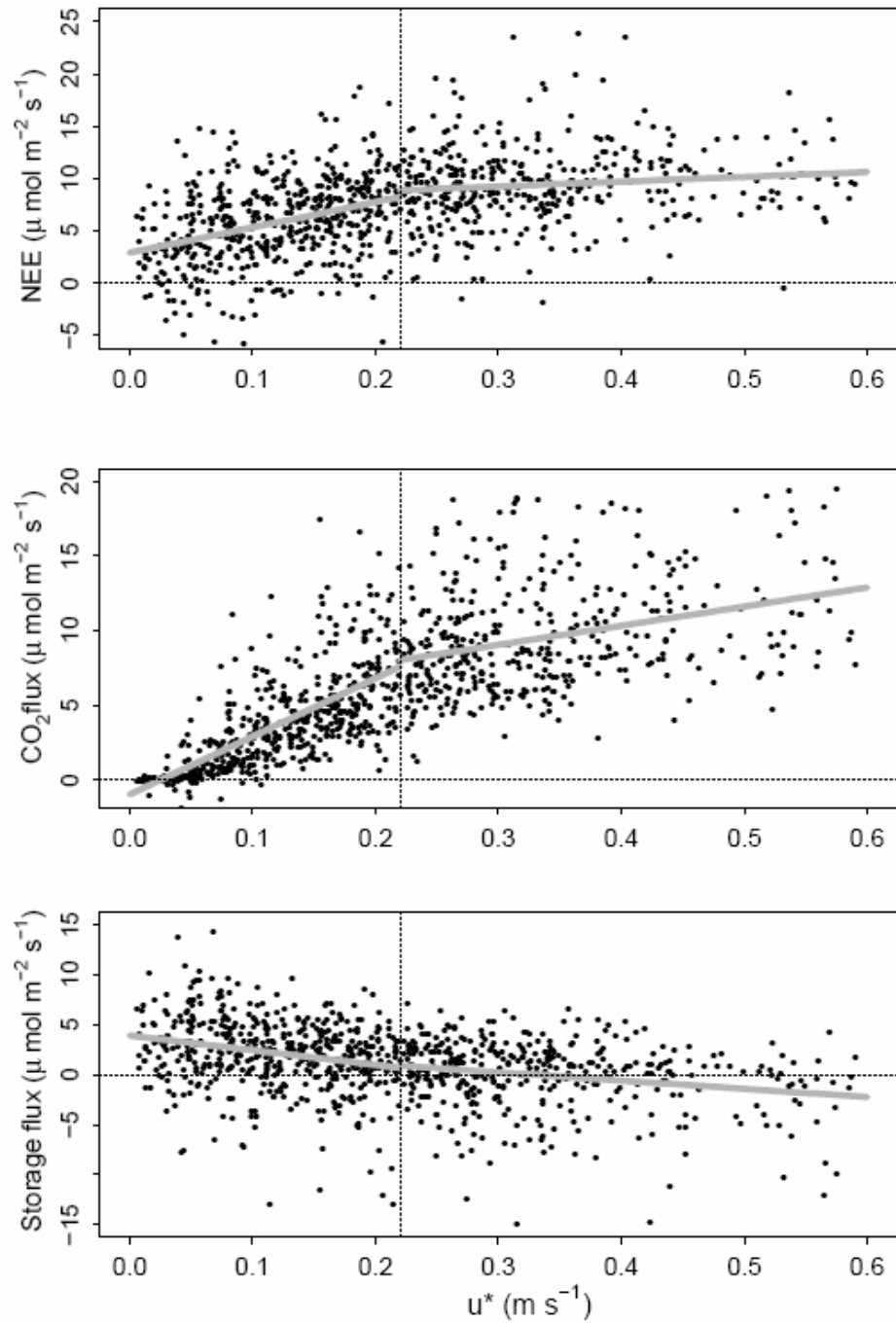


Figure 3.3: A. Nighttime NEE (A) showed evidence of ‘lost flux’ as evidenced by the positive relationship with turbulence under calm conditions ($u^* < 0.22 \text{ m s}^{-1}$). CO_2 flux (B) and canopy storage (C) also showed correlations with turbulence, but some flux was still lost to advection processes. Slope relationships are illustrated using linear regression based on a u^* threshold of 0.22 m s^{-1} .

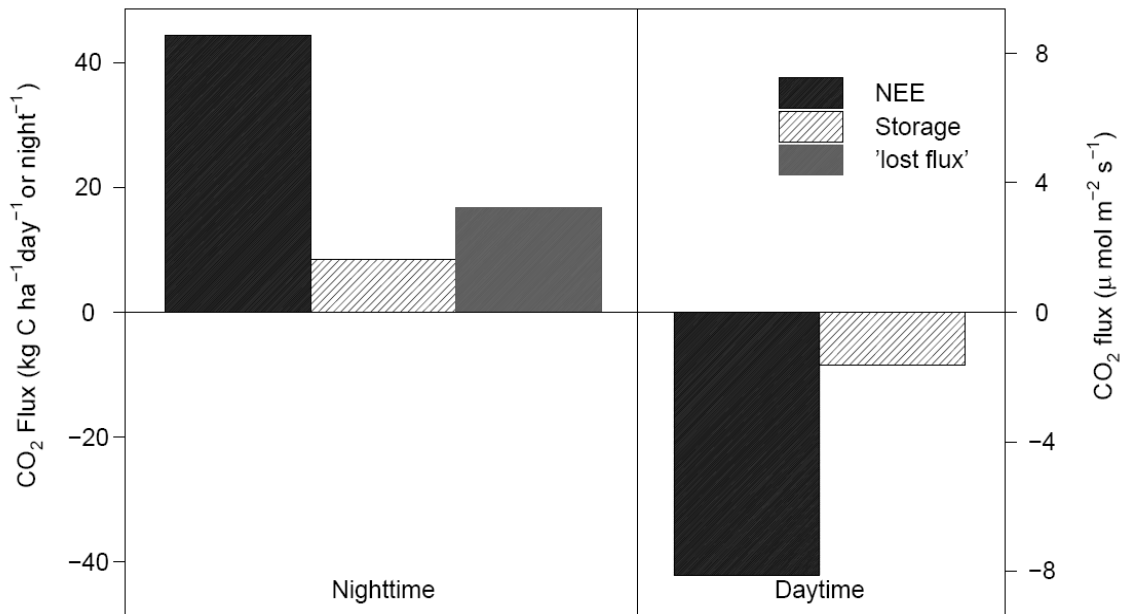


Figure 3.4: Accumulated nighttime (1800 – 0500, LT) and daytime (0600-1700, LT) u_* -corrected NEE, storage and 'lost' nocturnal flux. The mean 24-hour storage fluxes is zero, with $8.4 \text{ kg C ha}^{-2} \text{ night}^{-1}$ accumulating during the nighttime and $-8.4 \text{ kg C ha}^{-2} \text{ daytime}^{-1}$ venting during the daytime. The mean 'lost' nocturnal flux (the difference between u_* -corrected and uncorrected nighttime fluxes) was $16.7 \text{ kg C ha}^{-2} \text{ nighttime}^{-1}$.

3.4.3 Canopy CO₂ storage

Canopy CO₂ storage varies diurnally and as a function of boundary-layer turbulence (Figures 3.5 and 3.6). Figure 3.5 shows the canopy CO₂ concentrations and friction velocity (u_*) for a typical five day period in December 2005. Below the mean canopy height (40 – 45 m), nocturnal build-up of CO₂ approaches 100 ppm when u_* drops to near zero (DOY 340-343, Figure 3.5). During the night of December 9, 2005 (DOY 344) high atmospheric turbulence ($u_* > 0.22 \text{ m s}^{-1}$) resulted in a nearly well-mixed canopy profile and no significant build-up of CO₂. During the daytime well-mixed conditions are prevalent with a significant draw-down in canopy CO₂ concentration resulting from a

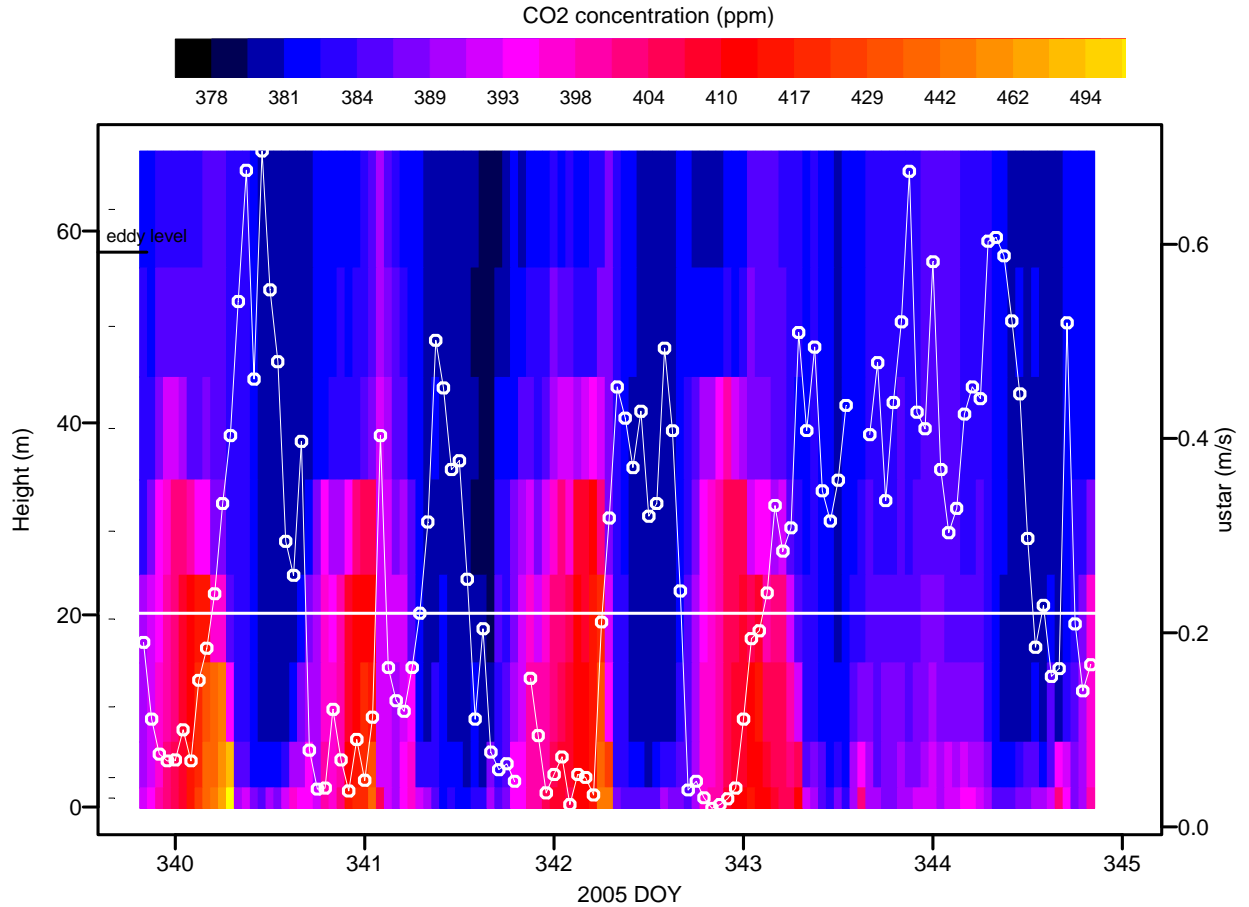


Figure 3.5: Hourly canopy CO_2 profile concentration (ppm) measurements interpolated across 8 measurement heights (62.2, 50.1, 39.4, 28.7, 19.6, 10.4, and 0.9 m) for days of year 340-345 (local time) in 2005. Canopy turbulence (u_* , $m s^{-1}$) is shown in the open circle points. The horizontal line at $0.22 m s^{-1}$ denotes the u_* threshold for data filtering to correct for lost flux. Note that the same time periods are illustrated in Figures 5 and 8, with the high-turbulence night on DOY 344 illustrating the influence of turbulence on canopy CO_2 storage.

combination of mixing with low- CO_2 containing air from aloft and carbon uptake through photosynthesis (Figure 3.5). Turbulence and canopy storage were strongly negatively correlated, with storage lagging turbulence by approximately 1 hour ($R^2 = 0.75$, Figure 3.6). However, as shown in Figure 3.5 conditions can vary substantially from day to day and night to night.

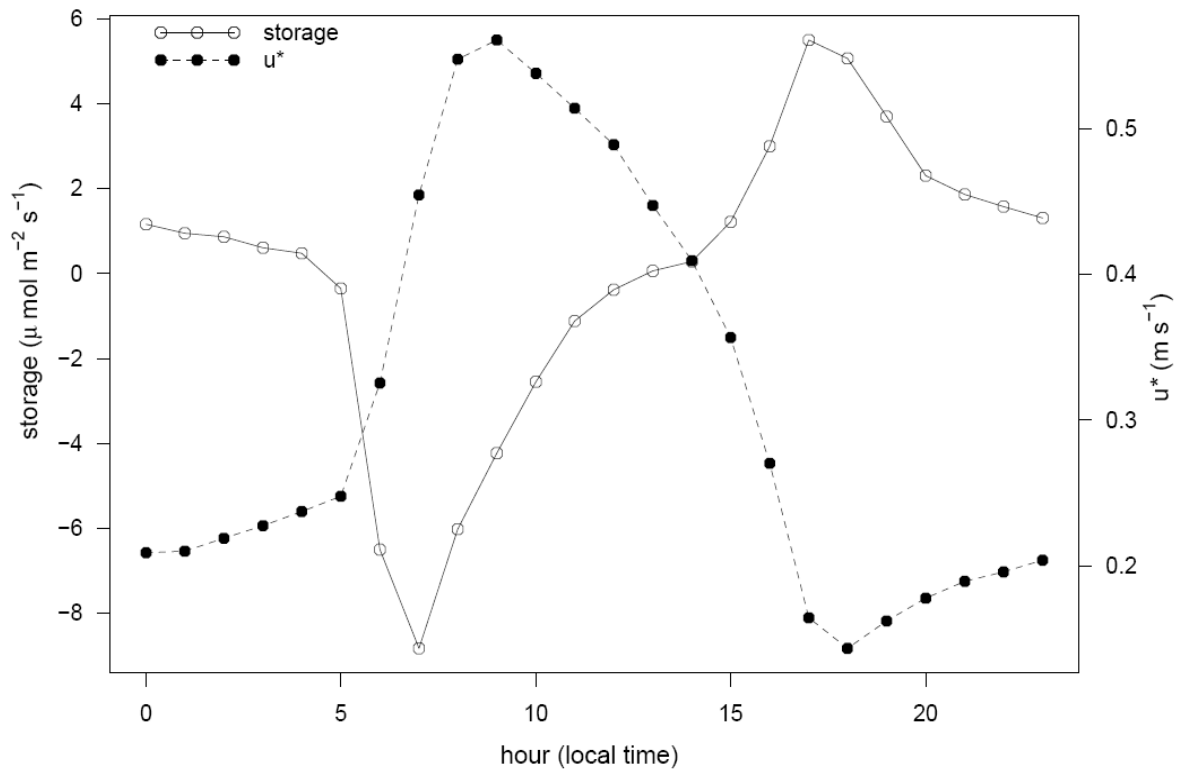


Figure 3.6: Turbulence (u_*) and canopy CO_2 storage were strongly, negatively correlated with changes in turbulence, with a time lag (storage delayed) of approximately 1 hour ($R^2 = 0.75$).

Gaps in canopy storage measurements are common at many forest flux tower sites, particularly in areas with extreme climate such as in tropical and boreal forests [cf. Iwata *et al.*, 2005]. If not corrected, significant errors in carbon balance estimates can result (Figures 3.1 and 3.2, B panels). Tables 3.1 and 3.2 show the model coefficients for fitting the S_1 model for canopy storage at km 67 and Table 3.3 shows the mean diel S_d model values. Figure 3.7 illustrates the relationship between measured accumulated nighttime storage and the time-weighted u_{*w} parameter used in formulating the S_1 model ($df = 1319$, $R^2 = 0.37$). A seasonal difference in the linear relationship between the weighted turbulence (u_{*w}) and storage was expected, but the seasonal model fits were

| | a_1 | a_2 | R^2 | p-value |
|------------------|-----------------|------------------|-------|---------|
| Annual model | 34.8 ± 0.64 | -75.4 ± 2.69 | 0.37 | <0.0001 |
| Dry season model | 35.2 ± 0.96 | -78.0 ± 4.3 | 0.39 | <0.0001 |
| Wet season model | 33.9 ± 0.85 | -71.9 ± 3.55 | 0.34 | <0.0001 |

Table 3.1: Annual and season model coefficient values for total nighttime CO_2 canopy storage in the Iwata et al. [2005] model. The Dry season extends from day of year 196 through 349.

| Local Time | 6:00 | 7:00 | 8:00 | 9:00 | 10:00 | 12:00 | 13:00 | 14:00 | 15:00 | 16:00 | 17:00 | 18:00 |
|------------|-------|-------|-------|-------|-------|-------|-------|-------|-------|-------|-------|-------|
| Coef. | -0.34 | -0.45 | -0.31 | -0.21 | -0.12 | -0.05 | -0.02 | 0.002 | 0.017 | 0.06 | 0.15 | 0.29 |

Table 3.2: Values of daytime hourly model coefficients ($\mu\text{mol } CO_2 \text{ m}^{-2} \text{ s}^{-1}$) for daytime depletion cycle of forest canopy storage based on the annual model described in Table 3.1.

| Local time | Coefficient ($\mu\text{mol } CO_2 \text{ m}^{-2} \text{ s}^{-1}$) |
|------------|--|
| 0600 | -6.49 ± 0.22 |
| 0700 | -8.82 ± 0.25 |
| 0800 | -6.02 ± 0.20 |
| 0900 | -4.23 ± 0.15 |
| 1000 | -2.54 ± 0.13 |
| 1100 | -1.13 ± 0.10 |
| 1200 | -0.38 ± 0.08 |
| 1300 | 0.07 ± 0.08 |
| 1400 | 0.29 ± 0.09 |
| 1500 | 1.21 ± 0.09 |
| 1600 | 3.00 ± 0.12 |
| 1700 | 5.49 ± 0.13 |
| 1800 | 5.07 ± 0.14 |
| 1900 | 3.7 ± 0.15 |
| 2000 | 2.31 ± 0.16 |
| 2100 | 1.86 ± 0.16 |
| 2200 | 1.57 ± 0.16 |
| 2300 | 1.31 ± 0.18 |
| 2400 | 1.16 ± 0.19 |
| 0100 | 0.95 ± 0.18 |
| 0200 | 0.88 ± 0.19 |
| 0300 | 0.62 ± 0.19 |
| 0400 | 0.48 ± 0.19 |
| 0500 | -0.35 ± 0.19 |

Table 3.3: Diel storage model, S_d , hourly values.

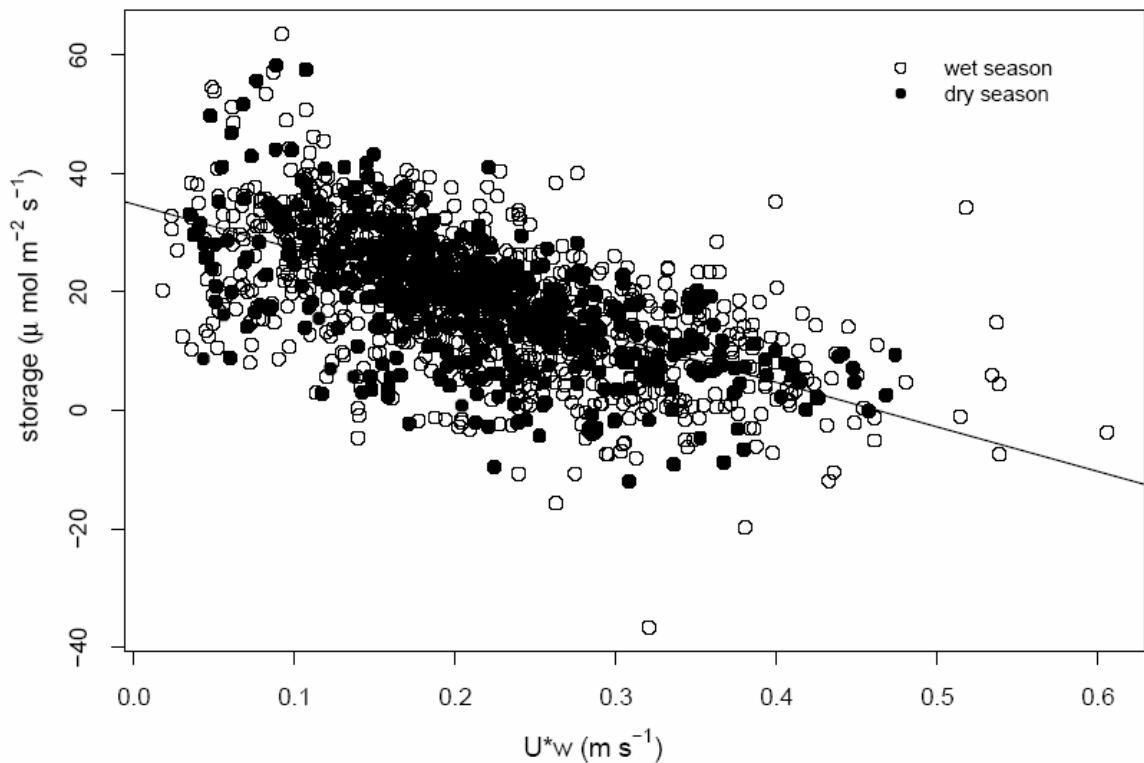


Figure 3.7: Measured hourly u^*_{w} plotted against total nighttime accumulated canopy storage with the filled circles denoting the dry season and the open circles denoting the wet season. No significant seasonal difference was detected in the relation and a single nighttime accumulation model was utilized, $R^2 = 0.37$.

statistically indistinguishable (Table 3.1) and an annual model was utilized for subsequent analysis. The overall model fit at the Tapajos site was comparable to the results reported by *Iwata et al.* [2005] for the Jaru and Caxiunã Amazonian flux tower sites notwithstanding that much less data were available for model calibration at the other flux tower sites. The errors on the diel S_d model values converged by approximately 2400 hours (100 days) of measured storage data.

Figure 3.8 shows a comparison between the S_d and S_I models and observations. During the nighttime, the S_I model roughly captured the accumulated nighttime storage, both under

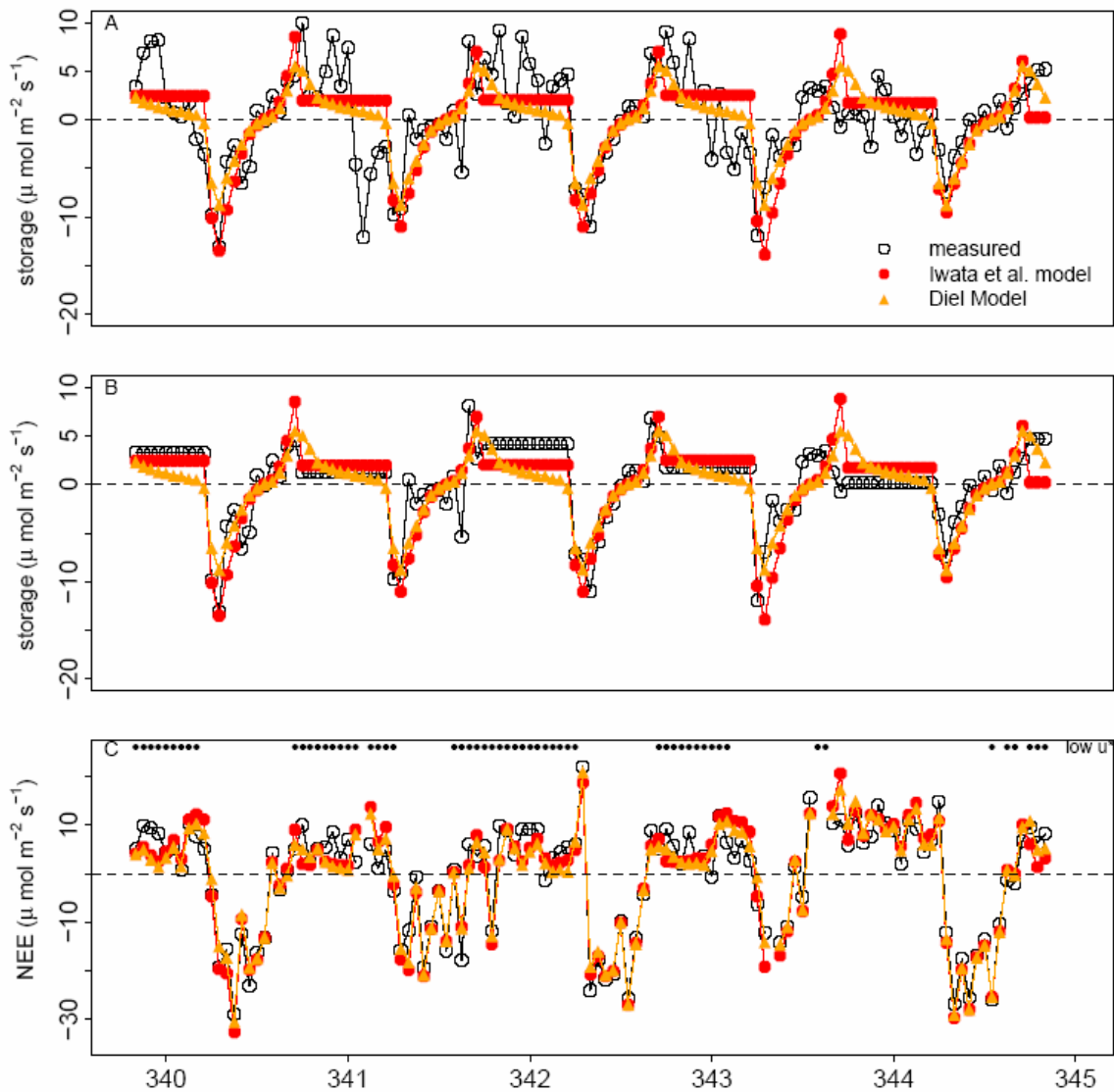


Figure 3.8: Time series comparison for measured and modeled canopy CO_2 storage and NEE for days of year 340-345 (local time) in 2005. The S_d and S_l storage models showed good agreement with the hourly measured storage (A) and with the nighttime mean storage (B). Measured NEE (CO_2 flux + storage) and estimated NEE (CO_2 flux + modeled storage) also agreed well (C). The points along the top of panel C indicate hours with low turbulence ($u_* < 0.22 \text{ m s}^{-1}$) which would be removed through filtering in the ‘best estimates’ of NEE and R. Note that the same time periods are illustrated in Figures 5 and 8, with the night on DOY 344 highlighting the influence of turbulence on canopy CO_2 storage.

and over-predicting the mean accumulation. The S_I model represented the morning drawdown and afternoon build-up well, but the results are largely comparable to the much simpler diel S_d model. The S_d model did not capture hourly variability (Figure 3.8A), but represented the overall mean behavior. Figure 3.8B shows the daily measured mean nighttime storage averaged for better comparison with the S_I model and shows that both the S_I and S_d models comparably capture the general patterns of the nighttime accumulation. Figure 3.8C shows a comparison between the estimated NEE (CO_2 flux + storage) based on the storage models and the measured NEE. The agreement between the modeled and observed NEE data is extremely good, but it is not surprising considering that CO_2 flux is the major term in NEE and differences between measured and modeled storage are small relative to the overall NEE (also see Figure 3.4). Overall, both the S_I and S_d models did capture the mean storage behavior, explaining 44% and 54% of the total observed hourly variance in canopy CO_2 storage, respectively.

The S_I and S_d models, with parameterizations from the km 67 tower site, were tested against the observed storage at the nearby km 83 forest tower site (3.0103° S, 54.5815° W; *Miller et al.*, 2004) and were found to explain significantly less of the observed hourly variance at the nearby site, only capturing 35% and 37%, respectively. The effects of aggregating the modeled data to longer time scales are discussed later in this paper. The km 67 and 83 towers sites are approximately 16 km apart, with similar flux measurement equipment, and extremely similar forest structure [*Miller et al.*, 2004; *Hutyra et al.*, 2007]. The km 83 site has more varied topography and even small differences in microclimate, topography, and/or canopy architecture evidently translate

into significant differences in air drainage and wind profile distributions. Given that the parameters for the S_I and S_d models were not found to be applicable across these proximate sites, site specific model storage parameterizations must be utilized.

3.4.4 Tower-based respiration flux measurements

3.4.4.1 Best estimates of ecosystem respiration

The validity of eddy-correlation measurements and adjustments to account for missing flux during calm conditions can be assessed by considering independent estimates of ecosystem R. We considered several alternatives for estimating R from the eddy-covariance data (Figure 3.1, panel A). During the nighttime hours, NEE represents ecosystem R, since photosynthesis is zero. Our best tower-based estimate of ecosystem R was $8.6 \pm 0.11 \mu\text{mol m}^{-2} \text{s}^{-1}$, based on the use of a u_* filter for the nighttime NEE calculated using hourly measured CO_2 flux and storage from January 2002 – January 2006. Our first alternative estimate derives R based on the intercept value of a hyperbolic light curve fit to the relationship between daytime NEE and photosynthetically active radiation (PAR) (Figure 3.9; see *Hutyra et al.*, 2007). This approach works particularly well at the TNF because no significant temperature relationship was observed for nighttime NEE [*Hutyra et al.*, 2007], Figure 3.9. The mean light curve intercept value was $8.9 \pm 0.6 \mu\text{mol m}^{-2} \text{s}^{-1}$, based on all available daytime data ($\text{PAR} \geq 40 \mu\text{mol m}^{-2} \text{s}^{-1}$; no u_* filter applied), and was statistically indistinguishable from our best estimate of ecosystem R. The light curve intercept and nighttime flux measurements are independent since entirely disjoint data were used in the comparison, and no u_* filter is applied to the daytime data.

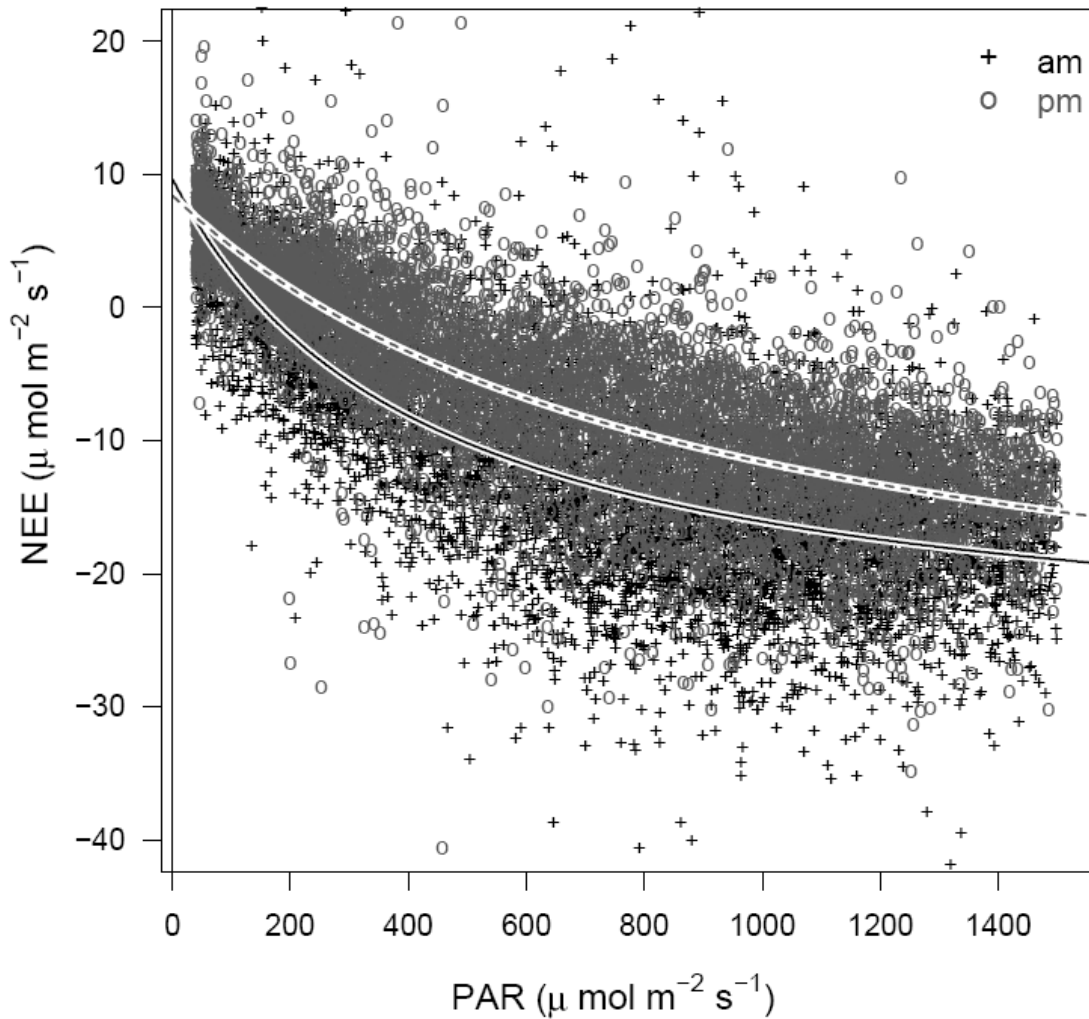


Figure 3.9: Net ecosystem exchange of CO_2 (NEE , $\mu\text{ mol m}^{-2} \text{ s}^{-1}$) as a function of photosynthetically active radiation (PAR , $\mu\text{ mol m}^{-2} \text{ s}^{-1}$), January 2002 – January 2006. Two separate nonlinear least squares approximation (hyperbolic function) are plotted through the data for the morning ($\text{PAR} > 40$ and before 1200) and afternoon periods ($\text{PAR} > 40$ and after 1200). The vertical line denotes $0 \mu\text{ mol m}^{-2} \text{ s}^{-1}$ PAR. The morning (cooler, moister, dashed line) and afternoon (warmer, drier, solid line) intercept values were statistically indistinguishable at 9.68 ± 0.98 and $8.43 \pm 0.56 \mu\text{ mol m}^{-2} \text{ s}^{-1}$. The overall intercept value (all data $\text{PAR} > 40 \mu\text{ mol m}^{-2} \text{ s}^{-1}$) was $8.9 \pm 0.6 \mu\text{ mol m}^{-2} \text{ s}^{-1}$.

Martens *et al.* [2004] independently assessed raw and u^* corrected NEE measurements at night at the TNF by comparing CO_2 eddy-covariance data with CO_2 fluxes inferred from ^{222}Rn profiles and ^{222}Rn soil flux measurements. Nighttime NEE derived from ^{222}Rn was

found to average $9.0 \pm 1.0 \mu\text{mol m}^{-2} \text{s}^{-1}$ in the wet season and $6.4 \pm 0.6 \mu\text{mol m}^{-2} \text{s}^{-1}$ in the dry season, agreeing very well with u_* filtered NEE measurements during the same time period (8.7 ± 1.1 and 6.6 ± 0.73 , respectively) [Martens *et al.*, 2004]. Scaling for the length of the local wet and dry seasons, the mean annual respiration rate inferred from the ^{222}Rn measurements was $7.9 \pm 0.81 \mu\text{mol m}^{-2} \text{s}^{-1}$ (Figure 3.1, panel A), equivalent to our best estimate with confidence bounds.

3.4.4.2 Treatments of canopy CO_2 storage

We tested the sensitivity of ecosystem R estimates to the treatment of canopy storage and u_* filtering to quantify possible errors and biases. An estimate of annual mean ecosystem R based only on CO_2 flux (u_* filtered) at the top of the tower (excluding canopy storage measurements) agreed very well with our best estimate of mean R and the independent estimates (Figure 3.1, panel B). Application of the u_* filter effectively removed nighttime periods of significant canopy CO_2 accumulation due to calm conditions. However, the combination of excluding storage and applying a u_* filter, introduced a serious temporal bias when integrating diurnally, since CO_2 accumulated and vented at different times of the day (Figures 3.4, 3.5, and 3.6). The overall mean nighttime measured storage was $1.2 \pm 0.06 \mu\text{mol m}^{-2} \text{s}^{-1}$. When a u_* filter was applied, the mean nighttime storage was reduced to only $-0.18 \pm 0.11 \mu\text{mol m}^{-2} \text{s}^{-1}$. But, during the daytime filtering is not effective, due to the predominance of well-mixed conditions; the mean daytime canopy storage was $-2.1 \pm 0.04 \mu\text{mol m}^{-2} \text{s}^{-1}$ and applying a u_* filter only changed the estimated storage value slightly to $-2.4 \pm 0.08 \mu\text{mol m}^{-2} \text{s}^{-1}$.

Hence, using only u^* filtered flux (no storage), we obtained a reasonable R value, but we got a biased 24-hour mean NEE estimate because of correlation between u^* and storage (*i.e.*, daytime NEE was biased positive, Figures 3.1, 3.2, and 3.6). The accumulation of CO_2 in the canopy, which was excluded by using only the flux (no storage) and a u^* filter, is released during the daytime hours and must therefore be carefully included in carbon budget computations. Omitting storage also strongly affected the light curve, biasing estimates of R due to the morning and evening patterns in storage (Figures 3.6 and 3.9); without the inclusion of storage, the intercept value was reduced to only $6.9 \pm 0.4 \mu\text{mol m}^{-2} \text{s}^{-1}$ (daytime data, no u^* filter), significantly underestimating the ecosystem R.

If we utilized either the S_I or S_d models for canopy storage, we obtained an underestimation of ecosystem R, due to the models' not adequately accounting for the influence of turbulence on nighttime storage (Figure 3.1, panel B). The overall mean nighttime storage for S_I and S_d models was 1.5 and 1.2 $\mu\text{mol m}^{-2} \text{s}^{-1}$, respectively, comparable to the observed mean storage without a u^* filter, but the design of these models does not allow for lost flux corrections such as u^* filtering. The mean observed respiration (CO_2 flux + measured storage) without the inclusion of a u^* filter, but using fluxes plus S_I or S_d , was only was $\sim 6.4 \pm 0.25 \mu\text{mol m}^{-2} \text{s}^{-1}$ (Figure 3.1, panel B). Not surprisingly, the estimates based on the modeled storage and measured CO_2 flux were consistent with the unfiltered nighttime NEE (Figure 3.1, panel B). However, nighttime NEE based on the S_I and S_d models did not agree with independent estimates of respiration from u^* filtered NEE, ^{222}Rn , bottom-up, or light-curve intercept (Figure 3.1, panel A).

3.4.5 Tower-based net ecosystem exchange measurements

Mean daily NEE (24-hour average summing photosynthesis and respiration) observed at this site was $0.25 \pm 0.04 \mu\text{mol m}^{-2} \text{s}^{-1}$ (u_* filtered, including measured storage, January 2002 – January 2006) and agreed well with the independent bottom-up estimate of $0.41 \pm 0.15 \mu\text{mol m}^{-2} \text{s}^{-1}$ (Figure 3.2, panel A). Mean NEE without the inclusion of a u_* filter was $-0.9 \pm 0.12 \mu\text{mol m}^{-2} \text{s}^{-1}$, as in the case of respiration, this value does not agree with independent estimates due to biases from missing nighttime respiration (Figure 3.2, panel B and Figure 3.4). NEE based on measured flux and modeled storage (no u_* filter) also resulted in a large estimated carbon sink, again due to biases from missing nighttime flux. The mean CO_2 flux (no storage included) measured at the top of the tower was 0.8 ± 0.12 or $-0.9 \pm 0.08 \mu\text{mol m}^{-2} \text{s}^{-1}$ with and without the inclusion of a u_* filter, respectively. Entirely excluding storage during both the daytime and nighttime resulted in a severe bias due to the combined effects of missing nighttime storage and daytime venting of nocturnal accumulations within the canopy.

When integrated across 24 hours, application of a u_* filter does not negate the need for storage measurements since it excludes periods of significant CO_2 accumulation within the canopy (nighttime), but includes the subsequent daytime venting (negative storage), resulting in a strong bias. Failing to apply a u_* filter to fluxes, without storage, also gives biased results.

3.4.6 Diurnally varying storage models

We devised and tested a diurnally varying storage model (DVSM) for estimating NEE when storage was missing. In the DVSM formulation, days and nights were treated separately to allow for differential treatment of storage patterns. During the nighttime (local time 1800 – 0600), we estimated NEE using only CO₂ flux measurements (no

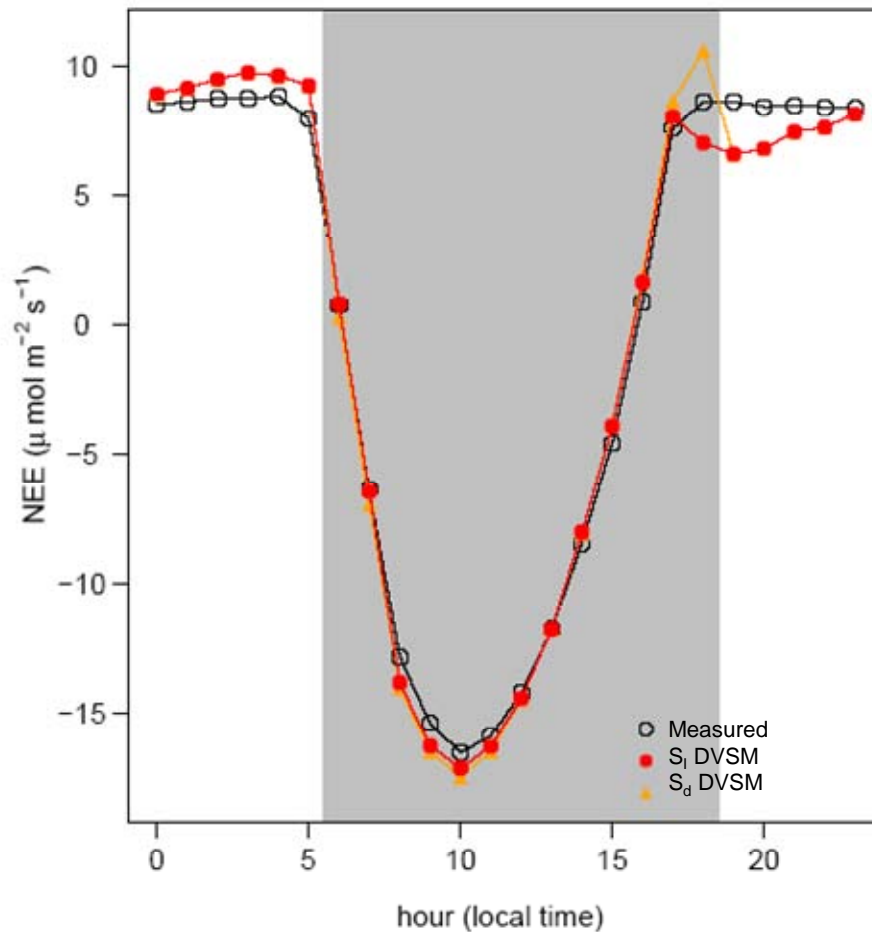


Figure 3.10: Diurnal cycle of NEE comparing measured ('Best estimate') with the S_1 and S_d diurnally varying storage models (DVSM). In the DVSM days and nights were treated separately to allow for differential treatment of the different storage patterns. During the nighttime (local time 1800 to 0600), NEE was estimated using only CO₂ flux measurements (no storage) from well mixed times ($u^* \geq 0.22 \text{ m s}^{-1}$) and during the daytime (local time 0700 – 1700) canopy storage models were included in the NEE estimation (CO₂ flux + storage) to capture the venting of accumulated CO₂ from the previous night.

storage) from well mixed times which allowed for accurate estimation of nighttime respiration (see *section 3.4.2*). But, during the daytime (local time 0600 – 1800), canopy storage model coefficients were included in the NEE estimate (CO_2 flux + storage) to capture the venting of nighttime storage accumulation. Both the S_I and S_d DVSM were able to accurately estimate the daytime venting of stored CO_2 , and the mean net carbon balance agreed well with the independent estimates (Figures 3.1, 3.2, and 3.10). Both S_I and S_d DVSM produced comparable results, with the error on both models maximizing at sunset due to the highly variable and quickly changing conditions during that time.

3.5 Discussion & Conclusions

Figures 3.1 and 3.2 compare independent estimates of mean NEE and ecosystem R with a range of different possible estimates based on the treatment of missing storage data and lost flux. There was a wide array of possible estimates of both NEE and R, but not all permutations were equally credible.

In the case of ecosystem R, we report three independent estimates of ecosystem R that did not use any type of ‘lost flux’ corrections: bottom-up measurements of the major respiration processes (a lower bound estimate of total R), estimates based on similarity with local ^{222}Rn flux measurements, and the light curve intercepts (as $\text{PAR} \rightarrow 0$). These independent estimates provide rigorous tests for eddy-covariance estimates of ecosystem R using nighttime flux data and a u^* filter. Our ‘best’ eddy-covariance based estimate of

ecosystem R (applying a u^* filter, including measured storage, and a filling algorithm for gaps) agreed very well with the three independent estimates (Figure 3.1, panel A).

Ecosystem R estimated using only CO_2 flux (applying a u^* filter, excluding canopy storage) at the top of the tower also agreed with our best estimate and with the independent validations (Figure 3.1, panel B). However, flux-only estimates of NEE were biased when examined on a 24-hour basis (Figure 3.2, panel B), with or without a u^* filter. If no u^* filter was applied to flux-only data, nighttime R was far too low and NEE was negatively biased. If a u^* was applied to flux-only data at night, R was well represented, but NEE during the day was positively biased. Utilizing the S_I and S_d canopy storage models throughout the day and night resulted in an underestimate of ecosystem respiration due to unaccounted for 'lost flux'. Both canopy storage models tested here were based only on the bulk mean hourly or nightly storage accumulation patterns and could not account for short-term and diurnal changes associated with turbulence. On an hourly or single night basis the storage models agree very well with observations, but did not allow for filtering based on turbulence or other corrections for the known lost nocturnal flux.

We derived and tested a diurnally varying canopy storage model to estimate NEE in the absence of direct canopy storage measurements. This model allows for both the correction of lost nocturnal flux by using measurements from turbulent time periods and captures the daytime venting of nocturnally accumulated CO_2 through the incorporation of the average daytime storage profile. The DVSM can allow for extensive data recovery

from sites where canopy CO₂ storage is not routinely measured. The close agreement between our best estimate of R and NEE and the independent estimates provide strong confirmation the validity of our lost flux corrections.

3.6 Implications and future research

Eddy-covariance is a widely utilized and accepted method for quantifying ecosystem carbon exchange. Integration of flux data to daily, seasonal and annual timescales involves assumptions about which data are representative of the ecosystem fluxes, requiring careful treatment to account for unrepresentative data. Small errors and biases in correction algorithms can have a significant effect on ecosystem carbon balances when integrated over long timescales, and must therefore be reduced to a negligible magnitude to accurately determine net carbon balances. Results should be evaluated and validated against independent constraints for both NEE and R to gain insights into the mechanisms controlling exchange processes and ensure ecological realism.

The tropics provide particularly challenging field conditions due to the deep forest canopy, high temperatures, and abundant rainfall, but data from the tropics are especially important for constraining global carbon budgets and modeling possible forest responses to a changing climate regime.

In this paper we discussed the biases associated with lost nighttime flux and missing storage measurements that need to be considered and applied to any site employing the

eddy-covariance technique, especially relevant to tropical data. There was clear evidence of lost flux under conditions of low turbulence at this site, and a u_* filter was therefore applied. Ideally, canopy CO_2 storage should be continuously measured for determination of NEE. If logistics or instrument failures make such measurements impractical, then campaign-based measurements of canopy storage should be undertaken to parameterize storage models. At our site we found that storage model errors converged with approximately 100 days of data, but also, model parameters were site-specific. Short-term measurements of storage may be used to develop a diurnally varying storage model of the type described above, using flux only during the night, u_* filtered, and flux plus modeled storage during the daytime. Undertaking these steps will provide estimates of NEE as robust and unbiased as possible.

The robust correction approaches presented above allow for a method to utilize and integrate flux measurements from the multitude of flux tower sites where storage is not routinely measured and for correcting and validating nighttime data at the numerous sites with 'lost' nighttime flux, providing knowledge of ecosystem carbon exchange across a wide range of ecosystems. The analytical framework laid out in this paper can serve as a general template for validation and assessment of biases in flux measurements. Each site and measurement approach comes with a unique set of challenges. Integrative studies that combine multiple approaches and which assess mechanisms underlying the observed patterns are essential for utilizing eddy-covariance data.

3.7 Acknowledgements

This study was part of the Brazil-led Large Scale Biosphere-atmosphere Experiment in Amazonia and was funded by NASA grants NCC5-341, NCC5-684, and NNG06GG69A to Harvard University. The authors would like to thank Elaine Gottlieb, Daniel Amaral, Lisa Merry, Bethany Reed, Dan Hodkinson, and the staff of the LBA Santarem office for their extensive data processing, logistical and field assistance. We wish to also thank Simone Vieira, Amy Rice, Greg Santoni, Daniel Curran, and Joost van Haren for their extensive assistance with the biometric field measurements. We also thank Allison Dunn for her valuable comments on earlier drafts of this paper. Finally, the authors are also extremely grateful to Eric Davidson, Dan Nepstad, Jeff Chambers, Michael Keller, Mike Goulden, Scott Miller, and David Fitzjarrald for sharing the data that made the independent comparisons in this paper possible.

Chapter 4: Climatic variability and vegetation vulnerability in Amazônia

Hutyra, L.R., Munger, J.W., Nobre, C.A., Saleska, S.R., Vieira, S.A., Wofsy, S.C.,
Climatic variability and vegetation vulnerability in Amazônia, *Geophysical Research
Letters*, 32, L24712, 2005.

4.1 Abstract

Models of climate change predict close coupling between increases in aridity and conversion of Amazonian forests to savanna. Here we assess the vulnerability and resilience of Amazonian vegetation to climate change by analyzing observed climate-vegetation relationships using climate data, observed vegetation distributions, and evapotranspiration rates inferred from eddy flux data. We found that drought frequency is an excellent predictor of the forest-savanna boundary, indicating the key role of extreme climatic events for inducing vegetation change, and highlighting particularly vulnerable regions of Amazônia.

4.2 Introduction

Vegetation change in Amazônia has long been recognized as a potentially significant component of climate change [Gash et al., 1996]. Early studies focused on climate change induced by deforestation [eg. Nobre et al., 1991], whereas coupled changes of climate and vegetation [e.g. Cox et al., 2004] are the current interest. Roughly 50% of Amazon precipitation is evaporated from the forest [Salati and Vose, 1984], so that changes in either vegetation or climate propagate through the entire vegetation-climate system. Large departures from mean climate conditions have been shown to result in increased tree mortality [Williamson et al., 2000], forest fires [Nepstad et al., 2004], and global atmospheric CO₂ anomalies [Clark et al., 2003], hence both mean climate and climate variability are important.

It is very difficult to capture the variability of natural systems in models. Both climate and vegetation can have multiple states that are persistent and resilient [Holling, 1973; Sternberg, 2001]. Many natural systems show hysteresis and lags. After small perturbations, the system returns to the initial state, but a large disturbance may cause a shift to a new persistent state. The perturbation needed to return the system to a prior long-term state may be larger than the one that triggered the shift. For example, Amazon forests have expanded during moist periods of the Holocene and contracted in dry periods [Oliveira and Marquis, 2002]. The last contraction, in a brief mid-Holocene dry interval, persisted despite the return of wetter conditions [Ledru, 1998].

Changes in the frequency or magnitude of disturbance [*Katz and Brown, 1992*], and covariance between perturbing factors (e.g. temperature, precipitation, sources of ignition) may make vegetation change inevitable and irreversible, but initially nothing may happen. Vegetation change can be unannounced, catastrophic, and persistent [*Scheffer et al., 2005*].

Climate and weather are primary mechanisms for disturbance and principal determinants of the size, age, and species structure of ecosystems [*Connell, 1978*]. The ratio of potential evapotranspiration to precipitation (PET/P) is a key determinant of vegetation in the tropics, with $PET/P < 1$ typically observed in biologically rich, closed-canopy forests and $PET/P > 1$ associated with sparser, fire-adapted vegetation [*Holdridge, 1947*]. *Cox et al.* [2004; cf. *Huntingford et al. 2004*] predicted dramatic shifts in vegetation in response to increased aridity in future climate, whereas *Friedlingstein et al.* [2002] inferred persistence of moist tropical forests. This divergence highlights the importance of understanding the resilience of Amazonian vegetation and the factors regulating the vegetation assemblage.

In this paper, we assess the vulnerability and resilience of Amazonian vegetation to climate change by analyzing observed climate-vegetation relationships in a statistical framework using climate data, observed vegetation distributions, evapotranspiration rates based on eddy flux data (ET, includes evaporation of surface water and soil moisture, and transpiration by vegetation [*Oke, 1996*]), and water balances. We re-evaluate the *Nix*

[1983] criteria for forest-savanna boundaries, and formulate a drought criterion to capture the influence of climatic variability on vegetation.

4.3 Measurements & Empirical model

Common formulas for ET (e.g. *Monteith* 1983; *Gash* 1979; *Hodnett et al.* 1996) could not be used for our analysis of drought because required data are not available from climate reconstructions. Hence we derived a similar formula for Amazonian forest ET, using only temperature, by analyzing eddy flux data that we collected in Tapajós National Forest (54°58'W, 2°51'S, near km 67 of the Santarém-Cuiaba highway, BR-163). This site was selected for study in the Brazilian-led Large Scale Biosphere-Atmosphere Experiment in Amazonia (LBA-ECO) because it lies at the dry end of the climate zone supporting evergreen equatorial forests.

Data for water fluxes and temperature [*Saleska et al.*, 2003], from January 2002 through November 2004, were combined to develop a model of actual ET for evergreen Amazonian tropical forest, denoted forest evapotranspiration (FET):

$$\text{FET (mm/day)} = -6.7084 + 0.3764 * T, \quad (4.1)$$

where T is monthly mean temperature (°C). When fit to 38 months of environmental measurements, Eq. (4.1) explained 68% of the total variance (Figure 4.1; see section 4.4.2).

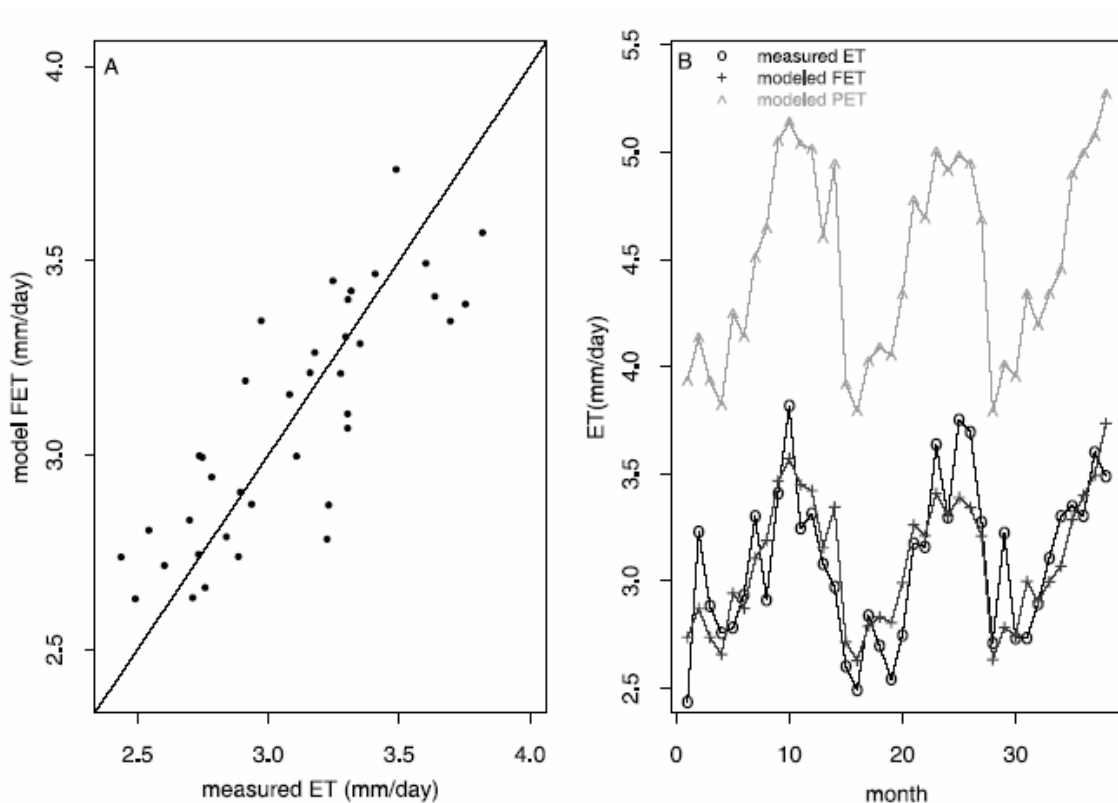


Figure 4.1: (a) Observed and modeled forest ET for the Santarém study site, $R^2 = 0.68$; (b) time series for measured forest ET, the FET model (4.1), and modeled PET [Thornwaite, 1948].

We used the Climate Research Unit's (CRU) 100-year gridded ($0.5^\circ \times 0.5^\circ$) time series for temperature and precipitation [New *et al.*, 1999; updated by Mitchell, 2003], in which monthly mean and variance fields are interpolated separately (Figure 4.2). For the few points (7.7%) where the CRU temperature was outside the range observed at Tapajós ($24^\circ - 28^\circ\text{C}$), FET was set to 75% of PET as given by Thornwaite [1948], the mean ratio of Eq. (4.1) to PET across the Basin. PET exceeds actual ET because it does not account for soil and vegetation limitations on water exchange, but our observed ET is a nearly constant fraction of PET (Figure 4.1b)

4.4 Drought assessment

To derive a measure of drought occurrence, we computed the quantity of soil water available trees (Plant Available Water, or PAW; units: mm H₂O),

$$PAW_i = PAW_{i-1} + P_i - FET_i, \quad (4.2)$$

where i indexes the month of the 100 year record. Values exceeding PAW_{max} were assumed lost as runoff. The spatial distribution of PAW_{max} was adapted from *Kleidon* [2004], who applied inverse methods to a land surface model optimizing photosynthesis (Figure 4.3). This PAW_{max} applies to current vegetation assemblages, under current climate. PAW in 1900 was set to PAW_{max} at all grid cells.

A drought was assessed at any grid cell where PAW declined to less than 75% of PAW_{max} for 5 or more months in a year, implying a dry period exceeding 6 or 7 months, longer than the mean dry season for most evergreen Amazon forests. Similar results were obtained using shorter-intervals of more extreme dryness, e.g. $PAW < 0.25 * PAW_{max}$ for 1 month (Figure 4.3).

The spatial distribution of estimated drought frequencies in 100 years was compared with vegetation in the legal Brazilian Amazon, classified using Landsat data from the early 1980s (prior to most forest clearing). These data were produced by the Tropical Rainforest Information Center (TRFIC), Michigan State University, without any reference to climate data. We aggregated 9 classes to 3 vegetation types: fire-adapted

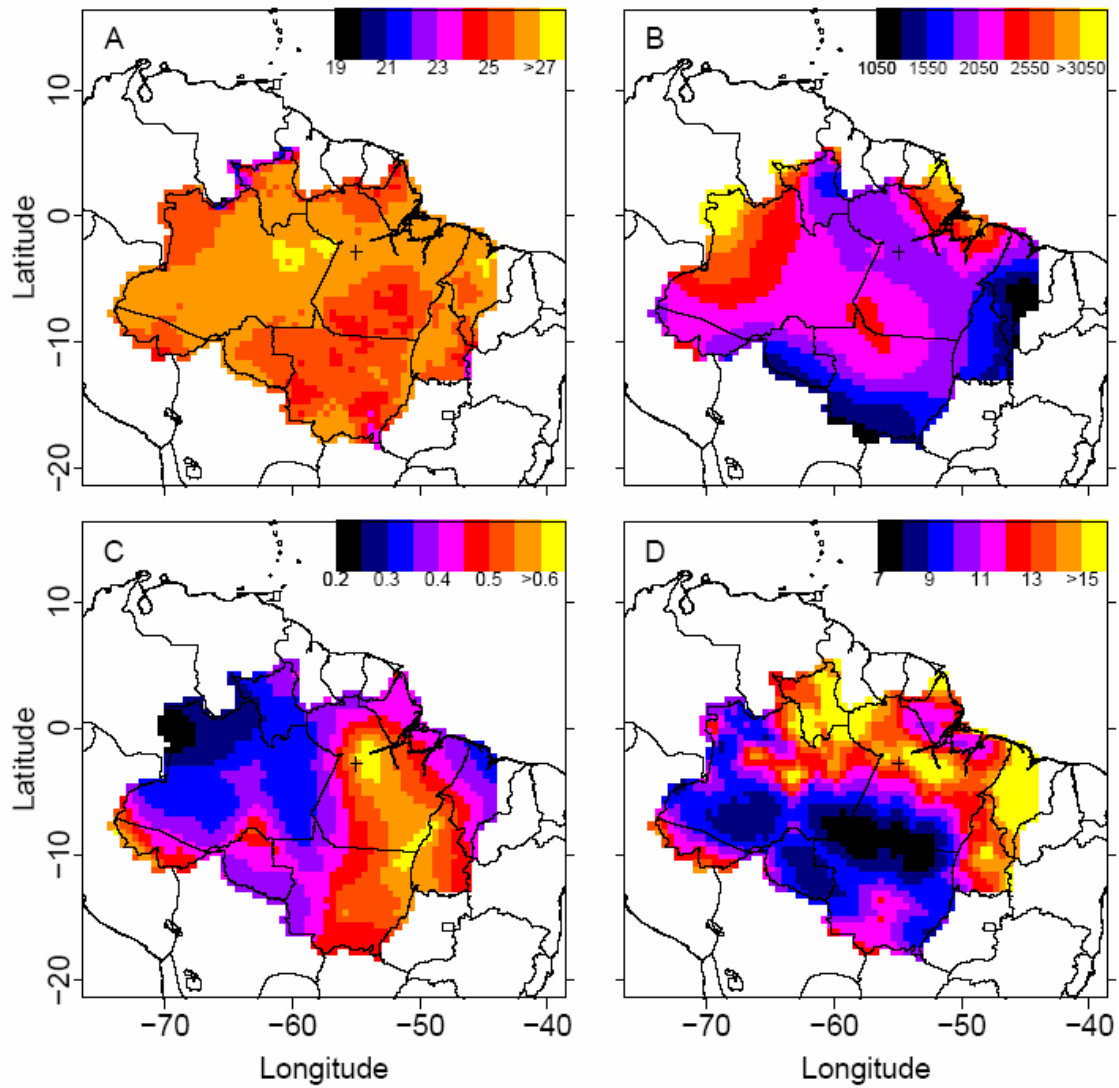


Figure 4.2: (A) Mean annual temperature ($^{\circ}\text{C}$); (B) mean annual precipitation (mm year^{-1}); (C) standard deviation for 100 year time series of temperature; (D) coefficient of variation for 100 year time series of precipitation (%).

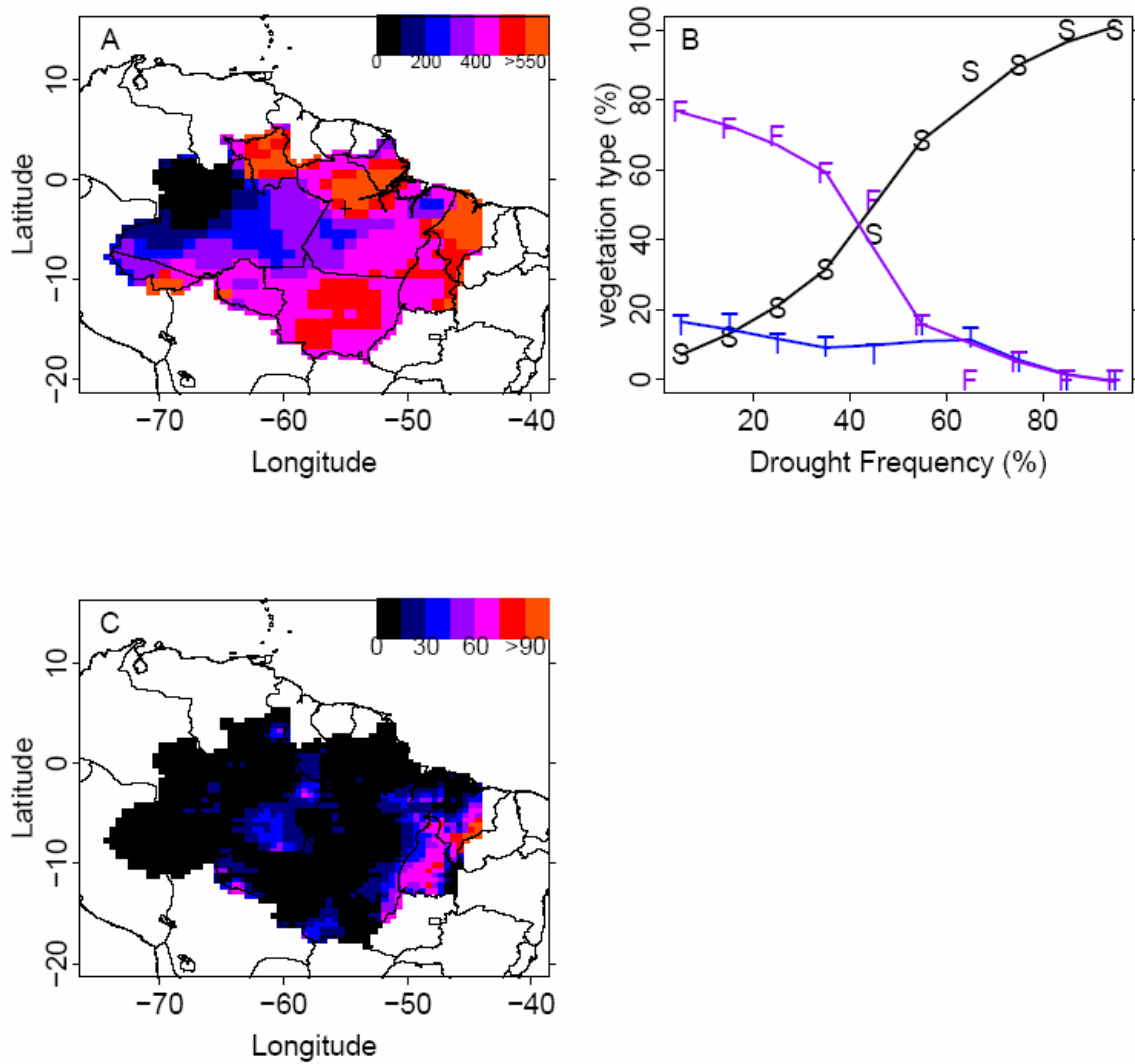


Figure 4.3: (A) PAWmax for the legal Amazon [Kleidon et al. 2004]; (B) fractional coverage of each vegetation type for pixels with a given drought ($PAW < 0.25 \cdot PAW_{max}$ for minimum of 1 month) incidence (%). (C) Percent of year with $PAW < 0.25 \cdot PAW_{max}$ for minimum of 1 month.

savanna and woodlands, seasonal transitional forest, and equatorial evergreen forest. Riparian zones were excluded and Caatinga in the NW basin was grouped with evergreen forests.

4.5 Results

4.5.1 Forest evapotranspiration

Equation 4.1 predicts significant spatial variation of mean annual FET (1.72 - 3.6 mm/day, Figure 4.4), highest near the Equator. Variability of FET is greatest in the southern portion of the Amazon (Figure 4.4). Few accurate multi-year measurements are available to test Fig. 2. Near Santarém (2.75°S, 54.75W°), Manaus (2.75°S, 59.75W°), and Ji-Paraná (10.75°S, 61.25°W) mean FET values are 3.1 (± 0.34 , 1 σ), 3.5 (± 0.24), and 2.9 (± 0.37) mm day⁻¹ respectively, in good agreement with observations (3.07 [*this work*] and 3.51 [*da Rocha et al.*, 2004], 3.05 [*Mahli et al.*, 2002] and 3.45 [*Shuttleworth et al.*, 1984], and 3.69 (wet season) and 3.83 (dry season) [*Von Randow et al.*, 2004], respectively). Both FET and measured ET maximize in the dry season when incident radiation and vapor pressure deficits are highest.

4.5.2 Drought and vulnerable vegetation areas

Our values for drought frequency (Figure 4.5) are highest along the southern and eastern edges of the legal Amazon, but less frequent droughts occurred in the central basin.

Areas with high drought frequency are associated with regional precipitation minima and/or high

temperature

variability. The

current distribution of vegetation (Figure 4.5

B) strikingly follows

drought frequency,

with savanna replacing

forest and transitional

vegetation as drought

frequencies increase

(Figure 4.5 C).

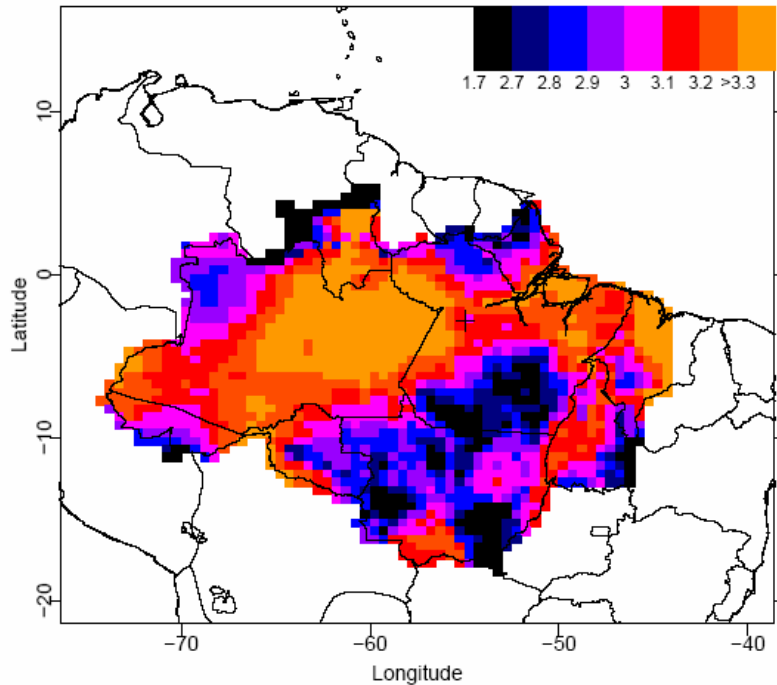


Figure 4.4: Mean annual modeled FET (mm/day) from equation (4.1).

Nix [1983] developed seven criteria to predict occurrence of tropical savannas (Table

4.1). The spatial patterns for attainment of his criteria 2-6 (Figure 4.5 D), utilizing the

CRU time series, showed a strong correlation with our PAW drought metric ($r = 0.69$, $p \approx$

0). The fraction of years attaining Nix criteria and vegetation type were also correlated, r

$= 0.59$ ($p \approx 0$). Correlations between individual Nix [1983] rules and vegetation (Table

4.1) imply that his most significant criteria are mean rainfall, which excludes very wet

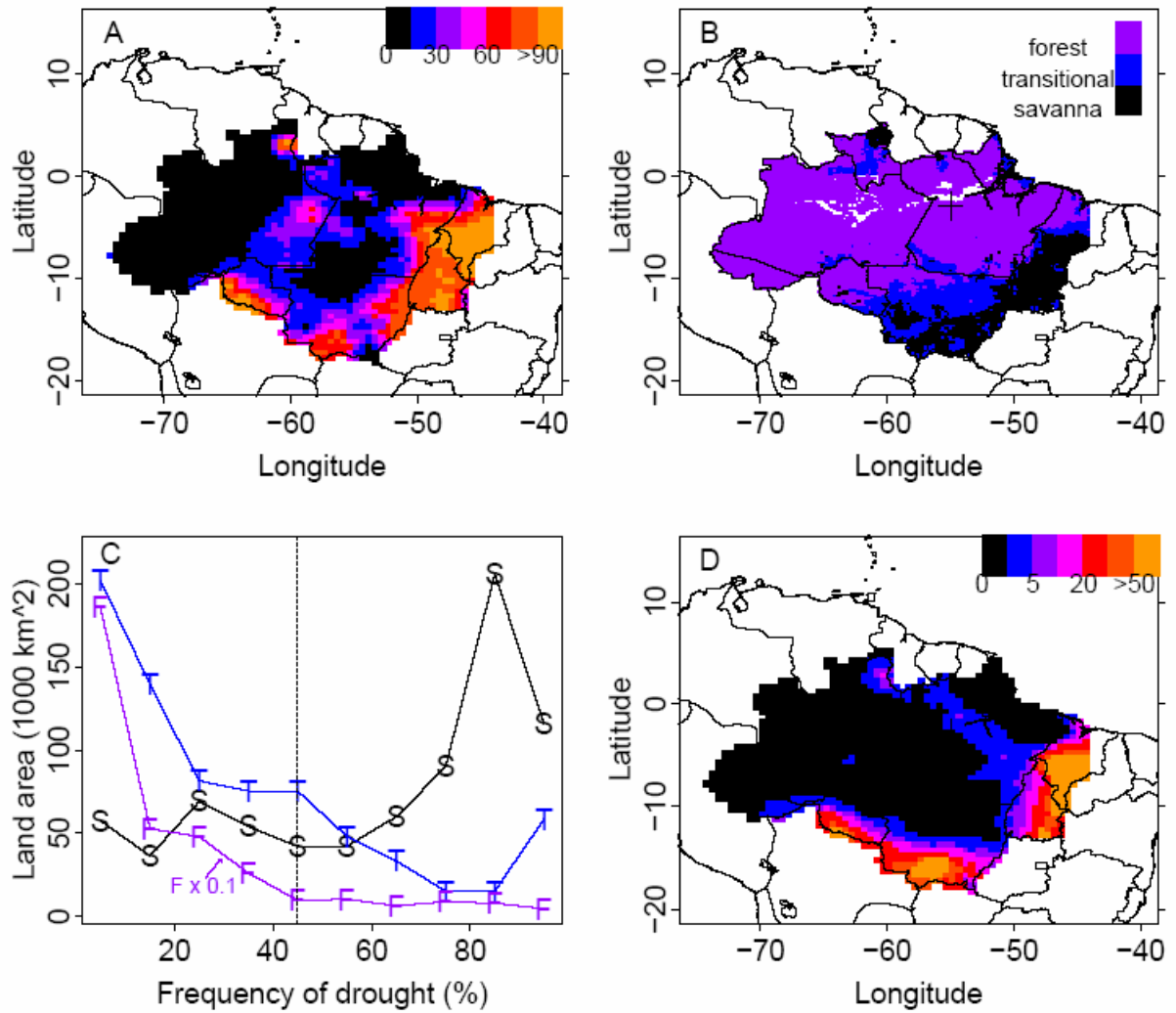


Figure 4.5: (a) Observed drought frequency (% years); (b) distribution of savanna, transitional vegetation, and forest across the legal Brazilian Amazon; (c) land area (1000 km²) of vegetation types for pixels with given drought frequency (%), forest land area is multiplied by 0.1 for scaling; (d) percent attainment of the Nix [1983] criteria for savanna vegetation in the last 100 years.

areas, and dry season precipitation, his aridity criterion. Since temperatures maximize in the dry season, the similarity with drought occurrence is unsurprising.

4.6 Discussion

Climatic variability is a principal driver for our PAW drought index, and implicitly for the *Nix* [1983] rules. Forest areas with high climate variability are vulnerable to loss of forest with *either* increased mean temperature, or increased with variability in temperature and/or precipitation. Our analysis provides a physical quantity (PAW

deficit) to predict

vegetation type, and it

supports the models of

Oyama and Nobre

[2004] indicating that

the *seasonality* of soil

moisture is a critical

factor determining

forest-savanna

boundaries. We support

the findings of *Nix*

| Nix [1983] Criteria | Correlation coefficient |
|---|-------------------------|
| 1. Annual totals of solar radiation between 6 and 8 GJ m ⁻² yr ⁻¹ | NA |
| 2. 1000 mm/yr < mean precipitation < 1500 mm year ⁻¹ | 0.56 |
| 2a. Mean precipitation > 1000 mm/yr | 0.28 |
| 2b. Mean precipitation < 1500 mm/yr | 0.56 |
| 3. High seasonality in rainfall | NA ^a |
| 4. Precipitation > 600 mm/yr during wettest 6 months | 0.05 |
| 5. Precipitation < 50 mm/yr during driest 3 months | 0.75 |
| 6. Mean temperature > 24°C | 0.08 |
| 7. Mean min temperature of coldest month between 13° and 18°C | NA |
| Parameters 2 and 5 | 0.59 |
| Parameters 2 through 6 | 0.58 |

^a *Satisfies entire basin.*

Table 4.1: Correlation coefficients between the percent attainment of the Nix [1983] criteria and observed vegetation.

[1983], by testing against the extensive CRU climate record and the TFRIC vegetation map. The apparent role of variability highlights the importance of correctly capturing high order statistical characteristics in coupled vegetation/climate models.

Fire is likely the event that actually shifts a forest to savanna. Historical records and charcoal found in soils show that fires have occurred in many evergreen tropical forests. Trees are sustained during dry periods by deep roots [*Nepstad et al.*, 1994] that access stored water, but small plants and dead organic matter can become combustible. Increased drought frequency would evidently raise susceptibility to ecosystem-transforming fires. Evergreen tropical forests are not fire-adapted, reflecting the long fire return interval. Fire return times of less than 90 years may eliminate rainforest species, and return intervals of less than 20 years may entirely eliminate trees [*Jackson*, 1968].

Other factors may interact synergistically with droughts, exacerbating vulnerability even in a stable climate [*Cochrane and Laurence*, 2002]. Fire frequency and intensity are expected to increase with fragmentation due to land conversion, due to desiccation at fragment edges, and with introduction of anthropogenic ignition sources [*Cochrane and Laurence*, 2003]. Areas of forest proximate to edges or to ignition sources have increased dramatically [*Cochrane*, 2003], and forest disturbance is currently significant in areas with notable climatic variability [e.g. Santarém and Rio Branco; Figure 4.1; *Vieira et al.*, 2004].

Oyama and Nobre [2003] have suggested that the Amazon may have an alternate persistent vegetation/climate state, where savannas take over large areas currently in tropical rainforests. A drier climate leads vegetation to rely on deeper water supplies to maintain green canopies, and flammability increases. Once large areas converted to savanna, overall aridity would increase because fire-adapted vegetation transpires much less than forests. Our study supports the view that forests in areas of high drought frequency (>45% drought probability) could shift to transition forests or savanna, if aridity increases as predicted by climate change models [*Cox et al.*, 2004; *Friedlingstein et al.* 2001]. Potentially at risk are over 600,000 km² of forest (Table 4.2, Figure 4.5), >11% of the total area. Savanna vegetation currently present in areas with low drought frequency (<45% droughts) are unlikely to shift to forest if aridity increases. Our maps show that increased aridity may lead to bisection of Amazonian equatorial forests.

The critical links between fire, climate, and land use are highly uncertain in current coupled climate-vegetation models. In order to assess vegetation vulnerability to climate change, models must capture variability of climate, the non-linear, hysteretic behavior of vegetation response to rising drought frequency, the synergistic effect of forest fragmentation and development, and the occurrence of landscape-changing fires.

| | Drought frequency 0-44 | Drought frequency 45-100 |
|--------------|---------------------------|-----------------------------|
| Forest | 3,176,751 km ² | 413,900 |
| Transitional | 550,023 | 197,027 |
| Savanna | 243,655 | 583,965 |

Table 4.2: Areas of the legal Amazon within the two drought frequencies regimes for each vegetation type. Grey cells indicate areas vulnerable to degradation with increased aridity. A 45% frequency of drought implies a mean return interval of 2.2 years.

4.7 Acknowledgements

The authors would like to thank Allison Dunn and Paul Moorcroft for insightful comments and suggestions, and David Skole, Walter Chomentowski, Elaine Gottlieb, and Axel Kleidon for kindly providing data. This work was supported by grants NASA NCC5-341 and NASA NCC5-684 to Harvard University.

Chapter 5: Conclusion

The Amazon forest is the earth's largest contiguous intact tropical forest and exerts substantial leverage over the global carbon cycle through its very large carbon stocks and high photosynthetic and respiratory rates of carbon exchange. The Amazon forest is currently estimated to be a large carbon sink ranging from 0.3 [Baker *et al.*, 2004] to 1.0 Pg C yr⁻¹ [Andreae *et al.*, 2002], but the results remain controversial [Ometto *et al.*, 2005]. The tropics have already experienced profound climate and atmospheric changes including increased CO₂ concentrations [IPCC, 2001], increased temperatures (with an average increases of $0.26 \pm 0.05^{\circ}$ C per decade since 1975 [Malhi and Wright, 2004]), and changed aerosol loads [Oliveira *et al.*, 2006] which are all known to significantly affect ecosystem function as well as the strength and stability of any Amazonian carbon sink [Clark, 2007].

General Circulation Model (GCM) simulations suggest that the Amazon is highly sensitive to changes in climate and/or vegetation cover, with models predicting declining productivity as warming proceeds [Fung *et al.*, 2005], despite possible benefits from CO₂ fertilization [Körner, 2003]. Some studies have predicted a dramatic collapse of the Amazon forest due to increasing aridity and consequently a slowing of the hydrological cycle under global climate change [Cox *et al.*, 2000; Betts *et al.*, 2006], but others have suggested that the Amazon will be very resilient to changes in both temperature and precipitation [Cowling and Shin, 2006]. Further, some models have suggested that continued deforestation, even in the absence of climate change effects, may result in an

alternative vegetated state, with widespread savanna vegetation occurring in areas currently dominated by forests [*Oyama and Nobre, 2003*]. However, our confidence in the model mechanisms responsible for this predicted change is limited. These models have difficulty in simulating such basics as the seasonal cycle of photosynthesis, respiration, evapotranspiration, and temperature in tropical ecosystems [*Lee et al., 2005; Saleska et al., 2003*].

This thesis addressed several important issues surrounding the controls on carbon and water exchange and ecosystem stability in Amazonian rainforests through the use of eddy-covariance data, ground-based measurements, long-term climate records, and numerical models.

5.1 Controls on ecosystem carbon balance

The carbon balance of an ecosystem is the result of disturbance and recovery dynamics over time scales of years and decades [*Saleska et al., 2003; Rice et al., 2004; Vieira et al., 2004; Hutya et al., 2007*]. Climate and weather are the primary mechanisms for disturbance and principal determinants of the size, age, and species structure of ecosystems [*Connell, 1979*].

Many process-based biogeochemical models [*e.g. Botta et al., 2002; Tain et al., 1998*] predict that moisture limitation during the dry season provides a strong constraint on canopy carbon uptake in ‘old-growth’ tropical rainforests like our study site in the

Tapajós National Forest (TNF). Four years of observations at the TNF do not support this paradigm. Carbon uptake was indeed reduced early in the dry season, but the decline began before the onset of the dry season and uptake consistently began to increase in the mid-dry season. We found that this forest maintained high rates of photosynthesis throughout the year because of adequate water supplies, high year-round temperatures, and high light levels [*Hutyra et al.*, 2007].

Temperature and moisture are the key environmental factors regulating ecosystem respiration rates, but the interaction between these variables, especially in tropical ecosystems, is still highly uncertain [*Raich and Schlesinger*, 1992; *Trumbore*, 2006].

Temperature and soil moisture are typically inversely correlated, but both factors simultaneously influence respiration by affecting enzyme activity, diffusion of solutes and O₂, growth of root tissue, and microbial populations [*Davidson et al.*, 2006]. Eddy-covariance data cannot distinguish the components of respiration, but the four year long dataset from the TNF did allow us to examine the aggregate effects of climatic variability on total ecosystem respiration.

We found that both temperature and precipitation were significant correlates of the total ecosystem respiration, with respiration rates negatively correlating with temperature, and positively correlating with precipitation. The total ecosystem respiration was lower during the dry season, but the decline in respiration consistently began during the latter part of the wet season, in synchrony with the decline in the canopy carbon uptake. The respiration tended to remain low throughout the dry season even as canopy uptake

increased. This observation highlighted a differential response between the autotrophic and heterotrophic respiration processes. The autotrophic respiration can be assumed to increase with increasing GPP; hence the reduction in dry season respiration represented moisture limitations on heterotrophic processes. We did not find a significant relationship between temperature and respiration on short timescales raising questions about the appropriateness of using Q-10 type relationships in ecosystem models of tropical rainforests.

This site in the TNF was a small overall carbon source to the atmosphere, reflecting long-term disturbance and recovery dynamics, phenology, and seasonal water limitations on ecosystem respiration [*Hutyra et al., 2007*].

5.2 Validation of flux measurements

Eddy-covariance is a widely utilized and accepted method for estimating ecosystem carbon exchange. Integration of flux data to daily, seasonal and annual timescales involves several assumptions about which data are representative and requires approaches to account for unrepresentative periods. Results must be evaluated and validated against independent constraints for both NEE and R to gain insights into the mechanisms controlling exchange processes and ensure ecological realism.

In the third chapter of this thesis I focused on constraining the measurements of NEE and ecosystem respiration at the TNF through a combination of four years of high quality

eddy-covariance measurements of the net ecosystem exchange of CO₂ (NEE) and independent ground-based measurements. I demonstrated that not all methods to obtain NEE and respiration from flux data are equally plausible by using approaches for validation and by conducting careful error analyses to constrain the estimates for both the respiratory fluxes and NEE. I also presented a detailed bottom-up budget for both ecosystem respiration and the net forest carbon balance using multiple datasets and repeated measurements. Finally, I proposed and validated a robust correction method for lost nocturnal flux and missing storage data and outlined a validation framework for eddy-covariance results that could be applied to any flux tower location.

5.3 Future Amazon stability

Historical records and charcoal found in soils show that fires have occurred in many evergreen tropical forests. Seasonal water limitations have the potential to reduce forest growth and place the forest at risk for fire. Future climate scenarios suggest that temperatures in the Amazon may increase while precipitation decreases [Fung *et al.*, 2005], likely decreasing water availability and increasing drought and flammability. Fire is a likely event that could shift a forest to a fire-adapted savanna type vegetation.

Based on local measurements in the TNF we found that even a forest with a long dry season (5 months at this study site) did not show water limitations in growth.

Evapotranspiration consistently increased at the start of the dry season and remained elevated throughout the entire dry season. Dry season evapotranspiration rates were

insensitive to dry season precipitation, being nearly constant across years even though dry season precipitation varied by as much as 40%. Given that water losses consistently exceeded inputs during the dry season it is clear that large stores of water were accessible to the trees. If precipitation rates were to decrease by a small amount at this site, but water supplies remained adequate for the trees, it is possible that the net carbon uptake could increase due to increased insolation and moisture constraints on heterotrophic respiration. However, a reduction in decomposition from drier conditions could also result in increased flammability due to a build up of litter. Alternatively, if the amount of available water for the trees were to decrease through logging (causing soil compaction), higher temperatures (increased the evaporative demands), or large decreases in precipitation (slowed recharge of deep water reservoirs) the flammability of this forest might increase and the forest may convert to a more drought adapted vegetation type.

Across the Amazon, increased drought frequency would raise susceptibility to ecosystem-transforming fires. Evergreen tropical forests are not fire-adapted, reflecting the long fire return interval. Fire return times of less than 90 years may eliminate rainforest species and return intervals of less than 20 years may entirely eliminate trees [Jackson, 1968]. Other factors may interact synergistically with droughts, exacerbating vulnerability even in a stable climate [Cochrane and Laurance, 2002]. Fire frequency and intensity are expected to increase with fragmentation due to land conversion, due to desiccation at fragment edges, and with introduction of anthropogenic ignition sources [Cochrane and Laurance, 2002]. Areas of forest proximate to edges or to ignition sources have increased dramatically [Cochrane, 2003], and forest disturbance is currently

significant in areas with notable climatic variability. In *Hutyra et al.* [2005] we found that over 600,000 km², more than 11% of the Brazilian Amazon, could shift to transitional forests or savanna, if aridity increases as predicted by climate change models [Cox et al., 2004; Friedlingstein et al., 2003]. Our analysis showed that increased aridity may lead to bisection of Amazonian equatorial forests.

The critical links between fire, climate, and land-use are highly uncertain in current coupled climate-vegetation models. In order to assess vegetation vulnerability to climate change, models must capture variability of climate, the non-linear, hysteretic behavior of vegetation response to rising drought frequency, the synergistic effect of forest fragmentation and development, and the occurrence of landscape-changing fires.

5.4 Future research

In thinking about future research needs in carbon cycle science, we need to acknowledge that any future changes will be complex and depend on both historical disturbance legacies and interactions between multiple driving forces. *Foster and Aber* [2004] described the challenge accurately in that ‘most landscapes and natural ecosystems bear strong legacies of the past events. In fact, as we anticipate future changes in our forests, we fully expect that these will be driven as much by recovery from historical processes as by responses to novel conditions.’ In the case of the TNF, historical disturbance legacies caused large carbon losses due the decomposition of excess of coarse woody debris (CWD) believed to have been the result of an *El Niño* driven climate anomaly [*Rice et*

al., 2004]. Many studies of Amazonian carbon cycling fail to include a complete accounting for all the ecosystem carbon additions and losses (such as CWD) that are required to accurately assess the carbon balance and elucidate the mechanisms controlling carbon exchange [*cf. Rice et al.*, 2004]. Eddy-covariance towers alone provide important information about the net exchange, but it is only in conjunction with ground-based measurements and model simulations that we can synergistically further our understanding of the ecosystem processes.

All individual study sites and measurement methods come with a unique set of challenges. We as a community need to move beyond arguments of data representivity from individual studies or methods to more integrative analyses combining datasets. We need more collaboration, integration, and sharing of data to pool our resources and understanding to truly progress in elucidating the controls on carbon exchange and ecosystem stability.

Appendix A

A.1 Water vapor concentrations

Accurate measurement of H₂O vapor concentration in tropical forests is challenging due to the high H₂O concentrations, large amount of rain, very tall canopies, and the large quantity of dust and aerosols. Mounting a dew point generator on a 65 m tall tower in central Amazonia is not a practical calibration option. A standard addition gas could not be added to check the calibration for H₂O, therefore we used two independent calibrations for the IRGA concentration measurements: (a) the nighttime relationship between ambient temperature measurements and sonic temperature measurements; (b) a chilled mirror dew point hygrometer mounted on the tower.

The sonic air temperature, T_s reported by the CSAT-3 is derived the properties of dry air and differs from the kinetic air temperature, T_k , by several degrees due to variation in the concentration of water vapor. The molar mass of water vapor, 18.016 g, is less than the mean molar mass of air, 28.97 g, therefore higher water vapor concentrations imply lower the mean air density and thus $T_s > T_k$. The speed of sound measured by the CSAT-3 reports T_s using the following equation:

$$T_s = \frac{c^2 M_d}{R} \times \frac{c_{vd}}{c_{pd}} \quad (\text{A.1})$$

Where c is the measured speed of sound (m s^{-1}), M_d is the molecular weight of dry air, R is the universal gas constant ($8.3144 \text{ J mol}^{-1} \text{ K}^{-1}$), c_{vd} and c_{pd} are the specific heats of dry air at constant volume and pressure, respectively (0.7176 and $1.0047 \text{ kJ mole}^{-1}$). To relate the T_s , T_k , and the molar fraction of water vapor, F_w , we used the following equations:

$$c^2 = \frac{c_{pd}}{c_{vd}} \times \frac{P}{\rho_d} = \frac{c_{pd}}{c_{vd}} \times \frac{k}{M_d} \times T_s \quad (\text{A.2})$$

$$c^2 = \frac{c_{pw}}{c_{vw}} \times \frac{k}{M_w} \times T_k \quad (\text{A.3})$$

Thus,

$$\frac{T_s}{T_k} = \frac{M_d}{M_w} \times \frac{c_{pw}}{c_{vw}} \bigg/ \frac{c_{pd}}{c_{vd}} \quad (\text{A.4})$$

Where P is the atmospheric pressure (N m^{-2}), ρ_d is density of dry air (kg m^{-3}), k is Boltzmann's constant ($1.38 \times 10^{-23} \text{ J K}^{-1}$), M_w is the molecular weight of water vapor, c_{vw} and c_{pw} are the specific heats of water vapor at constant volume and pressure, respectively (1.47 and 1.09 kJ kg^{-1}). The right-hand side of equation A.4 can be approximated for our conditions as

$$\frac{T_s}{T_k} \cong 1 + 0.322 \times F_w \quad (\text{A.5})$$

To calibrate the Licor 6262 H_2O signal, F_w^L , we fit parameters a and b to obtain:

$$T_s - T_k = a + b \times 0.322 \times F_w^L \times T_k \quad (\text{A.6})$$

Where a is the average observed offset between T_s and T_k and b is the water vapor calibration coefficient that relates F_w^L to F_w .

This water vapor calibration was done using 30-minute averaged nighttime data for data bins about 20 days in length. Nighttime data were used to ensure that radiative heating effects did not contaminate the calibration. The data bin length varied depending on distribution of data gaps due to system failures and deterioration of sample inlet filters.

As a second independent calibration approach we used an EdgeTech 200M dew point hygrometer was mounted on the tower at 57.9 m. The mirrors in the sensor were cleaned frequently using alcohol and calibrated according to manufacturer specifications. When the hygrometer was operating within specifications (~ 50% of the time), these data could also be used for calibration.

The calibration values from these two methods, chilled mirror hygrometer and sonic to ambient temperature, were individually smoothed through time using a loess smoothing filter and then averaged to get the best possible water vapor calibration. The two methods agreed within 10%.

A.2 Latent heat flux calculation

The latent heat flux (LE , $W m^{-2}$) was calculated as follows:

$$LE = \langle w'h' \rangle \times \frac{kg}{m^3} \times \lambda \quad (A.5)$$

and

$$\lambda = 2501 - 2.3601 \times T_k \times 10^3 \quad (A.6)$$

Where $\langle w'h' \rangle$ is the covariance between vertical wind velocity fluctuations (w') and fluctuations in the concentration of the scalar (h' , H_2O mol mol⁻¹) and λ is the latent heat of vaporization (J kg⁻¹). Ambient pressure was measured at the site and the density calculations used measured half-hourly data.

A.3 Sensible Heat Flux

The sensible heat flux (H , W m⁻²) was calculated as follows:

$$H = \langle w'T_s' \rangle \times (c_{pd} \times \rho_d + c_{pw} \times \rho_w) \quad (A.5)$$

Where $\langle w'T_s' \rangle$ is the covariance between vertical wind velocity fluctuations (w') and fluctuations in the concentration of the scalar (T_s'), ρ_w is density of water vapor (kg m⁻³). Both the moist and dry components of the density and heat capacity are included in this calculation because T_s is sensitive to the water vapor concentration. Ambient pressure was measured at the site and the density calculations used measured half-hourly data.

A.4 Supplemental Figures and analyses for chapter 2

Figure A.1 shows the results of a cospectral analysis of CO₂, H₂O, and heat flux measurements to assess the reliability of the flux data and to verify if appropriate averaging intervals have been used to capture all of the flux-carrying eddies. An Ogive analysis provided an independent check on the adequacy of sample intervals by looking for an asymptotic plateau in the cumulative sums of the cospectra (between 1 Hz and 32.4 minutes). The daytime ogives for CO₂, H₂O, and heat fluxes (Figure A.1.) indicate that for this site a 30 minute averaging period is appropriate. We did not examine averaging

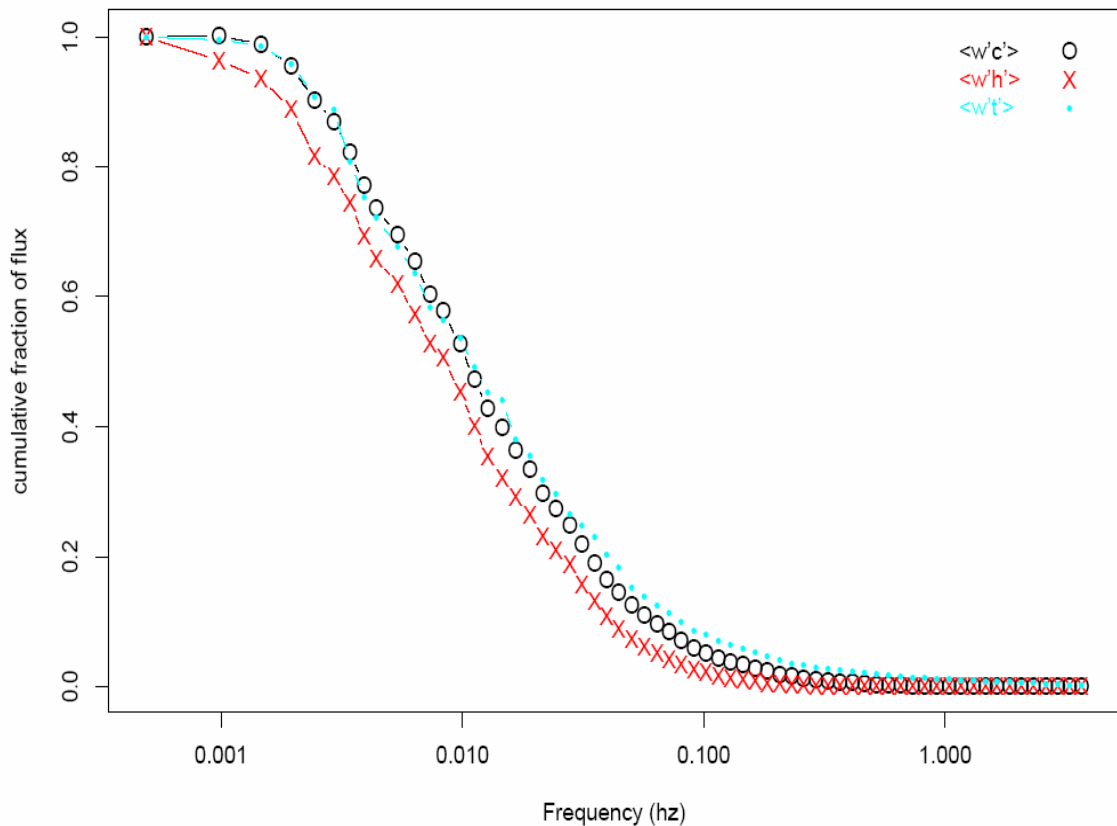


Figure A.1: Ogive, cumulative sum of the cospectra, plots for CO₂, H₂O, and heat fluxes. The curves are the composite averages of 12 individual co-spectra calculated during daytime periods in February 2004.

intervals beyond 34.2 minutes due to the instrument calibration schedule, but the ogives indicate that the low frequency fluxes are being adequately captured. There was some attenuation of high frequency (above 0.1 Hz) components of the water vapor flux due to adsorption and desorption along the sample tube walls and inlet filters, but overall high frequency attenuation was low (< 2%) because of the short sample tube lengths.

Figure A.2 shows the nighttime net ecosystem exchange (NEE) as a function turbulence (as measured by u^*) on a seasonal basis. We expect that ecosystem respiration should be largely independent of the turbulence intensity; nevertheless, measured NEE decreased in calm conditions (Figure A.2) suggesting that there was lost flux. Approximately 57% of the nighttime hours at this site were calm, with $u^* < 0.22 \text{ m s}^{-1}$. We therefore corrected for

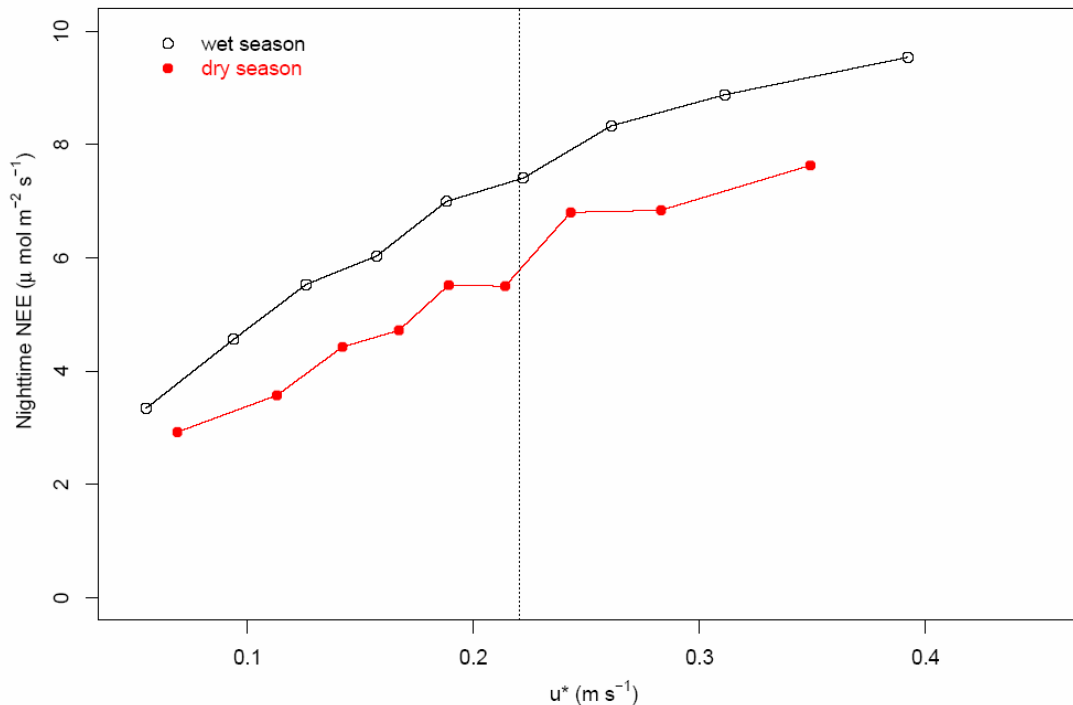


Figure A.2: Seasonal nighttime (0000 – 0400 LT) hourly net ecosystem exchange (NEE, $\mu\text{mol m}^{-2} \text{ s}^{-1}$, by u^* decile) vs. u^* (m s^{-1} , median of each decile) for 2002-2005. The vertical line at 0.22 m s^{-1} denotes the u^* filtering threshold.

lost flux by filtering calm night periods and replacing the data with the mean value of nearby well mixed time periods.

Figure A.3 shows the seasonal light curves from 2002 through 2005. Daytime data where $\text{PAR} \leq 40 \mu\text{mol m}^{-2} \text{s}^{-1}$ were excluded since these data represent periods of high atmospheric stability and rapid change, where hourly average values are not representative. The intercept, a_1 , of this overall model provides an extrapolation to derive an independent estimate of the mean ecosystem R at sunrise and sunset. The light-curve intercepts (based on all available data, no u^* filter applied), $8.9 \pm 0.6 \mu\text{mol m}^{-2} \text{s}^{-1}$, was not significantly different from the mean nighttime u^* filtered NEE, $8.6 \pm 0.13 \mu\text{mol m}^{-2} \text{s}^{-1}$. Comparisons of light-curve intercepts and nighttime, u^* filtered mean NEE examined seasonally also agree within <5% (Figure A.3).

Figure A.4 shows the time series for the mean enhanced vegetation index (EVI) over the TNF tower site, forest canopy efficiency (P_c ; gross primary production where photosynthetically active radiation is $725 - 875 \mu\text{mol m}^{-2} \text{s}^{-1}$), mean observed leaf litter fall rates, and daily precipitation values.

Figure A.5 we examined the intercept values (a_1) of seasonal morning versus afternoon light-curve extrapolations (equation (2.5)) and found no significant difference in the respiration estimates in the dry season, although temperature differences were near their maximum. In contrast, during the wet season we found that morning respiration estimates were higher than the afternoon estimates in three of four observed wet seasons (Figure

A.4). Higher morning respiration would again highlight the dominance of moisture in controlling heterotrophic respirations rates since nighttime precipitation is very common.

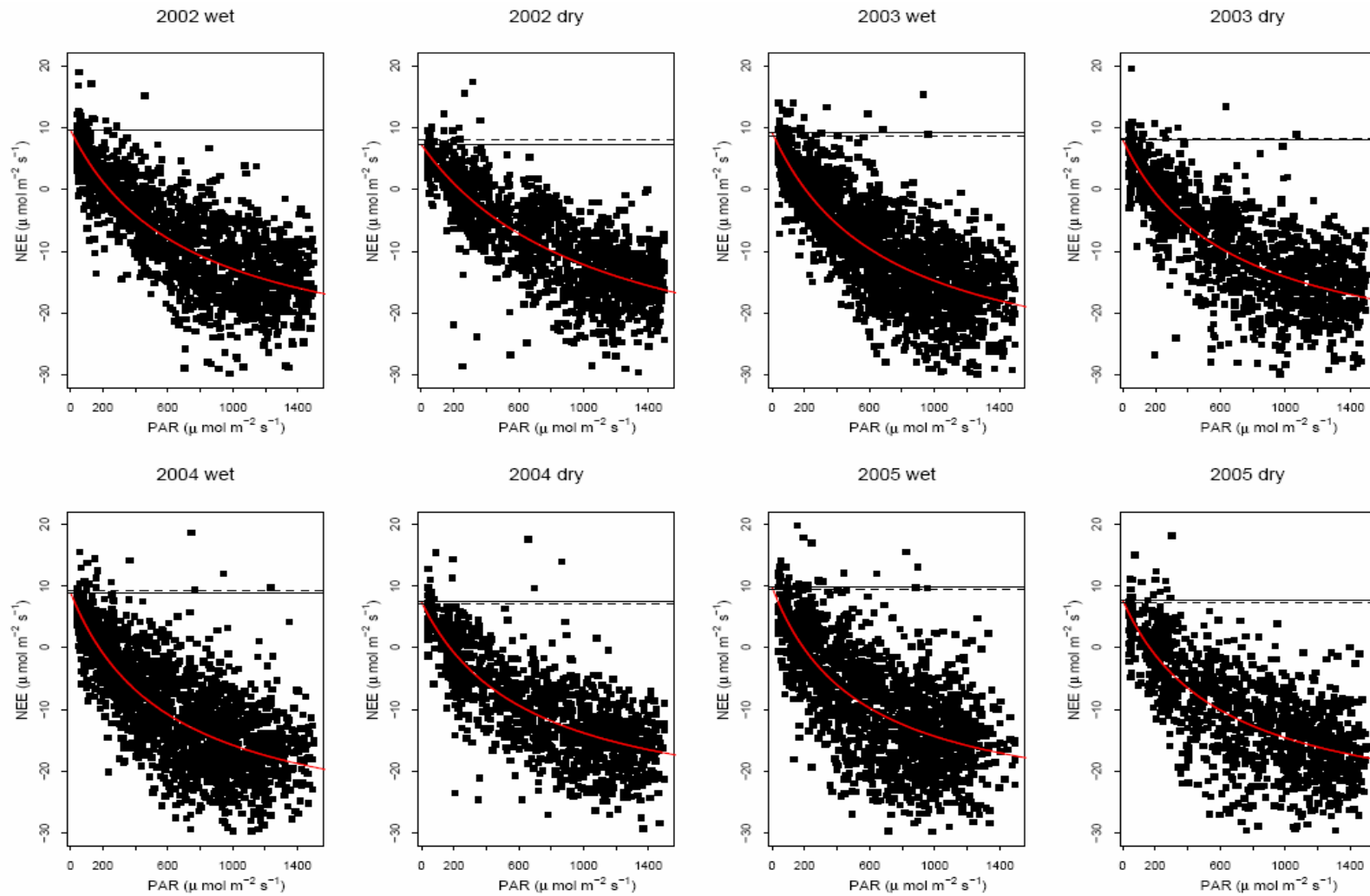


Figure A.3: Net ecosystem exchange of CO_2 ($NEE, \mu\text{mol m}^{-2} \text{s}^{-1}$) as a function of photosynthetically active radiation (PAR, binned by $15 \mu\text{mol m}^{-2} \text{s}^{-1}$). The vertical line denotes $0 \mu\text{mol m}^{-2} \text{s}^{-1}$ PAR. The horizontal line is the mean nighttime NEE during the given seasonal interval ($u^* \geq 0.22$). At low light levels, the light curve intercept (ecosystem respiration estimate) is approximated using a linear least squares fit.

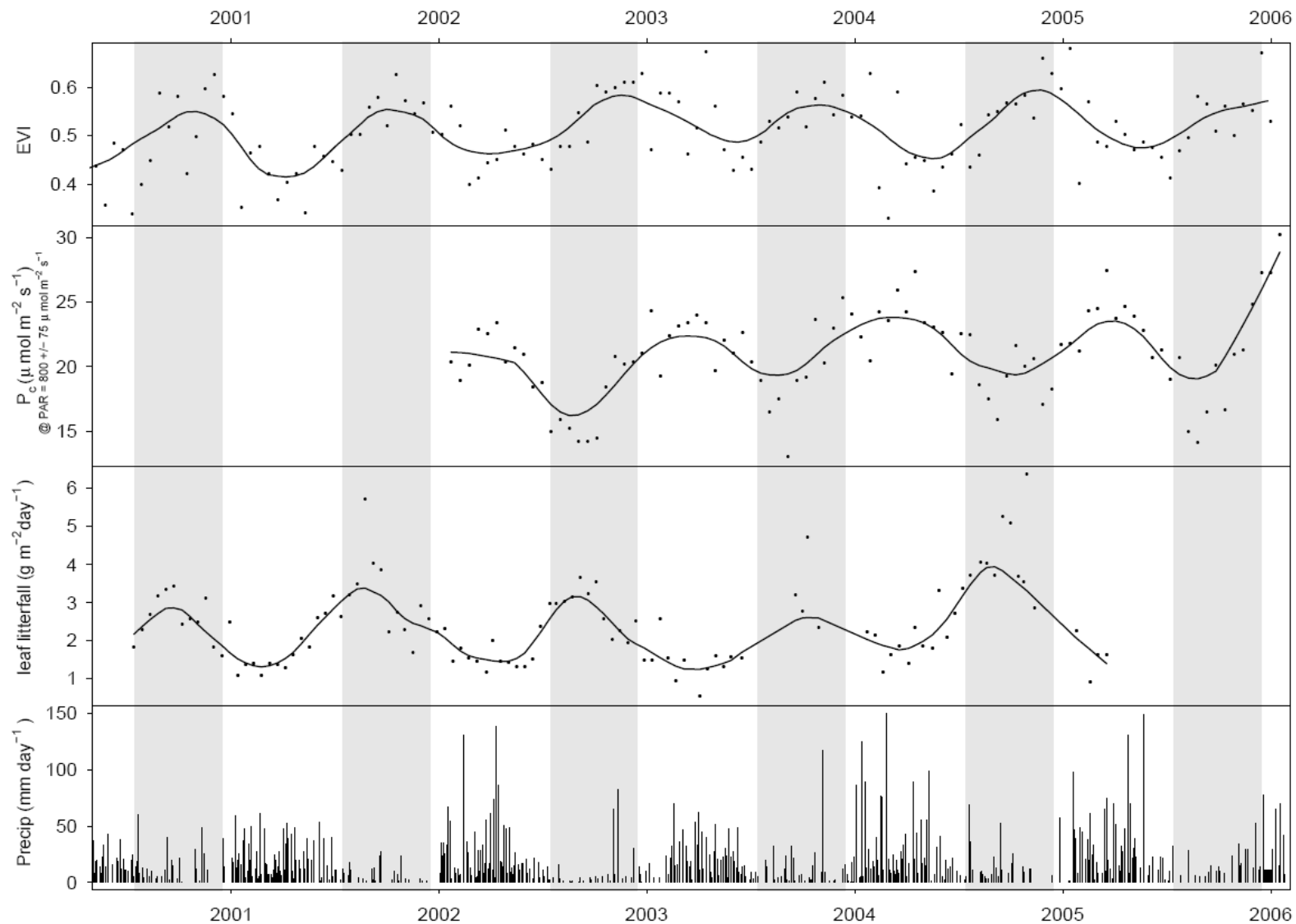


Figure A.4: (a) 16-day mean enhanced vegetation index (EVI) over the TNF tower site. (b) 16-day mean forest canopy efficiency (P_c ; gross primary production where photosynthetically active radiation is 725 – 875 $\mu\text{mol m}^{-2} \text{s}^{-1}$). (c) 14-day mean observed leaf litter fall rates. (d) daily precipitation values.

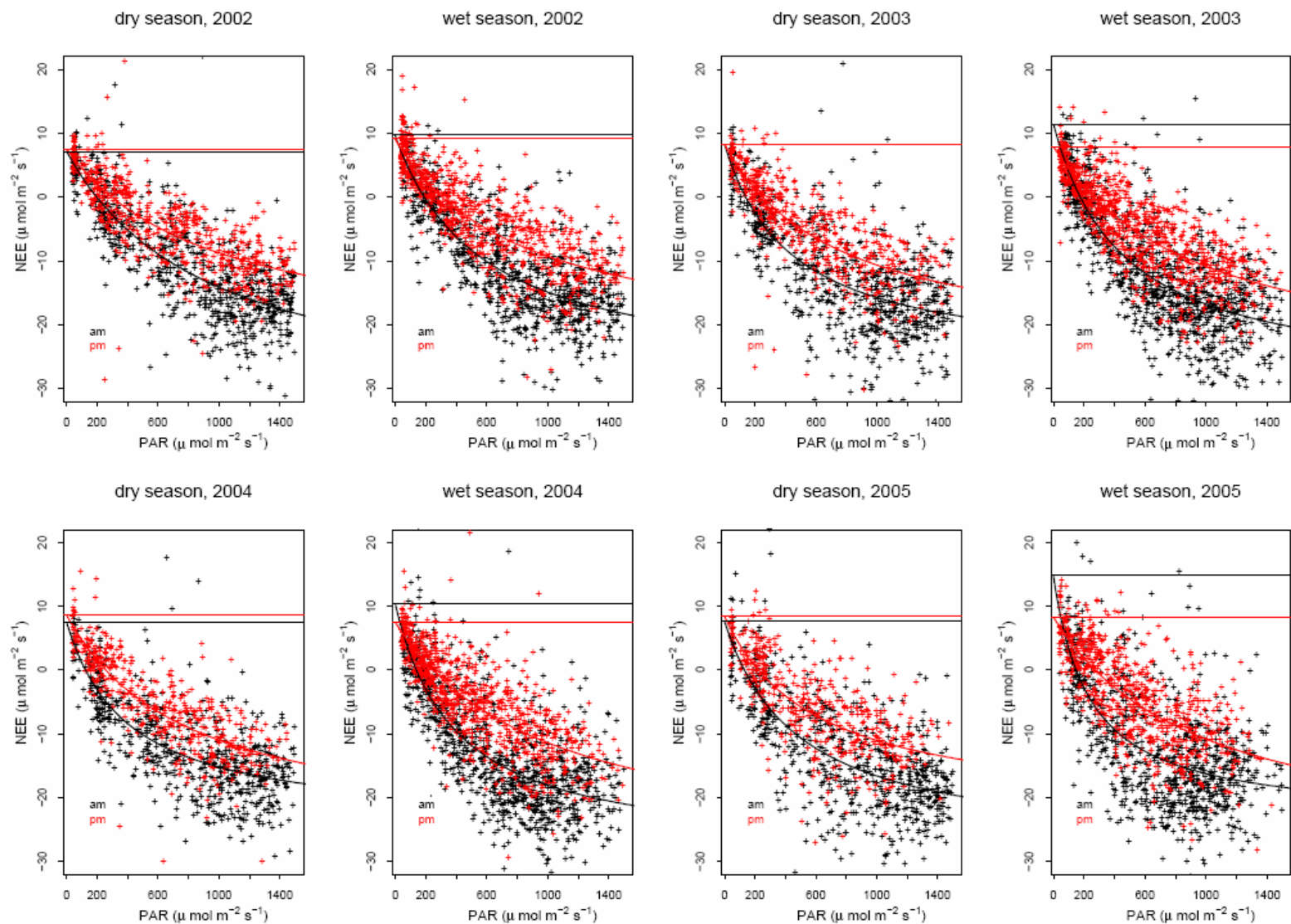


Figure A.5: Net ecosystem exchange of CO_2 (NEE , $\mu\text{mol m}^{-2} \text{s}^{-1}$) as a function of photosynthetically active radiation (PAR , $\mu\text{mol m}^{-2} \text{s}^{-1}$) fit by season. Morning (black points) and afternoon (red points) NEE was fit separately to test for a difference in respiration estimate (a_1). The solid horizontal lines highlight the individual a_1 intercept terms from the hyperbolic fits (equation (2.5)) estimating respiration.

References

- Anderson, J.M., Spencer, T., Carbon, nutrient and water balances of tropical rain forest ecosystems subject to disturbance., pp. 93, UNESCO, Paris, 1991.
- Araujo, A.C., et al., Comparative measurements of carbon dioxide fluxes from two nearby towers in a central Amazonian rainforest: The Manaus LBA site, *Journal of Geophysical Research-Atmospheres*, 107 (D20), Art. No. 8090, 2002.
- Baker, T.R., et al., Increasing biomass in Amazonian forest plots, *Philosophical Transactions of the Royal Society of London, Series B - Biological Sciences*, 359, 353-365, 2004.
- Baldocchi, D.D., B.B. Hicks, T.P. Meyers, Measuring biosphere-atmosphere exchanges of biologically related gases with micrometeorological methods, *Ecology*, 69 (5), 1331-1340, 1988.
- Barford, C.C., Wofsy, S.C., Goulden, M.L., Munger, J.W., Pyle, E.H., Urbanski, S.P., Hutyra, L., Saleska, S.R., Fitzjarrald, D., Moore, K., Factors controlling long- and short-term sequestration of atmospheric CO₂ in a mid-latitude forest, *Science*, 294, 1688-1691, 2001.
- Botta, A., Ramankutty, N., Foley, J.A., Long-term variations of climate and carbon fluxes over the Amazon basin, *Geophysical Research Letters*, 29 (9), Art. No. 1319, 2002.
- Brown, S., Lugo, A.E., The storage and production of organic-material in tropical forests and their role in the global carbon-cycle, *Biotropica*, 14 (3), 161-187, 1982.
- Carswell, F.E., Costa, A.L., Palheta, M., Malhi, Y., Meir, P., Costa, J.D.R., Ruivo, M.D., Leal, L.D.M., Costa, J.M.N., Clement, R.J., Grace, J., Seasonality in CO₂ and H₂O flux at an eastern Amazonian rain forest, *Journal of Geophysical Research-Atmospheres*, 107 (D20), Art. No. 8076, 2002.
- Chambers, J.Q., Higuchi, N., Schimel, J.P., Ferreira, L.V., Melack, J.M., Decomposition and carbon cycling of dead trees in tropical forests of the central Amazon, *Oecologia*, 122 (3), 380-388, 2000.
- Chambers, J.Q., dos Santos, J., Ribeiro, R. F., Higuchi, N., Tree damage, allometric relationships, and above-ground net primary production in a central Amazon forest., *Forest Ecology and Management*, 152, 73-84, 2001.
- Chambers, J.Q., et al., Respiration from a tropical forest ecosystem: Partitioning of sources and low carbon use efficiency, *Ecological Application*, 14 (4), S72-S88, 2004.

- Choudhury, B.J., DiGirolamo, N.E., A biophysical process-based estimate of global land surface evaporation using satellite and ancillary data - I. Model description and comparison with observations, *Journal of Hydrology*, 205, 164-185, 1998.
- Clark, D., Detecting tropical forests' responses to global climatic and atmospheric change: Current challenges and a way forward, *Biotropica*, 39 (1), 4-19, 2007.
- Clark, D.A., Piper, S.C., Keeling, C.D., Clark, D.B., Tropical rain forest tree growth and atmospheric carbon dynamics linked to interannual temperature variation during 1984-2000, *Proc. Natl. Acad. Sci. USA*, 100 (10), 5852-5857, 2003.
- Clark, D.B., Abolishing virginity, *Journal of Tropical Ecology*, 12, 735-739, 1996.
- Cochrane, M.A., Laurance, W.F., Fire as a large-scale edge effect in Amazonian forests, *Journal of tropical ecology*, 18 (311-325), 2002.
- Cochrane, M.A., Fire science for rainforests, *Nature*, 421, 913-919, 2003.
- Connell, J.H., Diversity in tropical rainforests and coral reefs., *Science*, 199, 1302-1310, 1978.
- Cox, P.M., Betts, R.A., Jones, C.D., Spall, S.A., Totterdell, I.J., Acceleration of global warming due to carbon cycle feedbacks in a coupled climate model, *Nature*, 408, 817-833, 2000.
- Cox, P.M., Betts, R.A., Collins, M., Harris, P.P., Huntingford, C., Jones, C.D., Amazonian forest dieback under climate-carbon cycle projections for the 21st century, *Theoretical and applied climatology*, 78, 137-156, 2004.
- da Rocha, H.R., Goulden, M.L., Miller, S.D., Menton, M.C., Pinto, L.D.V.O, de Freitas, H.C., Figueira, A.M.S., Seasonality of water and heat fluxes over a tropical forest in eastern Amazonia, *Ecological Application*, 14 (4), S22-S32, 2004.
- Davidson, E.A., Ishida, F.Y., Nepstad, D.C., Effects of an experimental drought on soil emissions of carbon dioxide, methane, nitrous oxide, and nitric oxide in a moist tropical forest, *Global Change Biology*, 10, 718-730, 2004.
- Davidson, E.A., Janssens, I.A., Luo, Y.Q., On the variability of respiration in terrestrial ecosystems: moving beyond Q(10), *Global Change Biology*, 12 (2), 154-164, 2006.
- Davidson, E.A., Janssens, I.A., Temperature sensitivity of soil carbon decomposition and feedbacks to climate change, *Nature*, 440, 165-173, 2006.
- Dickinson, R.E., and Henderson-Seller, A., Modeling tropical deforestation-a study of GCM land surface parameterizations, *Quarterly Journal of the Royal Meteorological Society*, 114 (480), 439-462, 1988.

- Domingues, T.F., Berry, J.A., Martinelli, L.A., Ometto, J.P.H.B., Ehleringer, J.R., Parameterization of canopy structure and leaf-level gas exchange for an eastern Amazonian tropical rain forest (Tapajos National Forest, Para, Brazil), *Earth Interactions*, 9, Art. 9, 2005.
- Doughty, C.E., Goulden, M.L., Miller, S.D., da Rocha, H.R., Circadian rhythms constrain leaf and canopy gas exchange in an Amazonian forest, *Geophysical Research Letters*, 33 (15), Art. No. L15404, 2006.
- FAO, Third interim report on the state of tropical forests, Food and Agriculture Organization, Rome, 1992.
- Farquhar, G.D., Sharkey, T.D., Stomatal conductance and photosynthesis, *Annual Review of Plant Physiology and Plant Molecular Biology*, 33, 317-345, 1982.
- Finnigan, J., Advection and modeling, in *Handbook for Micrometeorology*, edited by X. Lee, Massman, W., Law, B., Kluwer Academic Publishers, Dordrecht, 2004.
- Freeland, R.O., Effect of age of leaves upon the rate of photosynthesis in some conifers., *Plant physiology*, 27, 685-690, 1952.
- Friedlingstein, P., Bopp, L., Ciais, P., Dufresne, J.L., Fairhead, L., LeTreut, H., Monfray, P., Orr, J., Positive feedback between future climate change and the carbon cycle., *Geophysical Research Letters*, 28 (8), 1543-1546, 2001.
- Fung, I.Y., Doney, S.C., Lindsay, K., John, J., Evolution of carbon sinks in a changing climate, *Proceedings of the National Academy of Sciences of the USA*, 102 (32), 11201-11206, 2005.
- Garstang, M., Massie, H.L., Halverson, J., Greco, S., Scala, J., Amazon coastal squall lines. 1. Structure and kinematics, *Monthly Weather Review*, 122 (4), 608-622, 1994.
- Gash, J.H.C., An analytical model of rainfall interception by forests, *Q. J. R. Meteorol. Soc.*, 105, 43– 55, 1979.
- Gash, J.H.C., Nobre, C.A., Roberts, J.M., Victoria, R.L., *Amazonia deforestation and climate*, John Wiley & Sons, Chichester, 1996.
- Goulden, M.L., Munger, J.W., Fan, S.M., Daube, B.C., Wofsy, S.C., Measurements of carbon sequestration by long-term eddy covariance: Methods and a critical evaluation of accuracy, *Global Change Biology*, 2 (3), 169-182, 1996.
- Goulden, M.L., Miller, S.D., da Rocha, H.R., Menton, M.C., Freitas, H.C., Figueira, A.M., de Sousa, A.C.D., Diel and Seasonal Patterns of Tropical Forest CO₂ Exchange, *Ecological Application*, 14 (4), S43-S54, 2004.

- Grace, J., Lloyd, J., McIntyre, J., Miranda, A., Meir, P., Miranda, H., Moncrieff, J., Massheder, J., Wright, I., Gash, J., Fluxes of carbon dioxide and water vapor over an undisturbed tropical forest in south-west Amazonia, *Global Change Biology*, 1 (1), 1-12, 1995.
- Grace, J., Malhi, Y., Meir, P., Productivity of tropical rain forests., in *Terrestrial global productivity*, edited by M.H. Saugier B, pp. 401-426, Academic, San Diego, 2001.
- Gu, L.H., Baldocchi, D.D., Wofsy, S.C., Munger, J.W., Michalsky, J.J., Urbanski, S.P., Boden, T.A., Response of a deciduous forest to the Mount Pinatubo eruption: Enhanced photosynthesis, *Science*, 299, 2035-2038, 2003.
- Gut, A., *An intermediate course in probability*, Springer-Verlag, New York, New York, 1995.
- Hasler, N., Avissar, R., What controls Amazon evapotranspiration, *Journal of Hydrometeorology*, 2007, in review.
- Hodnett, M.G., Tomasella, J., Marques Filho, A. de O., Oyama, M.D., Deep soil water uptake by forest and pasture in central Amazonia: predictions from long-term daily rainfall data using a simple water balance model, in *Amazonian deforestation and climate*, edited by C.A.N. J.H.C. Gash, J.M. Roberts and R.L. Victoria, pp. 79-99, John Wiley & Sons, Chichester, 1996.
- Holdridge, L.R., Determination of world plant formations from simple climatic data, *Science*, 105 (2727), 367-368, 1947.
- Holling, C.S., Resilience and stability of ecological systems, *Annual review of ecology and systematics*, 4, 1-23, 1973.
- Houghton, R.A.a.S., D.L., Carbon, in *The Earth as transformed by human action.*, edited by W.C.C. B.L. Turner, R.W. Kates, J.F. Richards, J.T. Mathews, and W.B. Meyers, pp. 393-408, Cambridge University Press, Cambridge, 1990.
- Huete, A.R., Didan, K., Shimabukuro, Y.E., Ratana, P., Saleska, S.R., Yang, W. Nemani, R.R., Myneni, R., Hutya, L.R., Fitzjarrald, D., Amazon rainforests green-up with sunlight in dry season, *Geophysical Research Letters*, 33 (6), Art. No. L06405, 2006.
- Huntingford, C., Harris, P.P., Gedney, N., Cox, P.M., Betts, R.A., Marengo, J.A., Gash, J.H.C., Using a GCM analogue model to investigate the potential for Amazonian forest dieback, *Theoretical and Applied Climatology*, 78 ((1-3)), 177-185, 2004.
- Hutya, L.R., Munger, J.W., Nobre, C.A., Saleska, S.R., Vieira, S.A., Wofsy, S.C., Climatic variability and vegetation vulnerability in Amazonia, *Geophysical Research Letters*, 32, L24712, 2005.

Hutyra, L.R., Munger, J.W., Saleska, S.R., Gottlieb, E., Daube, B.C., Dunn, A.L., Amaral, D.F., de Camargo, P.B., Wofsy, S.C., Seasonal controls on the exchange of carbon and water in an Amazonian rainforest, *Journal of Geophysical Research - Biogeosciences*, 2007, in review.

Hutyra, L.R., Munger, J.W., Hammond-Pyle, E., Saleska, S.R., de Camargo, P.B., Wofsy, S.C., Resolving systematic errors in estimates of net ecosystem exchange of CO₂ and ecosystem respiration in a tall-stature forest: application to a tropical forest biome, *Agricultural and Forest Meteorology*, in review.

IPCC, *Climate Change 2001: The Scientific Basis.*, Cambridge University Press, Cambridge, UK, 2001.

Iwata, H., Malhi, Y., von Randow, C., Gap-filling measurements of carbon dioxide storage in tropical rainforest canopy airspace, *Agricultural and Forest Meteorology*, 132, 305-314, 2005.

Jackson, W.D., Fire, air water, and earth: an elemental ecology of Tasmania., *Proceedings of the ecological society of Australia*, 2, 9-16, 1968.

Kaimal, J.C., Izumi, Y., Wyngaard, J.C., Cote, R., Spectral characteristics of surface-layer turbulence, *Quarterly Journal of the Royal Meteorological Society*, 98 (417), 563-589, 1972.

Katz, R.W., Brown, B.G., Extreme events in a changing climate - variability is more important than averages, *Climatic Change*, 21 (3), 289-302, 1992.

Keller, M., Varner, R., Dias, J.D., Silva, H., Crill, P., de Oliveira, R.C., Soil-atmosphere exchange of nitrous oxide, nitric oxide, methane, and carbon dioxide in logged and undisturbed forest in the Tapajos National Forest, Brazil, *Earth Interaction*, 9, art 23, 2005.

Kleidon, A., Global datasets of rooting zone depth inferred from inverse methods, *Journal of Climate*, 17 (13), 2714-2722, 2004.

Kruijt, B., et al., The robustness of eddy correlation fluxes for Amazon rain forest conditions, *Ecological Applications*, 14 (4), S101-S113, 2004.

Ledru, M.P., Salgado Labouriau, M.L., Lorscheitter, M.L., Vegetation dynamics in Southern and Central Brazil during the last 10,000 year B.P., *Review of Palaeobotany and palynology*, 99 (2), 131-142, 1998.

Lee, J.E., Oliveira, R.S., Dawson, T.E., Fung, I., Root functioning modifies seasonal climate, *Proceedings of the National Academy of Sciences of the United States of America*, 102 (49), 17576-17581, 2005.

- Lee, X., Finnigan, J., Kyaw, T.P.U., Coordinate systems and and flux bias error, in *Handbook for Micrometeorology*, edited by X. Lee, Massman, W., Law, B., Kluwer Academic Publishers, Dordrecht, 2004.
- Lu, L.X., Denning, A.S., da Silva-Dias, M.A., da Silva-Dias, P., Longo, M., Freitas, S.R., Saatchi, S., Mesoscale circulations and atmospheric CO₂ variations in the Tapajós Region, Para, Brazil, *Journal of Geophysical Research-Atmospheres*, 110 (D21), Art. No. D21102, 2005.
- Malhi, Y., Nobre, A.D., Grace, J., Kruijt, B., Pereira, M., Culf, A., Scott, S., Carbon dioxide transfer over a central Amazonian rain forest, *Journal of Geophysical Research-Atmospheres*, 103, 31593-31612, 1998.
- Malhi, Y., Pegoraro, E., Nobre, A.D., Pereira, M.G.P., Grace, J., Culf, A.D., Clement, R., Energy and water dynamics of a central Amazonian rain forest, *Journal of Geophysical Research*, 107, Art. No. 8061, 2002.
- Martens, C.S., et al., Radon fluxes in tropical forest ecosystems of Brazilian Amazonia; night-time CO₂ net ecosystem exchange derived from radon and eddy covariance methods., *Global Change Biology*, 10, 618-629, 2004.
- McMillen, R.T., An eddy-correlation technique with extended applicability to non-simple terrain., *Boundary-Layer Meteorology*, 43 (3), 231-245, 1988.
- Melillo, J.M., McGuire, A.D., Kicklighter, D.W., Moore, B., Vorosmarty, C.J., Schloss, A.L., Global climate-change and terrestrial net primary production, *Nature*, 363, 234-240, 1993.
- Miller, S.D., Goulden, M.L., Menton, M.C., da Rocha, H.R., de Freitas, H.C., Figueira, A.M.E.S., de Sousa, C.A.D., Biometric and micrometeorological measurements of tropical forest carbon balance, *Ecological Applications*, 14 (4), S114-S126, 2004.
- Mitchell, T.D., Carter, T.R., Jones, P.D., Hulme, M., New, M., A comprehensive set of grids of monthly climate data for Europe and the globe: the observed record (1901-2000) and 16 scenarios., pp. 30, Tyndall Centre Working Paper, 2003.
- Monteith, J.L., Evaporation and environment, *Symp. Soc. Exp. Biol.*, 19, 205-234, 1983.
- Moore, C.J., G. Fisch, Estimating heat storage in Amazonian tropical forest, *Agricultural and Forest Meteorology*, 38, 147-169, 1986.
- Nascimento, H.E.M., Laurance, W.F., Biomass dynamics in Amazonian forest fragments, *Ecological Application*, 14 (4), S127-S138, 2004.
- Nepstad, D., Lefebvre, P., Da Silva, U.L., Tomasella, J., Schlesinger, P., Solorzano, L., Moutinho, P., Ray, D., Benito, J.G., Amazon drought and its implication for forest

flammability and tree growth; a basin-wide analysis, *Global Change Biology*, 10, 704-717, 2004.

Nepstad, D.C., de Carvalho, C.R., Davidson, E.A., Jipp, P.H., Lefebvre, P.A., Negreiro, G.H., da Silva, E.D., Stone, T.A., Trumbore, S.E., Vieira, S., The role of deep roots in the hydrological and carbon cycles of Amazonian forests and pastures., *Nature*, 372, 666-669, 1994.

Nepstad, D.C., et al., The effects of partial throughfall exclusion on canopy processes, aboveground production, and biogeochemistry of an Amazon forest, *Journal of Geophysical Research-Atmospheres*, 107 (D20), Art. No. 8085, 2002.

New, M., Hulme, M., Jone, P.D., Representing twentieth century space-time climate variability. Part 2: development of 1901-96 monthly grids of terrestrial surface climate., *Journal of Climate*, 13, 2217-2238, 2000.

Nix, H.A., Climate of tropical savannas, in *Ecosystems of the world, tropical savannas*, edited by F. Bourliere, pp. 37-61, Elsevier Scientific Publishing, Amsterdam, 1983.

Nobre, C.A., Sellers, P.J., Shulka, J., Amazonian deforestation and regional climate change, *Journal of Climate*, 4, 957-988, 1991.

Oke, T.R., *Boundary Layer Climates*, Routledge, Cambridge, U.K., 1987.

Oliveira, P.H.F., Artaxo, P., Pires, C.A., de Lucca, S., Procópio, A., Holben, B., Schafer, J., Cardoso, L.F., Wofsy, S.C., The effects of biomass burning aerosols and clouds on the CO₂ flux in Amazonia, *Tellus B*, 2007, in review.

Oliveira, P.S., Marquis, R.J., *The cerrados of Brazil : ecology and natural history of a neotropical savanna*, Columbia University Press, New York, 2002.

Oliveira, R.S., Dawson, T.E., Burgess, S.S.O., Nepstad, D.C., Hydraulic redistribution in three Amazonian trees, *Oecologia*, 145 (3), 354-363, 2005.

Oyama, M.D., Nobre, C.A., A new climate-vegetation equilibrium state for Tropical South America, *Geophysical Research Letters*, 30 (23), 2199, 2003.

Oyama, M.D., and C. A. Nobre, A simple potential vegetation model for coupling with the Simple Biosphere Model (SiB), *Rev. Bras. Meteorol.*, 19, 203-216, 2004.

Parrotta, J.A., Francis, J.K., De Almeida, R.R., *Trees of the Tapajos*, United States Department of Agriculture, Rio Piedras, Puerto Rico, 1995.

Petit, J.R., et al., M., Climate and atmospheric history of the past 420,000 years from the Vostok ice core, Antarctica, *Nature*, 399, 429-436, 1999.

Phillips, O.L., Hall, P., Gentry, A.H., Sawyer, S.A., Vasquez, R., Dynamics and species richness of tropical rainforests, *Proc. Natl. Acad. Sci. USA*, 91 (7), 2805-2809, 1994.

Phillips, O.L., Malhi, Y., Higuchi, N., Laurance, W. F., Nunez, P. V., Vasquez, R. M., Laurance, S. G., Ferreira, L. V., Stern, M., Brown, S., Grace, J., Changes in the carbon balance of tropical forests: Evidence from long-term plots, *Science*, 282 (October 16), 439-442, 1998.

Prentice, I.C., Farquhar, G. D., Fasham, M. J. R., Goulden, M. L., Heimann, M., Jaramillo, V. J., and H.S. Keshgi, Le Quere, C., Scholes, R. J., Wallace, D. W. R., The carbon cycle and atmospheric carbon dioxide, in *Climate Change 2001: the Scientific Basis*, edited by J.T. Houghton, and e. al., pp. 183-237, Cambridge University Press, Cambridge, 2001.

Raich, J.W., Schlesinger, W.H., The global carbon-dioxide flux in soil respiration and its relationship to vegetation and climate, *Tellus Series B- Chemical and Physical Meteorology*, 44 (2), 81-99, 1992.

Rice, A.H., et al., Carbon balance and vegetation dynamics in an old-growth Amazonian forest, *Ecological Applications*, 14 (4), s55-s71, 2004.

Richardson, A.D., Hollinger, D.Y., Statistical modeling of ecosystem respiration using eddy covariance data: Maximum likelihood parameter estimation, and Monte Carlo simulation of model and parameter uncertainty, applied to three simple models, *Agricultural and Forest Meteorology*, 131 (3-4), 191-208, 2005.

Rivera, G., Elliott, S., Caldas, L.S., Nicolossi, G., Coradin, V.T.R., Borchert, R., Increasing day-length induces spring flushing of tropical dry forest trees in the absence of rain, *Trees-Structure and Function*, 16 (7), 445-456, 2002.

Salati, E., Vose, P.B., Amazon Basin: A system in equilibrium, *Science*, 225, 129-138, 1983.

Saleska, S.R., et al., Carbon in amazon forests: Unexpected seasonal fluxes and disturbance-induced losses, *Science*, 302, 1554-1557, 2003.

Saleska, S.R., Huttyra, L.R., Hammond-Pyle, E., de Carmargo, P.B., Vieira, S.A., Wofsy, S.C., From source to sink: tracing the effects of natural disturbance on tropical forest carbon balance, *Ecological Applications*, 2007, in prep.

Santoni, G.W., Nascimento, H.E.M., Hammond-Pyle, E., Huttyra, L.R., Laurance, W.F., Saleska, S.R., de Carmargo, P.B., Vieira, S.A., Wofsy, S.C., Landscape-scale dynamics of live and dead biomass in two Amazonian rainforests, *Ecological Applications*, 2007, in prep.

- Schaphoff, S., Lucht, W., Gerten, D., Sitch, S., Cramer, W., Prentice I.C., Terrestrial biosphere carbon storage under alternative climate projections, *Climatic Change*, 74 (1-3), 97-122, 2006.
- Scheffer, M., M. Holmgren, V. Brovkin, and M. Claussen, Synergy between small- and large-scale feedbacks of vegetation on the water cycle, *Global Change Biology*, 11, 1-10, 2005.
- Shuttleworth, W.J., Evaporation from Amazonian rainforest, *Proc. R. Soc. Lond. B.*, 233, 321-346, 1988.
- Silver, W.L., Neff, J., McGroddy, M., Veldkamp, E., Keller, M., Cosme, R., Effects of soil texture on belowground carbon and nutrient storage in a lowland Amazonian forest ecosystem, *Ecosystems*, 3, 193-209, 2000.
- Sternberg, L.D.L., Savanna-forest hysteresis in the tropics, *Global ecology and biogeography*, 10, 169-378, 2001.
- Tans, P.P., Fung, I.Y., Takahashi, T., Observational constraints on the global atmospheric CO₂ budget, *Science*, 247, 1431-1438, 1990.
- Thornwaite, C.W., An approach toward a rational classification of climate., *Geographic review*, 38, 55-94, 1948.
- Tian, H.Q., Melillo, J.M., Kicklighter, D.W., McGuire, A.D., Helfrich, J.V.K., Moore, B., Vorosmarty, C.J., Effect of interannual climate variability on carbon storage in Amazonian ecosystems, *Nature*, 396 (6712), 664-667, 1998.
- Trumbore, S.E., Carbon respired by terrestrial ecosystems - recent progress and challenges, *Global Change Biology*, 12 (2), 141-153, 2006.
- Urbanski, S., Barford, C., Wofsy, S., Kucharik, C., Pyle, E., Budney, J., McKain, K., Fitzjarrald, D., Czikowsky, M., Munger, J.W., Factors Controlling CO₂ Exchange on time scales from hourly to decadal at Harvard Forest, *Journal of Geophysical Research - Biogeosciences*, 2007, in press.
- Vieira, S., de Carmago, P.B., Selhorst, D., da Silva, R., Hutyra, L., Chambers, J.Q., Brown, I.F., Higuchi, N., dos Santos, J., Wofsy, S.C., Trumbore, S.E., Martinelli, L.A., Forest structure and carbon dynamics in Amazonian tropical rain forests, *Oecologia*, 140, 468-479, 2004.
- von Randow, C., Manzi, A.O., Kruijt, B., de Oliveira, P.J., Zanchi, F.B., Silva, R.L., Hodnett, M.G., Gash, J.H.C., Elbers, J.A., Waterloo, M.J., Cardoso, F.L., Kabat, P., Comparative measurements and seasonal variations in energy and carbon exchange over forest and pasture in South West Amazonia, *Theoretical and Applied Climatology*, 78, 5-26, 2004.

Vourlitis, G.L., Priante, N., Hayashi, M.M.S., Nogueira, J.D., Caseiro, F.T., Campelo, J.H., Seasonal variations in the evapotranspiration of a transitional tropical forest of Mato Grosso, Brazil, *Water Resources Research*, 38 (6), Art. No. 1094, 2002.

Wang, G.L., Eltahir, E.A.B., Biosphere-atmosphere interactions over West Africa II: Multiple climate equilibria., *J.Q. Roy. Met. Soc.*, 126, 1261-1280, 2000.

Webb, E.K., Pearman, G.I., Leuning, R., Correction of flux measurements for density effects due to heat and water-vapour transfer, *Quarterly Journal of Royal Meteorological Society*, 106, 85-100, 1980.

Werth, D., Avissar, R., The regional evapotranspiration of the Amazon, *Journal of Hydrometeorology*, 5 (100-109), 2004.

Whittaker, R.H., and Likens, G.E., The biosphere and man, in *Primary Productivity of the Biosphere*, edited by R.H. Whittaker, and Likens, G.E., pp. 305-328, Springer-Verlag, Berlin, 1975.

Williamson, G.B., Laurance, W.F., Oliveira, A.A., Delamonica, P., Gascon, C., Lovejoy, T.E., Pohl, L., Amazonian tree mortality during the 1997 El Nino drought, *Conservation Biology*, 14 (5), 1538-1542, 2000.

Wilson, K., et al., Energy balance closure at FLUXNET sites, *Agricultural and Forest Meteorology*, 113 (1-4), 223-243, 2002.

Wofsy, S.C., Goulden, M.L., Munger, J.W., Fan, S.M., Bakwin, P.S., Duabe, B.C., Bassow, S.L., Bazzaz, F.A., Net exchange of CO₂ in a midlatitude forest, *Science*, 260, 1314-1317, 1993.

Wright, S.J., van Schaik, C.P., Light and the phenology of tropical trees, *The American Naturalist*, 143, 192-199, 1994.